The Acheloos-Thessalia Water Transfer: Impact Assessment

Prepared by

Aris P. Georgakakos
Principal Investigator

Huaming Yao
Research Engineer

Developed for and sponsored by

The National Technical University of Athens

and

The Greek Ministry of Public Works (ΥΠΕΧΩΔΕ)

December 1997

ACKNOWLEDGMENTS

This work was sponsored by the Greek Ministry of Public Works (ΥΠΕΧΩΔΕ) through a subcontract with the National Technical University of Athens (NTUA), and the Georgia Institute of Technology, Atlanta, Georgia, USA.

We would like to thank Dr. Demetris Koutsoyiannis of NTUA for his close collaboration and support of this work effort.

CONTENTS

CHAPTER 1

INTRODUCTION

Thessalia valley is in central Greece and is a key agricultural region for the national economy. However, in recent years, the impacts of population growth and agricultural expansion have resulted in frequent droughts, diminishing water supplies, and ecosystem degradation. To reverse this trend and to maintain the sustainability of the land resources, a water diversion has been proposed from the nearby Acheloos River Basin. The diversion is planned to take place from Sykia, a new reservoir currently being constructed at the upper reaches of the Acheloos River. Figure 1.1 schematically depicts the existing and planned hydraulic works that would enable this inter-basin water transfer. The features of these projects are described in the following section.

Previous studies (*Georgakakos, et al., 1995*) have shown that a diversion of 600 million cubic meters per year would reduce energy generation at the existing hydropower facilities of the Acheloos River (Kremasta, Kastraki, and Stratos) by about 15% per year, without significantly affecting the other water uses in the Acheloos Basin. However, this is a partial assessment, and more detailed studies are needed to evaluate the overall impacts and benefits of the water resources system to be created after the diversion is in place.

With this background, the purpose of this study is to develop a mathematical model that incorporates all major elements of the new system configuration and use it to carry out the aforementioned integrated assessments. The model includes a control (i.e., optimization) and a control-simulation component. The purpose of the control model is to develop optimal reservoir operation policies, while that of the control-simulation model is to evaluate the performance of these policies over the historical inflow record.

The report includes five chapters and one appendix. In the following chapter, we give a short overview of the Acheloos reservoir system and discuss the data used in the study. In Chapter 3, we introduce the control model formulation, discuss our modeling assumptions, and

briefly describe the basis of a new optimization methodology implemented in this work. In Chapter 4, we present and elaborate on the model results, and in Chapter 5 we summarize the conclusions and suggest certain modifications and further investigations. Lastly, in the appendix, we include various reservoir characteristic curves and miscellaneous data.

We note that this report is not yet final, but it is issued to solicit the input of the funding and other interested agencies relative to (1) the validity and suitability of model assumptions and features and (2) additional operational and planning scenarios that would be of interest to them. In view of this, the model design is flexible to incorporate such modifications and support future investigations.

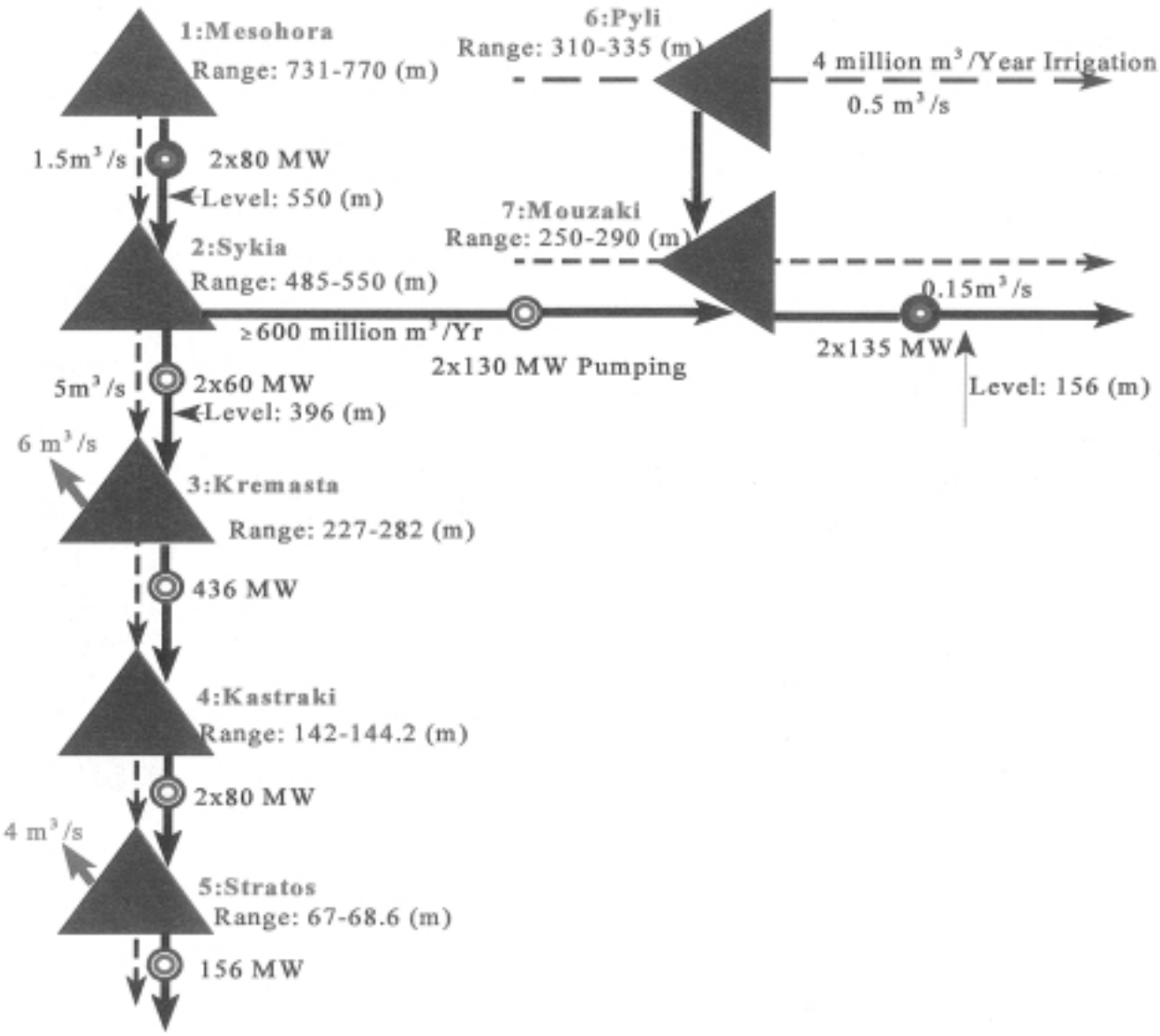

Figure 1.1: The Acheloos-Thessalia River System

CHAPTER 2

THE ACHELOOS-THESSALIA RESERVOIR SYSTEM

The Acheloos River basin (Figure 1.1) currently includes three reservoirs (Kremasta, Kastraki, and Stratos), while two other projects (Mesohora and Sykia) are presently under construction. Of the existing reservoirs, the largest is Kremasta with a total storage of $4,500 \times 10^6$ cubic meters, whereas the others are smaller projects with a combined storage of less than $1,500 \times 10^6$ cubic meters. The proposed water diversion to Thessalia would take place from the Upper Acheloos (Sykia). The Thessalia system includes two proposed reservoirs, Pyli and Mouzaki. The conservation storage of these reservoirs is used to support water supply, hydropower generation, and environmental protection and extends over the ranges reported in Table 2.1.

Table 2.1: Conservation Storage Ranges

Reservoir	Minimum		Maximum	
	Storage (10^6 m^3)	Elevation (m)	Storage (10^6 m^3)	Elevation (m)
Mesohora	132.8	731	358	770
Sykia	94	485	590.8	550
Kremasta	999	227	4500	282
Kastraki	750	142	800	144.2
Stratos	60	67	70.2	68.6
Pyli	21.7	310	125.4	355
Mouzaki	54.4	250	237.2	290

Average seepage losses amount to 6 m^3/sec at Kremasta and 4 m^3/sec at Stratos, while at others, they are either negligible or unavailable. Other reservoir data, including elevation versus storage and area versus storage curves, are included in Appendix A. All projects except Pyli have hydro electric generation units, the number and capacities of which are shown on Table 2.2.

Table 2.2: Hydroelectric Plant Characteristics

Reservoir	**(Number of Units) x (Installed Capacity - MW)**
Mesohora	2 x 80
Sykia	2 x 60
Kremasta	4 x 109 = 436
Kastraki	4 x 80 = 320
Stratos	2 x 75 + 2 x 3 = 156
Pyli	0
Mouzaki	2 x 135
Pefkofito	2 x 130

The water diversion from Sykia to Mouzaki passes through the power facility at Pefkofito. The turbines at Pefkofito and Mouzaki can also operate in a pumping mode.

An approximate relationship between power generation, reservoir elevation, and turbine discharge is provided in Appendix A for all power facilities. For lack of more detailed data, these relationships are used herein to model power generation at the monthly time scale.

Figures 2.1, 2.2, and 2.3 respectively summarize the monthly statistics of reservoir inflows (local drainage basins) for all reservoirs. A correlation analysis for the inflows indicates that the flows exhibit weak monthly correlations. The previous statistics are based on a 31-year record, extending from 1961 to 1991. Tables 2.3 and 2.4 report the monthly statistics of the evaporation and rainfall rates for all reservoirs based on same period.

Table 2.3. Monthly Evaporation Rate (mm)

Month	Mesohora	Sykia	Kremasta	Kastraki	Stratos	Pyli	Mouzaki
Jan	35.2	37.5	33.370	33.370	33.370	40.8	41
Feb	34.8	40.8	52.860	52.860	52.860	40.3	44.6
Mar	53.3	56.5	79.380	79.380	79.380	61.5	61.6
Apr	68.3	74.7	119.99	119.99	119.99	78.5	81.3

May	115.3	122.3	162.94	162.94	162.94	131.9	132.7
Jun	169.1	185.5	206.24	206.24	206.24	192.6	200.7
Jul	222.7	236.5	237.79	237.79	237.79	252.9	255.4
Aug	176.9	187.8	212.18	212.18	212.18	201	202.9
Sep	123.3	135.3	147.19	147.19	147.19	140.4	146.4
Oct	57.8	61.2	76.010	76.010	76.010	66.2	66.4
Nov	32.2	35.2	38.500	38.500	38.500	37.1	38.3
Dec	32.4	34.4	25.570	25.570	25.570	37.4	37.6

Table 2.4 Monthly Rainfall Rate (mm)

Month	Mesohora	Sykia	Kremasta	Kastraki	Stratos	Pyli	Mouzaki
Jan	223.04	266.65	149.18	134.45	134.45	207.49	194.09
Feb	212.66	251.06	144.55	136.78	136.78	200.61	175.27
Mar	159.56	184.66	115.17	104.32	104.32	161.85	143.27
Apr	133.80	158.36	95.880	78.790	78.790	144.87	125.73
May	101.20	109.24	72.310	51.170	51.170	104.88	86.61
Jun	48.060	53.460	37.620	33.730	33.730	43.520	40.54
Jul	36.750	39.060	23.300	18.600	18.600	28.040	25.53
Aug	34.200	45.060	20.100	22.860	22.860	33.900	29.77
Sep	64.790	75.440	50.030	42.790	42.790	60.350	57.36
Oct	165.00	174.91	108.29	103.88	103.88	181.36	154.15
Nov	255.52	293.29	216.31	206.34	206.34	225.85	197.54
Dec	295.99	340.50	210.69	187.13	187.13	287.74	245.11

Except for energy generation and flood protection, the reservoir system is expected to provide water for irrigation and maintain sufficient in-stream flows to preserve environmental

quality. Irrigation withdrawals amount to 35 m^3/sec during May through September, while 21 m^3/sec are mandated throughout the year for environmental preservation. Both of these requirements apply to downstream of Stratos. Thus, the minimum release from Stratos is 56 m^3/sec for May through September and 21 m^3/sec for the rest of the year. The annual irrigation requirement for Pyli is 4 million cubic meters distributed from May through September. The environmental release requirements are 0.5 and 0.15 m^3/s, respectively, for Pyli and Mouzaki. Table 2.5 reports the combined release constraints for all reservoirs.

Table 2.5: Monthly Release Constraints (m^3/s)

	Mesohora	Sykia	Kremasta	Kastraki	Stratos	Pyli	Mouzaki
Jan	1.5	5	0	0	21	0.5	0.15
Feb	1.5	5	0	0	21	0.5	0.15
Mar	1.5	5	0	0	21	0.5	0.15
Apr	1.5	5	0	0	21	0.58	0.15
May	1.5	5	0	0	56	0.67	0.15
Jun	1.5	5	0	0	56	0.86	0.15
Jul	1.5	5	0	0	56	0.97	0.15
Aug	1.5	5	0	0	56	0.91	0.15
Sep	1.5	5	0	0	56	0.55	0.15
Oct	1.5	5	0	0	21	0.5	0.15
Nov	1.5	5	0	0	21	0.5	0.15
Dec	1.5	5	0	0	21	0.5	0.15

Lastly, the proposed diversion of Acheloos water to the neighboring region of Thessalia is planned to take place from Sykia. The amount of the diversion is estimated at 600 million cubic meters annually, with the seasonal distribution shown on Table 2.6.

Table 2.6: Seasonal Distribution of the Proposed Thessalia Diversion

Month	Jan.-Mar.	April	May	June	July	Aug.	Sep.	Oct.-Dec.
%	0	5	11	23.6	30.2	26.4	3.8	0

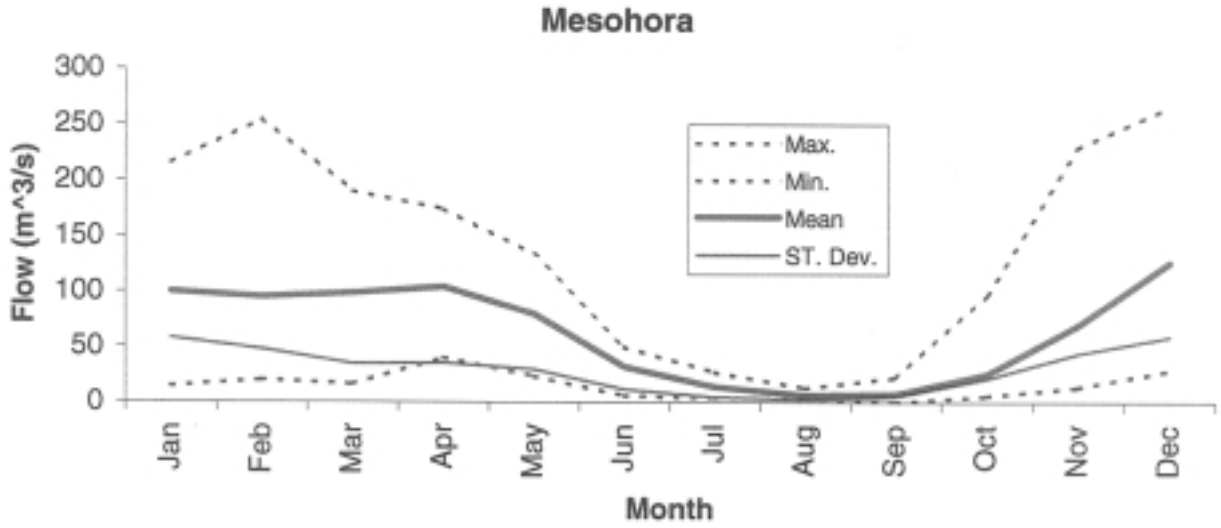

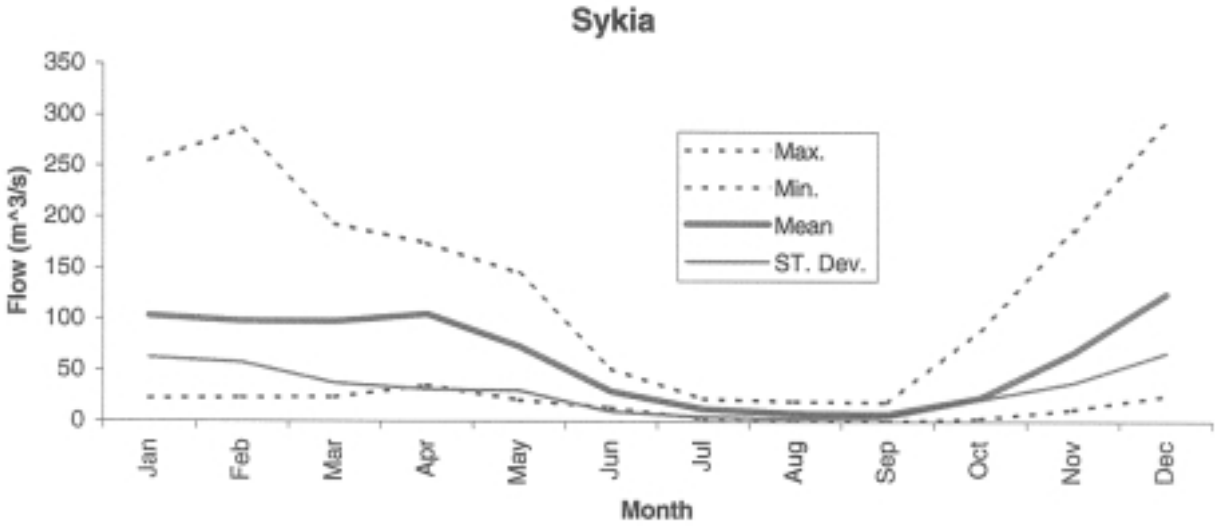

Figure 2.1: Inflow Statistics; Mesohora and Sykia

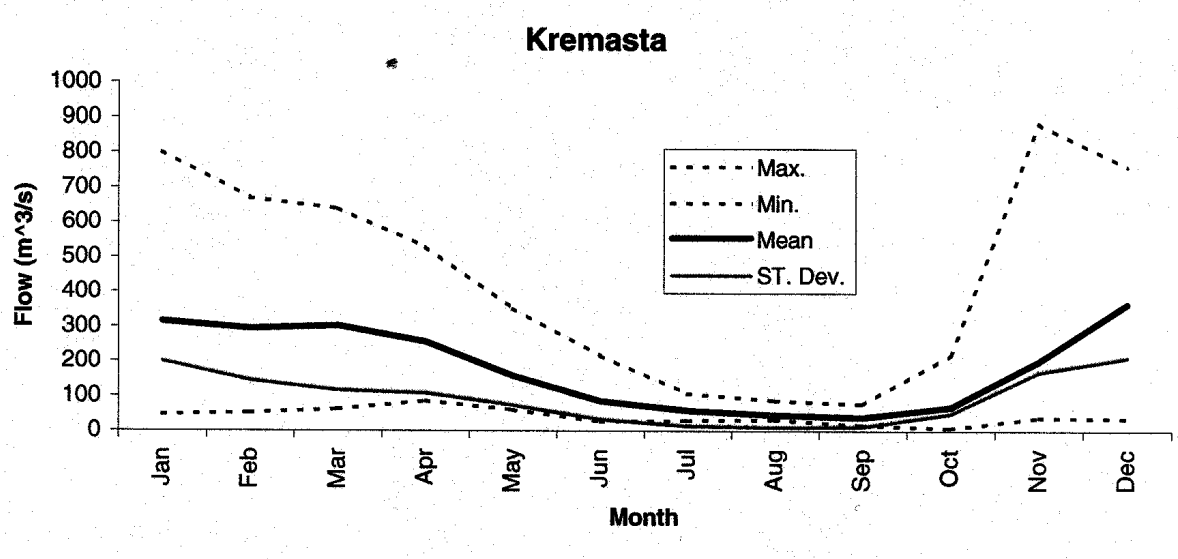

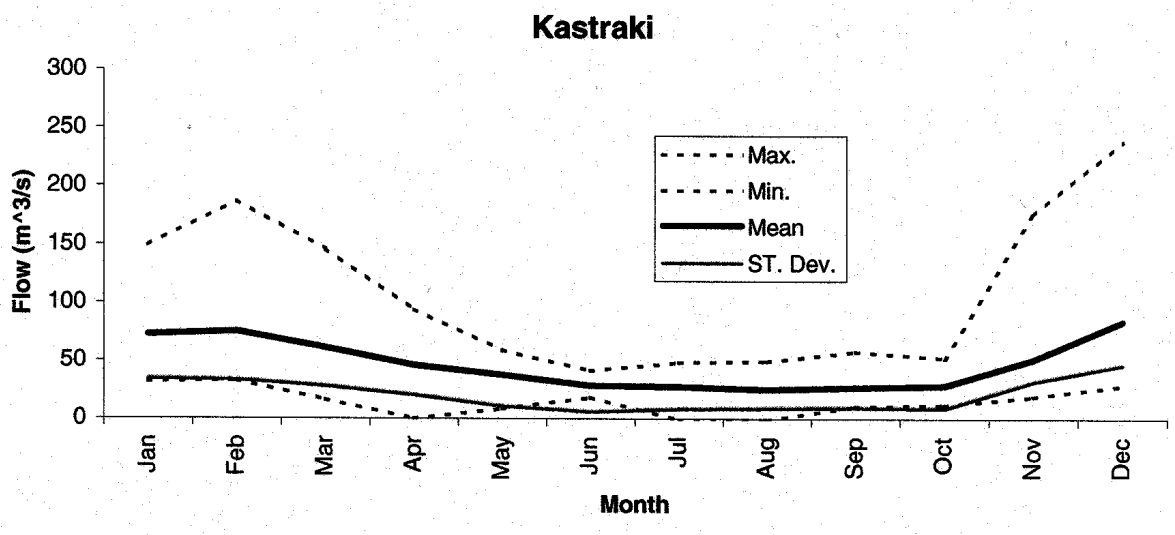

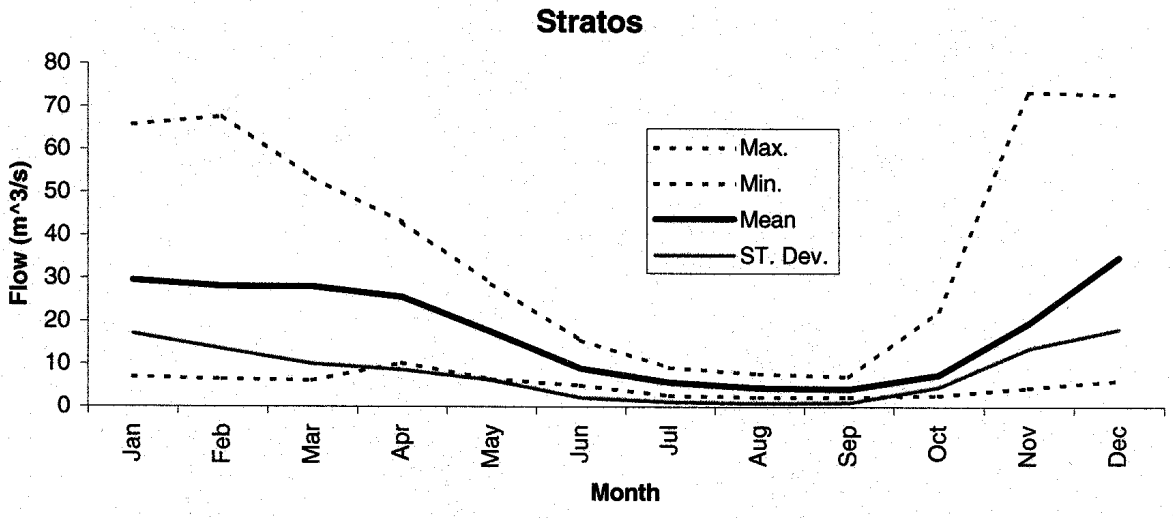

Figure 2.2: Inflow Statistics; Kremasta, Kastraki, and Stratos

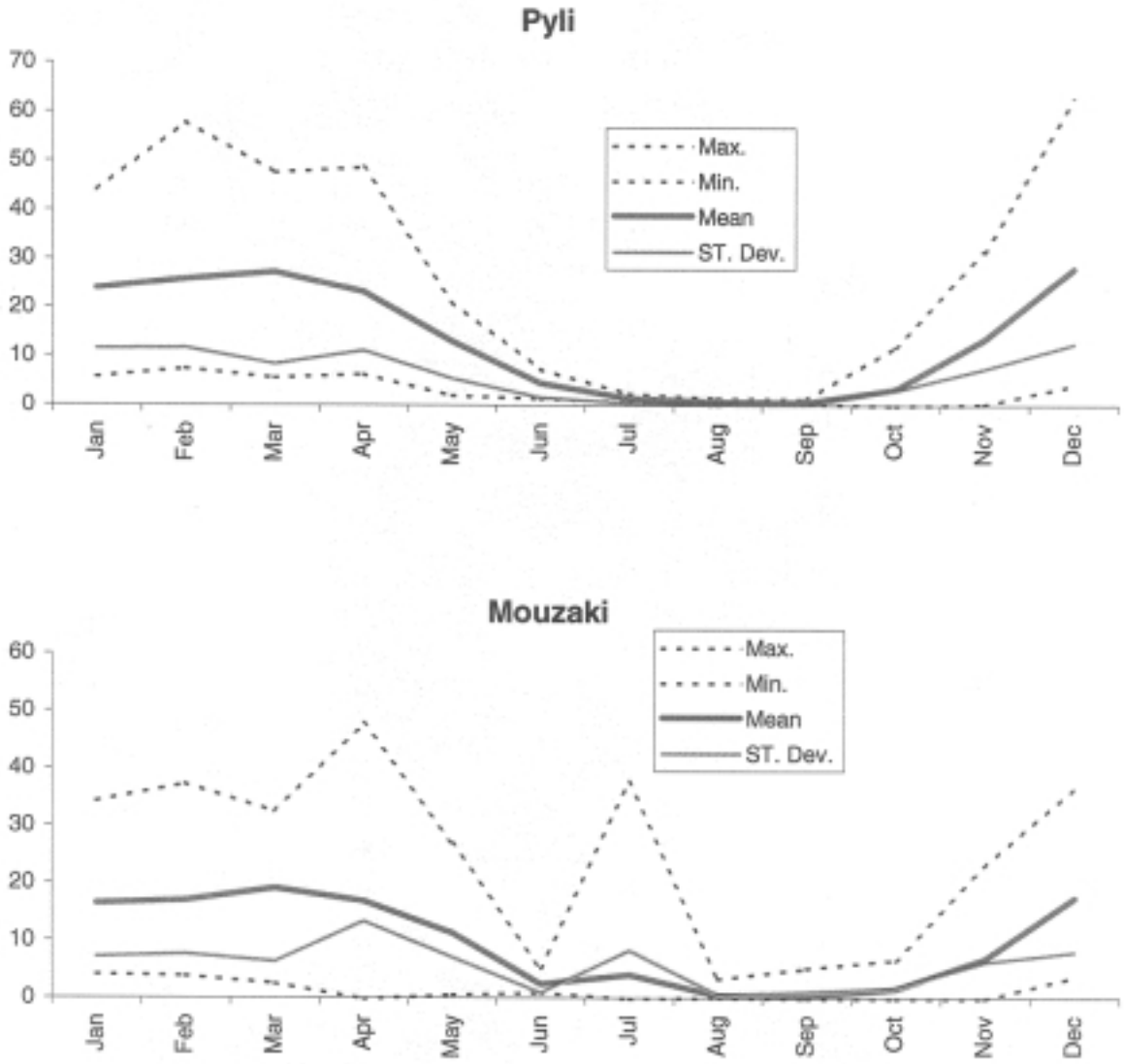

Figure 2.3: Inflow Statistics; Pyli and Mouzaki

CHAPTER 3

CONTROL MODEL

3.1 Formulation

3.1.1 System Dynamics

The entire reservoir system is modeled by the following water balance relationships:

$$
\begin{aligned}
S_1(k+1) &= S_1(k) - e_1(k)A_1[S_1(k)] - u_1(k) + w_1(k) - L_1(k) \ , \\
S_2(k+1) &= S_2(k) - e_2(k)A_2[S_2(k)] - u_2(k) + u_1(k) - u_8(k) + u_9(k) + w_2(k) - L_2(k) \ , \\
S_3(k+1) &= S_3(k) - e_3(k)A_3[S_3(k)] - u_3(k) + u_2(k) + w_3(k) - L_3(k) \ , \\
S_4(k+1) &= S_4(k) - e_4(k)A_4[S_4(k)] - u_4(k) + u_3(k) + w_4(k) - L_4(k) \ , \\
S_5(k+1) &= S_5(k) - e_5(k)A_5[S_5(k)] - u_5(k) + u_4(k) + w_5(k) - L_5(k) \ , \\
S_6(k+1) &= S_6(k) - e_6(k)A_6[S_6(k)] - u_6(k) + w_6(k) - L_6(k) \ , \\
S_7(k+1) &= S_7(k) - e_7(k)A_7[S_7(k)] - u_7(k) + u_6(k) + u_{10}(k) + w_7(k) - L_7(k) \ , \\
k &= 0,1,\ldots,N-1 \ ,
\end{aligned}
\tag{3.1}
$$

where the subscripts i = 1, to 7 respectively denote quantities pertaining to Mesohora, Sykia, Kremasta, Kastraki, Stratos, Pyli, and Mouzaki; k is the discretization time interval corresponding to one month; $S_i(k)$ is the storage of the ith reservoir at the beginning of the month; $e_i(k)$ is the evaporation rate; $A_i[S_i(k)]$ is the reservoir area versus storage function; $u_i(k)$ is the release volume; $w_i(k)$ is the inflow volume; $L_i(k)$ is the water loss; $u_8(k)$ is the release from Sykia to Mouzaki while $u_9(k)$ is the pumping volume from Mouzaki to Sykia; The difference of $u_8(k)$ and $u_9(k)$ represents the water diversion from Acheloos basin to Thessalia; $u_{10}(k)$ is the pumping volume from downstream of Mouzaki; and finally N is the control horizon in month. The characteristics of the inflow volumes, evaporation rates, area versus storage functions, reservoir losses, and of the planned diversion have been described in the previous chapter.

Storage and release variables are constrained to be within certain ranges as follows:

$$
\begin{aligned}
S_i^{\min}(k) \le S_i(k) \le S_i^{\max}(k) \ , \\
u_i^{\min}(k) \le u_i(k) \le u_i^{\max}(k) \ , \\
k = 0,1,...,N \ .
\end{aligned}
\tag{3.2}
$$

The upper and lower storage limits in (3.2) correspond to the reservoir conservation storage zones reported in the previous chapter. (Flood storage is not included in the controllable storage range because the study uses a monthly time discretization.) The lower release limit are constrained by the environmental and water supply requirements. The environmental requirements are constant through out the year while the water supply requirements are change seasonally. The releases are constrained by irrigation and environmental requirements which are discussed in the previous chapter (Table 2.5). The planned water diversion is 600 million cubic meters per year allocated according to the irrigation distribution. The difference of $u_8(k)$ and $u_9(k)$ is constrained by this distribution. The upper release bounds are determined based on the hydro plant capacity and the specific power generation curve (reported in Chapter 2 and Appendix A).

In view of the inflow uncertainty, storage constraints are more properly expressed in a probabilistic form:

$$
\begin{aligned}
Prob[S_i^{\min}(k) \le S_i(k)] \le \pi_i^{\min}(k) \\
Prob[S_i(k) \le S_i^{\max}(k)] \ge \pi_i^{\max}(k) \\
i = 1,2,...,7, \quad k = 0,1,...,N,
\end{aligned}
\tag{3.3}
$$

where $\pi^{\min}$ and $\pi^{\max}$ are reliability levels. These levels as well as the upper and lower storage and release thresholds are denoted here as time-varying, but are usually time-invariant.

Equations (3.1), (3.2), and (3.3) summarize the reservoir system model. In control systems terminology, reservoir storages are the state variables, and releases are the control variables. The goal of the control procedure is to identify the release sequences $\{u_i^*(k), i=1,2,...10; k=0,1,...,N-1\}$ such that system objectives and constraints are met successfully. The element of the formulation that brings this about and also measures the success of the various

operational alternatives is the performance index which we discuss next.

3.1.2 Performance Index

The goal of the control procedure is to maximize the benefit of the whole reservoir system, while meeting its environmental and water supply demands. To achieve this objective, we minimize the following performance index:

$$J = E\{\sum_{k=0}^{N-1}[\alpha\ P_{eng}(u(k),S(k)) + \beta P_h(S(k))] + \gamma P_h(S(N))\}, \tag{3.4}$$

where

$$\begin{aligned} P_{eng}(u(k),S(k)) = &-\lambda_p\{\sum_{i=1}^{7} E_{pi}(u_i(k),S_i(k)) + E_{p8}(u_8(k),S_2(k))\} \\ &-\lambda_s\{\sum_{i=1}^{7} E_{si}(u_i(k),S_i(k)) + E_{s8}(u_8(k),S_2(k)) - E_{s9}(u_9(k),S_2(k)) - E_{s10}(u_{10}(k),S_7(k))\}, \end{aligned} \tag{3.5}$$

and

$$P_h(S(k)) = \sum_{i=1}^{7} P_{hi}(S_i(k))$$

$$P_{hi}(k) = \begin{cases} (H_i(S_i(k)) - H_i^{\min}(k))^2, & H_i(S_i(k)) < H_i^{\min}(k) \\ (H_i(S_i(k)) - H_i^{\max}(k))^2, & H_i(S_i(k)) > H_i^{\max}(k) \\ 0, \quad \textit{otherwise} \end{cases} \tag{3.6}$$

In (3.4), E{ } denotes expectation of the quantity in the brackets with respect to the joint probability distribution of the reservoir inflows. This expectation is simplified by the fact that reservoir inflows exhibit only weak autocorrelation and can, therefore, be assumed to be statistically independent. There are two terms in the performance index, the first term represents the penalty for the energy value generated from all power facilities in the system including the

pumping stations. The energy generation consists of two parts: primary and secondary, with different prices. Primary energy is the energy generated during the peak hours of a day. The peak time is assumed to be 6 hours a day in this study. It is also assumed that the power facility will always generate energy during the peak time first, then use the off peak hours. The energy price is 11.5 dr/KWH for the peak hours (λ_p) and 6 or 8 dr/KWH for the off peak time (λ_s). The pump station can be operated in either a generation mode or a pumping mode. When at pumping mode, it always consumes secondary energy. The power functions for all facilities are discussed in the previous chapter. The negative signs in (3.5) implement a minimum objective.

The performance index should also include the benefit from irrigation. However, since we do not have information on whether water supply in excess of irrigation demand generates benefit, the irrigation benefit is limited by the irrigation demand, and the optimization results are not affected by the irrigation term. However, if the penalty or loss functions for not meeting the irrigation are known, then the performance index should include the irrigation benefit (loss) term.

The second term is intended to keep reservoir elevations within their respective bounds, $[H^{min}, H^{max}]$. As shown in (3.6), if reservoir elevation is outside its bounds, a quadratic penalty term is imposed.

Penalty parameters α, β, and γ are used to introduce priorities in the performance index terms. In this case, these parameters should be determined such that the second term is dominant. The logic is to determine feasible sequences (2nd term) guaranteed to maximize the energy values (1st term).

3.2 Modified DP Method

The control problem formulated in the previous section poses a challenge because of its large size. It can be solved using techniques such as the Extended Linear Quadratic Gaussian (ELQG) control method [*Georgakakos et al., 1997a,b,c]* ,and Dynamic Programming. ELQG is an iterative optimization procedure and computationally efficient, and especially-suited for uncertain multi reservoir systems. However, it requires strict conditions for the objective functions. Moreover, it is difficult to deal with complicate state and control constraints. On the other hand, Dynamic Programming is a very general optimization tool. It has no strict

requirements on the format of the objective function, and can handle any type of constraints. However, the "curse of dimensionality" is always the major obstacle preventing DP' s application to large systems.

In this work, we introduce a new procedure designed to optimize large reservoir systems based on the traditional DP. The idea of this approach is based on the fact that all reservoirs within a certain group are generally regulated uniformly. This means that if the operation rules of some dominant reservoirs are specified, the operation modes for the others can be determined accordingly. The dominant reservoirs are usually the large reservoirs in the system and are called primary reservoirs. The other reservoirs are small and are called secondary reservoirs.

With the help of classification of primary and secondary reservoirs, the dimension of the system is reduced to the number of primary reservoirs. The optimization is carried out on the primary reservoirs, with the operation of the secondary reservoirs determined based on the optimal results of the primary reservoirs.

Two issues need to be addressed in this new procedure: (1) classification of primary and secondary reservoirs and (2) relationship between the primary and the secondary reservoirs. There are no strict rules to assign a reservoir to which category. In fact, this classification is purely a mathematical simplification of the original system. The number of primary reservoirs should be selected first. This number depends on the computational power. Based on our experience thus far, 5 seems to be appropriate. As the computational power increases, more primary reservoirs can be included. An intuitive selection for primary reservoirs is one or two largest reservoirs on the same river. For this system, Sykia, Kremasta, and Mouzaki are assigned as primary reservoirs. The rest are assigned as secondary reservoirs. The classification of the reservoirs is labeled by the following vector:

$$NP = [NP_i] = [\ 0,\ \ 1,\ \ 1,\ \ 0,\ \ 0,\ \ 0,\ \ 1] \tag{3.7}$$

A value of "1" for NP_i indicates a primary reservoir, while a value of "0" indicates a secondary reservoir. This classification will split the state vector and control vector into two sub-vectors as

below:

$$S = [S_i] = [S_p,\ S_s]$$
$$S_p = [S_2,\ S_3,\ S_7],\quad S_s = [S_1,\ S_4,\ S_5,\ S_6] \tag{3.8}$$

$$u = [u_i] = [u_p,\ u_s]$$
$$u_p = [u_2,\ u_3,\ u_7,\ u_8,\ u_9],\quad u_s = [u_1,\ u_4,\ u_5,\ u_6] \tag{3.9}$$

More details on this new implementation of D.P. will be published elsewhere.

CHAPTER 4

CASE STUDIES

4.1 Control Experiments

In this section, we present some results of the control model. This sample run applies to the case of no pumping operation. The minimal water diversion of 600 x 10^6 m^3 is apportioned monthly according to the percentages reported in Chapter 2. The length of the control horizon is 12 months starting October 1st. The objective is to maximize the system benefit (total energy value) without violating the elevation and release bounds with reliability of more than 95% for the time. The minimum release from Stratos (for irrigation and environmental preservation) is 147 million cubic meters per month for May through September and 55.2 million cubic meters per month for the rest of the year. At the beginning of October, the water elevation is arbitrarily set at 765 meters at Mesohora, 540 meters at Sykia, 250 meter at Kremasta, 143 meters at Kastraki, 68 meters at Stratos, 335 meters at Pyli, and 270 meters at Mouzaki. Inflow forecasts are generated from a corridor model which generates 20 equally likely inflow traces for each reservoir. This model uses the values of the past three month inflows to select historical inflow traces that resemble the current hydrologic situation the most (in a Euclidian norm sense). All such traces then constitute the forecast ensemble.

Figures 4.1.1 through 4.1.14 show the results of this control model run. The figures respectively depict the traces of reservoir elevation, forecasted inflow, optimal releases, and the associated primary and secondary energy generation amounts. The elevation traces fully satisfy the reliability constraints. As allowed at the 95% reliability level, only one trace for Sykia and one for Stratos fall below the lower bounds. The water diversion traces (releases from Pefkofito) are shown in Figure 4.1.14. All traces are above the 600 mcm constraint (which is represented by the thick line in the figure). The irrigation requirements for Stratos are always met.

Table 4.1.1 includes a summary of the expected annual energy generation and its value by reservoir and for the entire system. The energy values are estimated based on a price of 11.5

dr/KWH for the primary energy and 6 dr/KWH for the secondary energy.

Table 4.1.1: Annual Expected Energy Statistics

	Expected Primary Energy / Value GWH / 10^6 drachma	Expected Secondary Energy / Value GWH/10^6 drachma	Expected Total Energy / Value GWH /10^6 drachma
Mesohora	278.6 / 3204	112.9 / 677	391.5 / 3881
Sykia	144.2 / 1658	128.2 / 769	272.3 / 2427
Kremasta	414.6 / 4768	58.0/ 348	472.6 / 5116
Kastraki	264.5 / 3042	72.5 / 435	336.9 / 3476
Stratos	158.5 / 1823	15.6 / 94	174.1 / 1917
Mouzaki	274.4 / 3156	20.8 / 125	295.3 / 3281
Pefkofito	291.4 / 3351	187.5 / 1125	479.0 / 4477
Total	1826.3 / 21002	595.4 / 3573	2421.7 / 24575

Figures 4.1.15 through 4.1.22 depict the exceedance probability curves for the annual values of primary energy, secondary energy, and energy values. These curves indicate the ability of the control model to fully assess the variability of the system outputs.

In the following section, the control model will be used in sequential control-simulation experiments to assess the impacts of the proposed water diversion.

4.2 Control-Simulation Experiments

In this section, we describe some tentative model runs in a control-simulation framework. The purpose of the control-simulation experiments is to quantify the performance of the system under different scenarios and with the guidance of the control model. The runs described herein are for demonstration purposes. More comprehensive scenarios will be tested at the next project phase.

The basis for the experiments presented herein is the 30-year long monthly historical inflow record (1961-1991) which is shown on Figures 4.2.1, 4.2.2, and 4.2.3. The control-simulation process is as follows: For each month of the historical record, the control model is activated first to generate the optimal reservoir release sequences. The control model is implemented with a 95% reliability for reservoir elevation constraint violations, 12-month control horizon, and inflow forecasts generated by the corridor forecasting model. The values of the initial reservoir elevations of each month are determined based on the results of the previous step. From the 12-month optimal release sequences, only the first month' s optimal releases are actually implemented, and the system response is simulated using the historically observed inflows. If the optimal releases result in feasible end-of-the-month reservoir elevations, the program completes this control-simulation step, records these elevations along with the releases and the energy generation amounts, and repeats this process at the next month. Otherwise, appropriate release adjustments are made so that all reservoirs stay within their feasible ranges. This control-simulation process is repeated for 360 (= 36 x 12) months and results in a long series of simulated reservoir elevations, releases, and energy generation amounts. This data series is then analyzed to develop statistics of system performance and make comparisons.

The first control-simulation experiment corresponds to the base case scenario with zero diversion and only three active reservoirs: Kremasta, Kastraki, and Stratos. The purpose of this simulation is to establish a baseline performance of the existing system. In this scenario, the inflows of Kremasta include all upstream local flows, i.e., local flows of Mesohora and Sykia. The simulated sequences of reservoir elevation, release, and energy generation are plotted in Figures 4.2.4 to 4.2.6. The release from Stratos meets the irrigation and environmental flow requirements *all* of the time. The primary and secondary energy generation are 1201 and 906 GWH,

respectively, for a total of 2107 GWH. The value of annual energy generation is 19248 million drachma, assuming that primary energy is valued at 11.5 dr/KWH, and the secondary energy at 6 dr/KWH.

The second experiment corresponds to a scenario where the entire reservoir system is operational, but without the possibility of pump-back operations. Namely, the pumping function at Pefkofito and Mouzaki is inactivated. The minimum water diversion is 600 million cubic meters per year. This volume is seasonally distributed according to Table 2.6. Depending on the hydrologic circumstances and the efficiency of the power facilities, the water transferred to Thessalia may exceed 600 mcm. The simulation sequences of all reservoirs are shown in Figures 4.2.7 to 4.2.14. The total annual system energy is 3097 GWH, of which 2014 GWH are primary energy and 1083 are secondary. Of the total energy generation, 2643 GWH is generated from the Acheloos system (Mesohora, Sykia, Kremasta, Kastraki, and Stratos). The total expected value of annual energy generation in this case is 29659 million drachma, which is 54% higher than the baseline scenario. The water actually diverted amounts to an average of 837 mcm per year. Water in excess of 600 mcm per year is diverted due to the high generation efficiency and value of power at Pefkofito. Again, the release requirements for irrigation and the environment are met *throughout* the simulation horizon.

In this case, the annual energy generation from Kremasta, Kastraki, and Stratos is reduced to 1766 GWH (as compared to 2107 GWH of the baseline scenario), of which 1098 GWH represent primary energy and 678 GWH represent secondary energy. Namely, the diversion results in a 16% decrease in average energy generation from these three reservoirs. The value of this energy generation is 16695 million drachma which represents a 13% reduction relative to the baseline scenario.

The third experiment has the same system configuration as the second, but includes pumping. The option to pump is decided by the control model based on the potential gains that may result from the relative difference between on- and off-peak energy pricing and the efficiency of the power facilities. Two runs with different off-peak energy prices (6 and 8 dr/KWH) are conducted. For the case of 6 dr/KWH off-peak energy, Pefkofito operates in a pumping mode *throughout* the simulation horizon, while Mouzaki never pumps. The total annual energy

generation is 2997 GWH which is a little less than the generation of the previous experiment (3097 GWH). However, primary energy generation amounts to 2216 GWH per year which is higher than the 2014 GWH of the previous case. The resulting annual energy value is increased to 30172 million drachma as compared to 29659 million of the previous run. The increase is approximately 2%. This result indicates that if off-peak energy price is 6 dr/KWH or less, it is beneficial to use off-peak energy to pump water back into Sykia and use it to generate during peak power demand. However, this does not apply to Mouzaki. The corresponding simulated sequences are shown in Figures 4.2.15 to 4.2.23.

The annual energy generation from Kremasta, Kastraki, and Stratos is 1812 GWH, of which 1113 GWH are primary energy and 698 GWH are secondary energy. Namely, in comparison to the second (no-pumping) experiment, this system now produces about 2.6% more energy per year, with a total value of 16988 million drachma. Compared to 16695 million of the second experiment, this represents a 1.8% value increase.

The second run with an off-peak energy price of 8 dr/KWH generates sequences identical to the second (no-pumping) experiment. Namely, both Pefkofito and Mouzaki never operate in a pumping mode. Thus, pumping operation is not profitable at the off-peak price of 8 dr/KWH or higher.

The annual energy generation and simulated diversion of all control-simulation runs are summarized in Table 4.2.1.

Figures 4.2.24 through 4.1.43 depict the exceedance probability curves for the annual values of primary energy, secondary energy, and energy value from the above three experimental runs. Figure 4.2.44 compares the system exceedance probability curves for these three runs. The figure indicates that primary energy output and value increased considerably from the baseline to the other two cases. In addition, pumping produces additional marginal benefits. The distribution of the secondary energy is similar in the first two cases. When pumping becomes an option, part of this energy is used to support the pumping operation.

Table 4.1: Summary Statistics of the Control-Simulation Experiments

	Base Case	**Full System; No Pumping; Off-Peak Price = 6 dr/KWH**	**Full System; Pumping Optional; Off-Peak Price = 6 dr/KWH**
Primary Energy (GWH/y)	1,201	2,014	2,216
Secondary Energy (GWH/y)	906	1,083	781
Total Energy (GWH/y)	2,107	3,097	2,997
Primary Energy Value (10^6 dr/y)	13,815	23,162	25,488
Secondary Energy Value (10^6 dr/y)	5,434	6,497	4,684
Total Energy Value (10^6 dr/y)	19,249	29,659	30,172
Simulated Diversion (10^6 m^3/y)	0	837	821

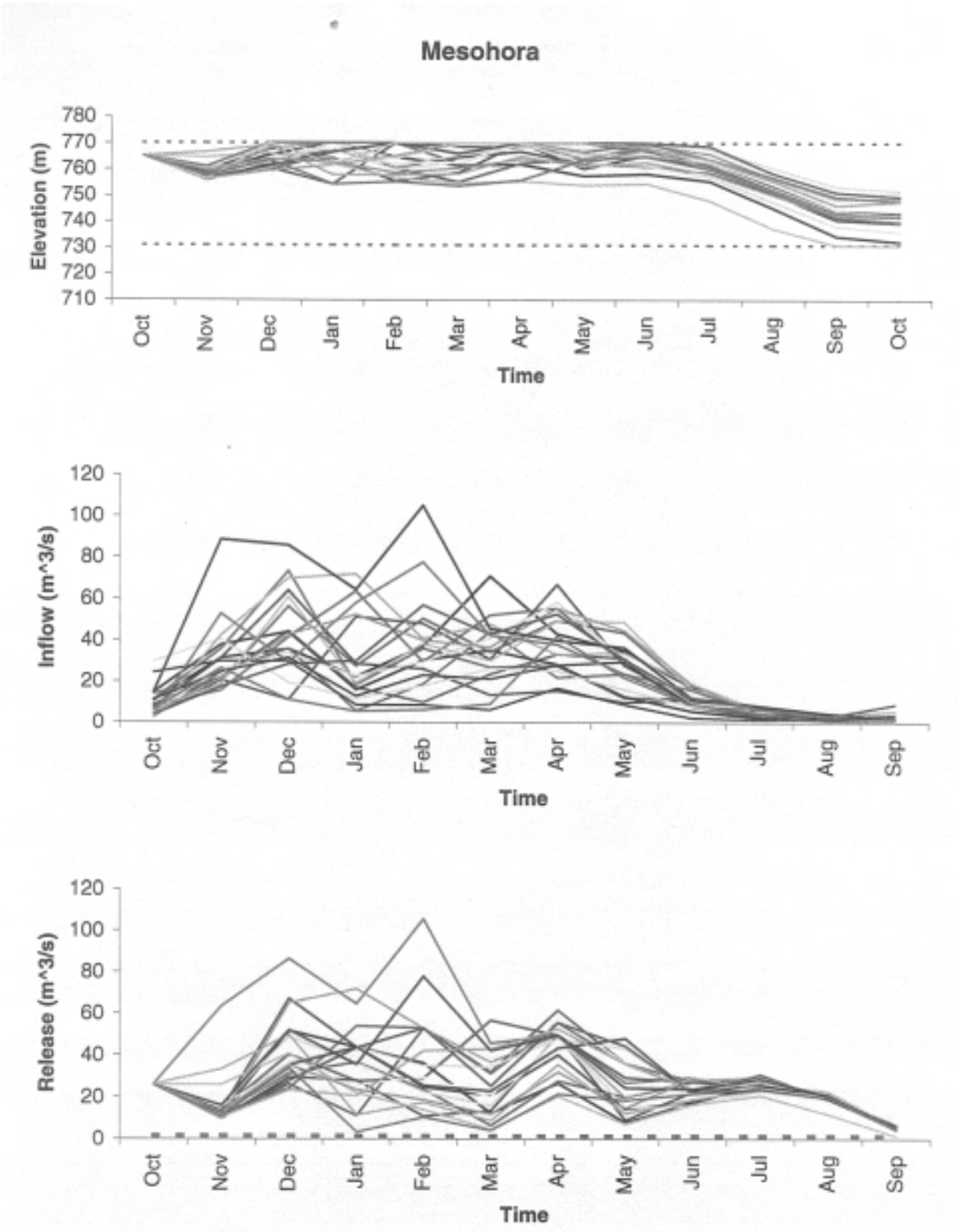

Figure 4.1.1: Mesohora Control Sequences (a)

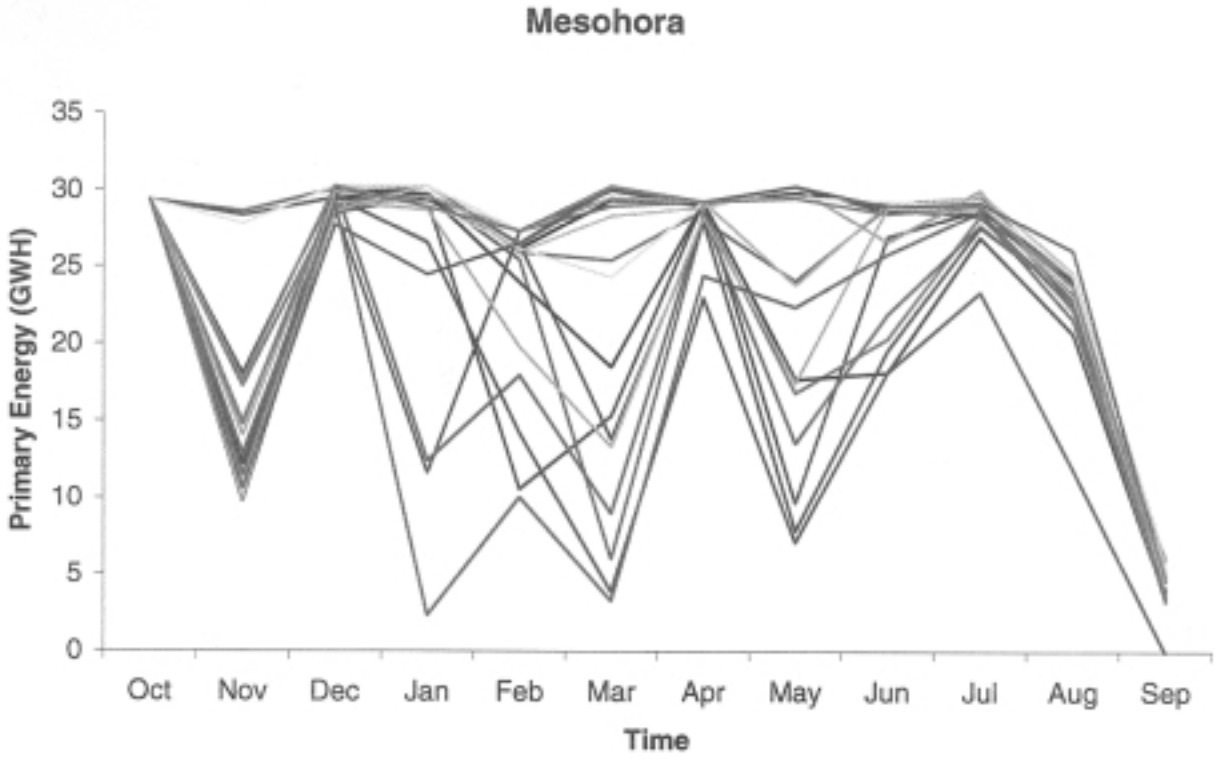

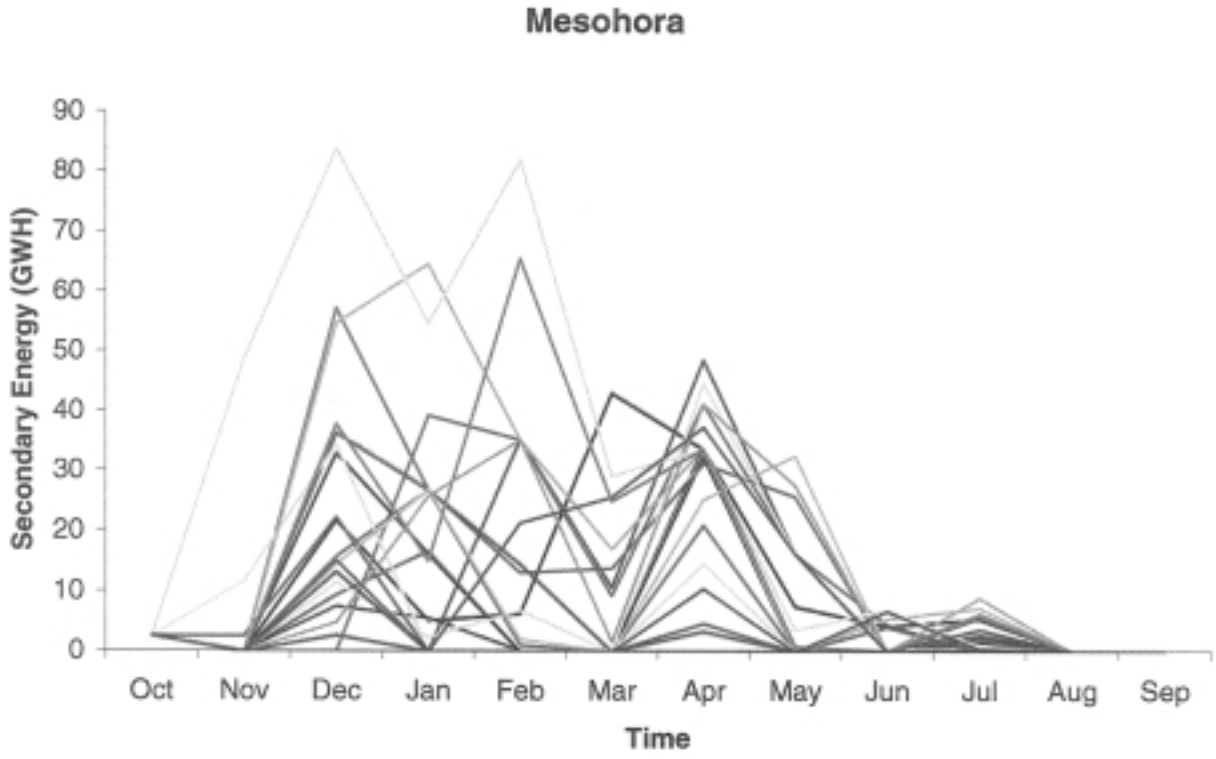

Figure 4.1.2: Mesohora Control Sequences (b)

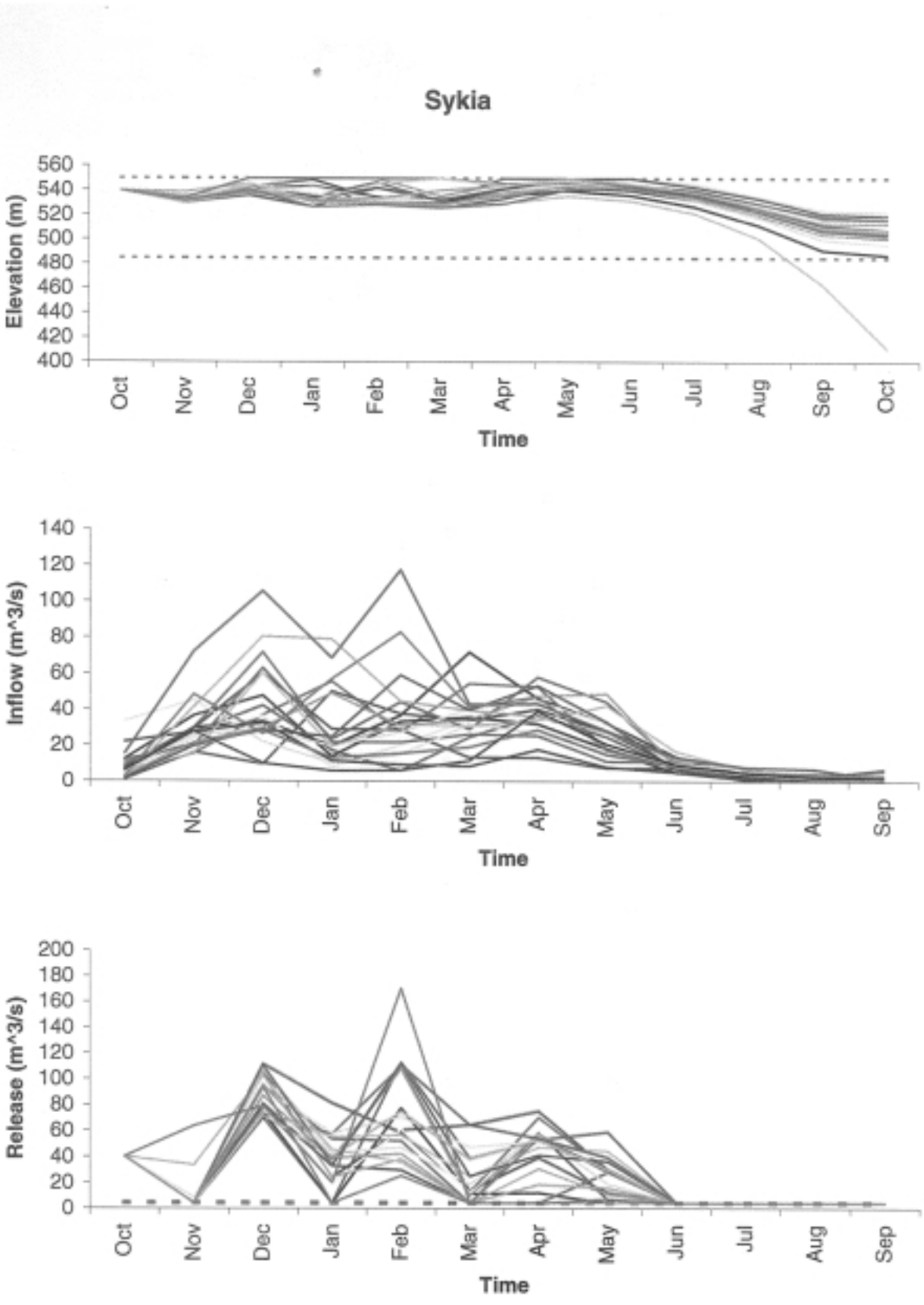

Figure 4.1.3: Sykia Control Sequences (a)

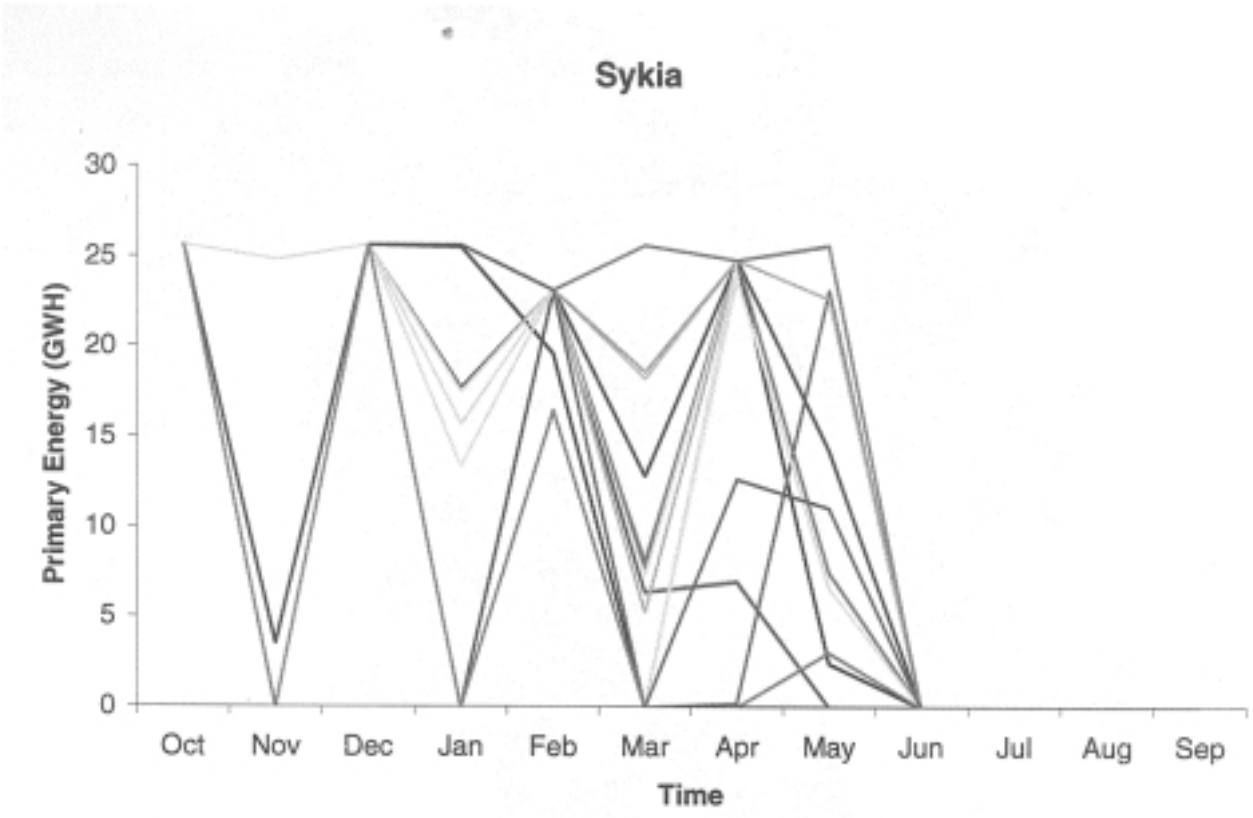

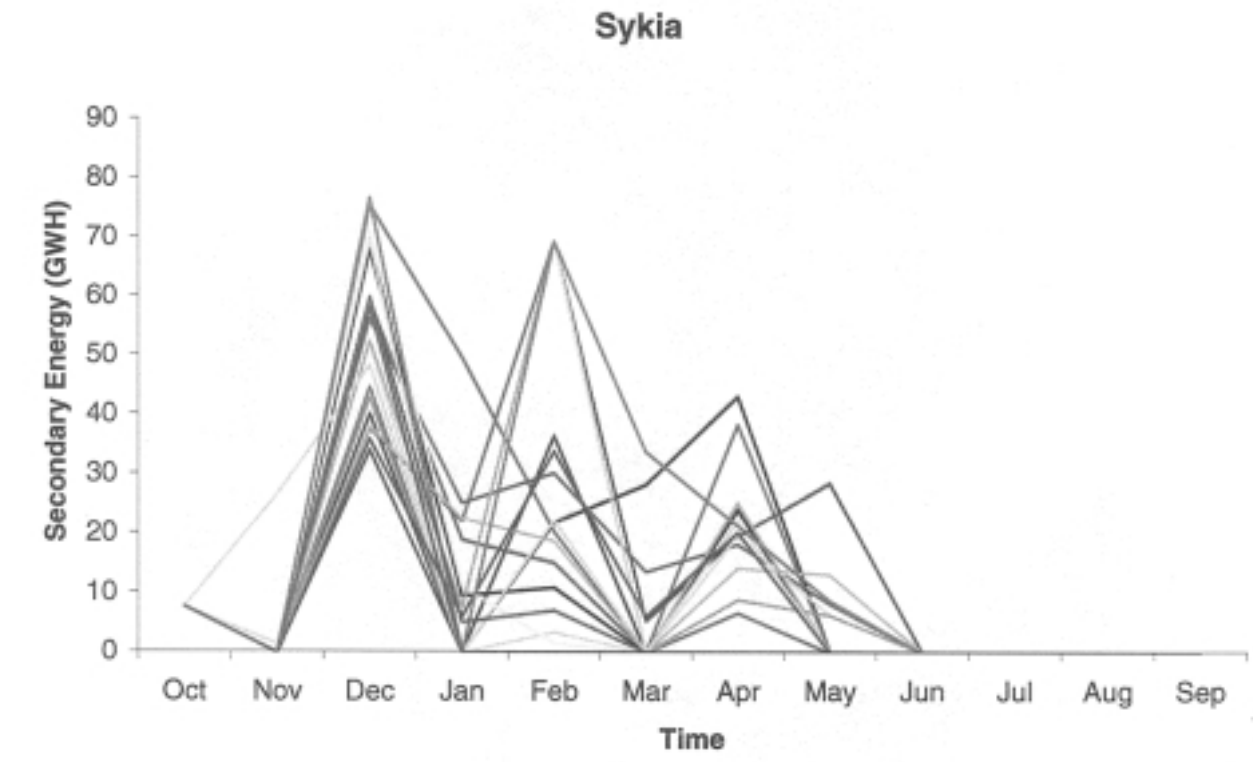

Figure 4.1.4: Sykia Control Sequences (b)

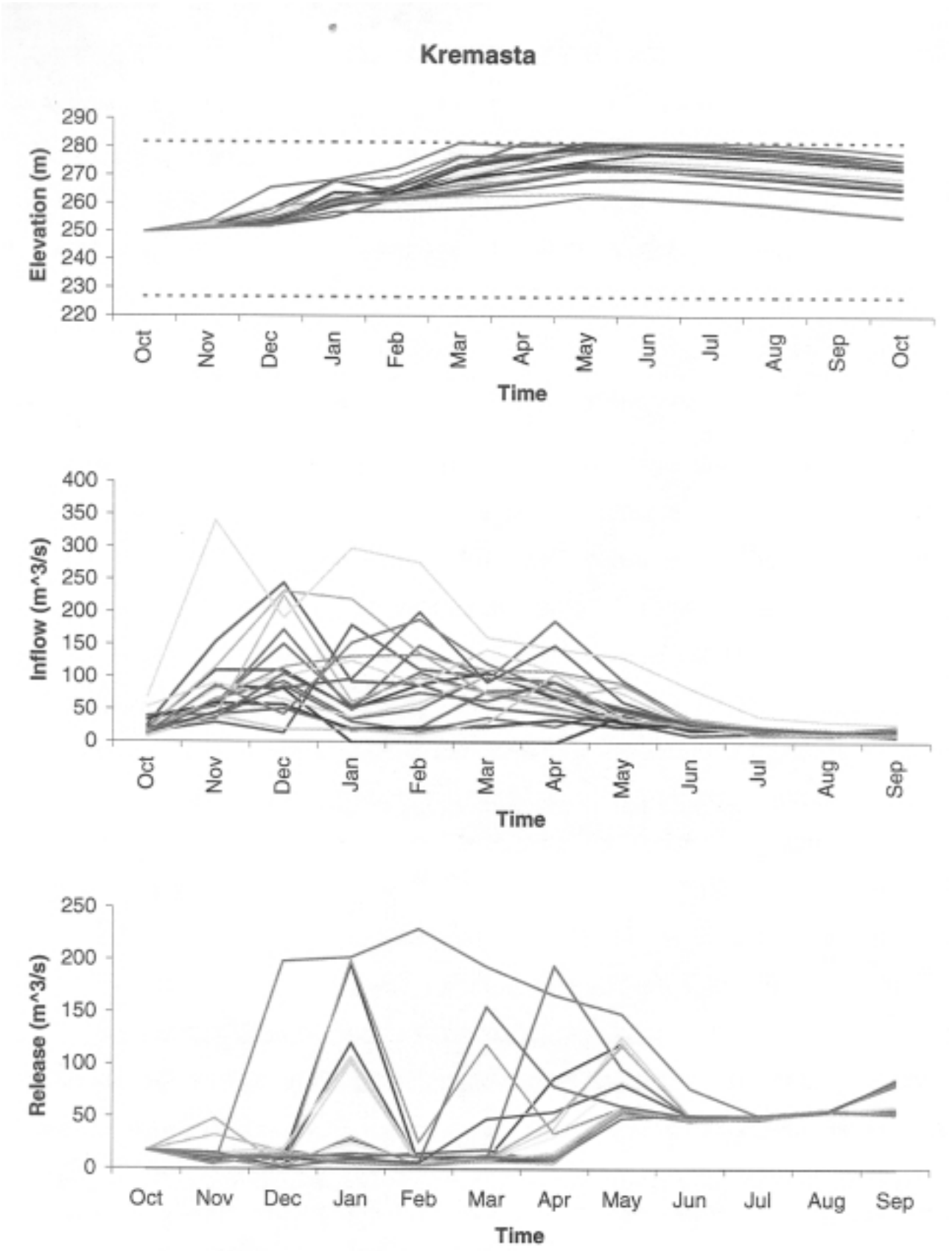

Figure 4.1.5: Kremasta Control Sequences (a)

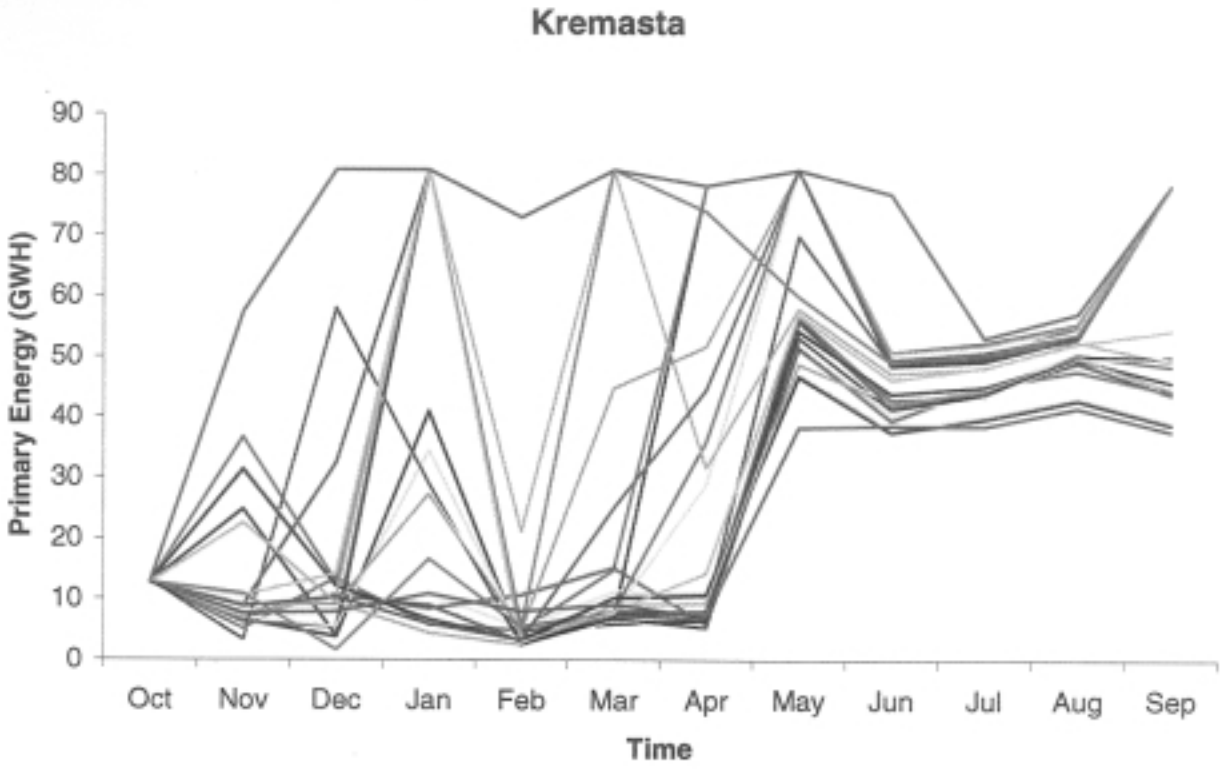

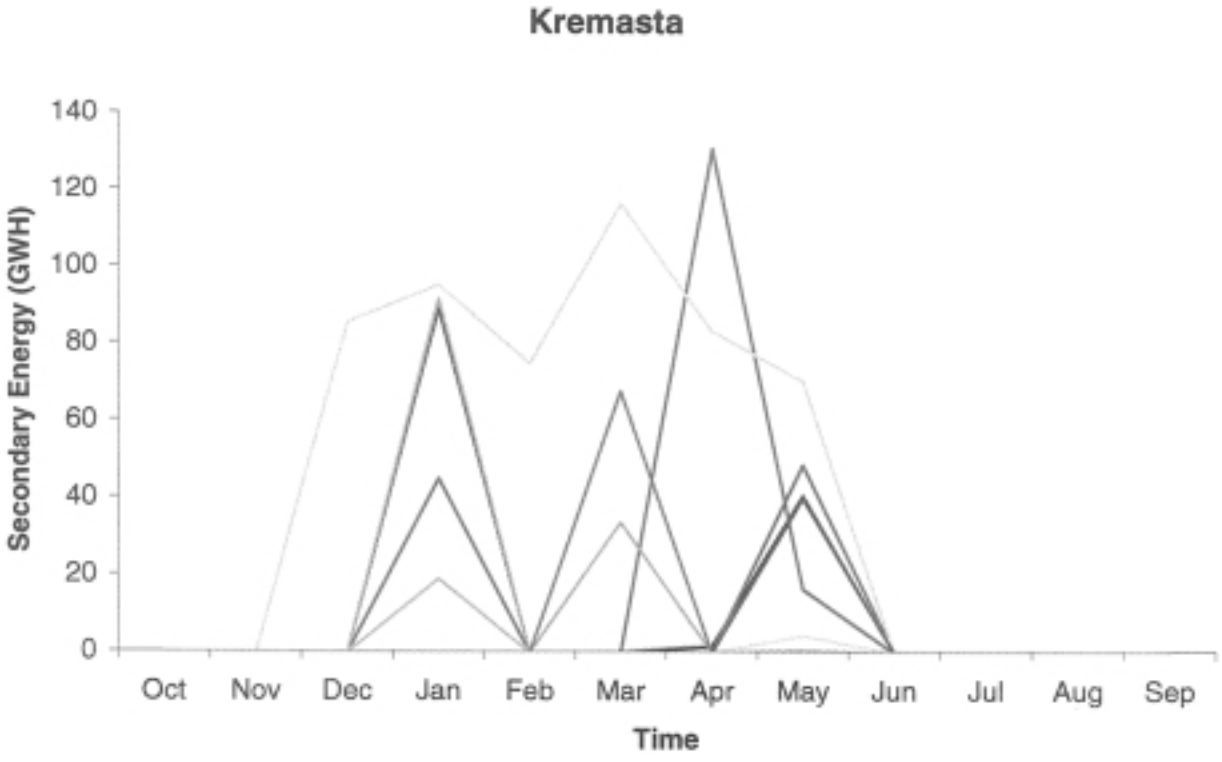

Figure 4.1.6: Kremasta Control Sequences (b)

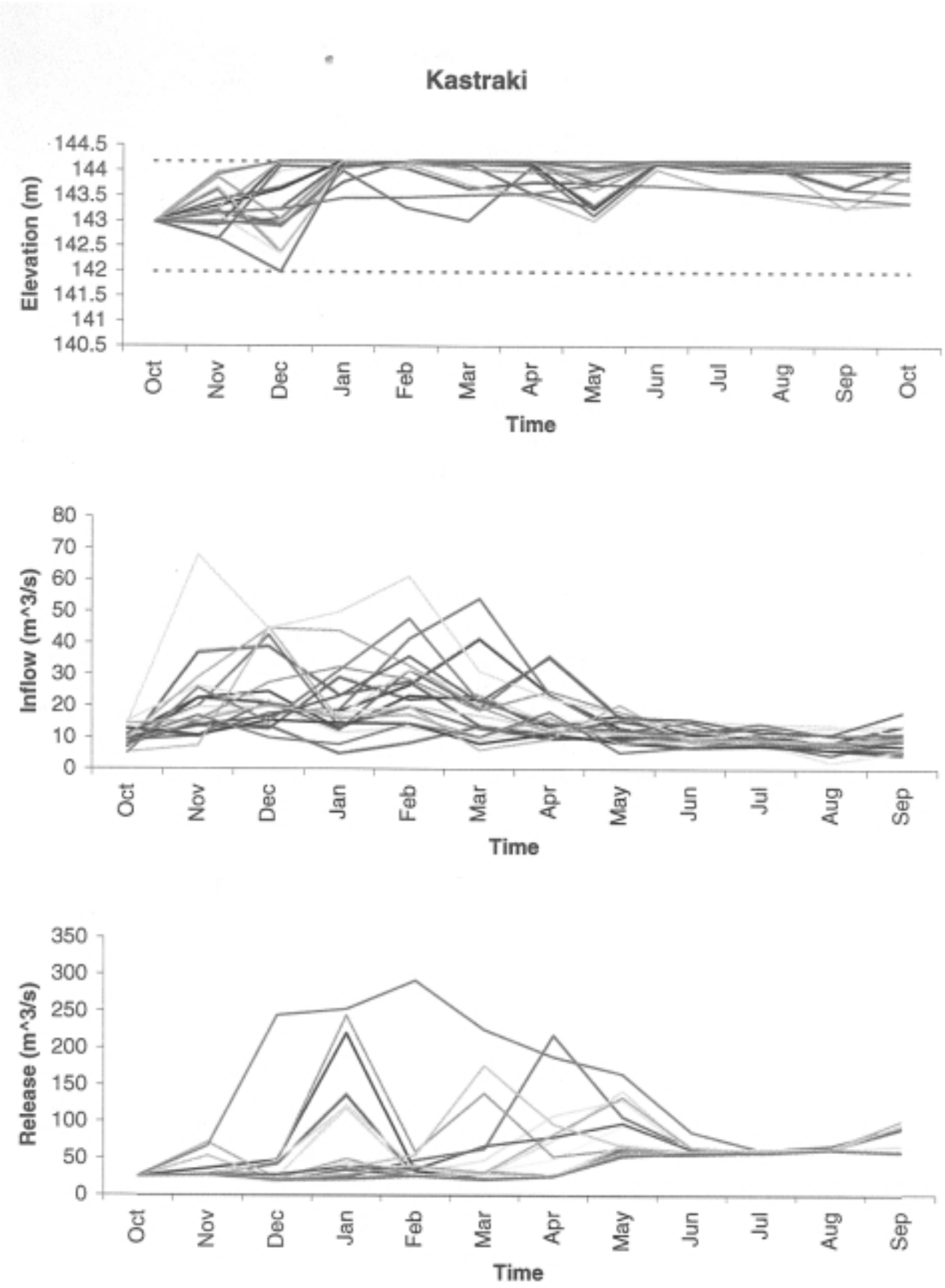

Figure 4.1.7: Kastraki Control Sequences (a)

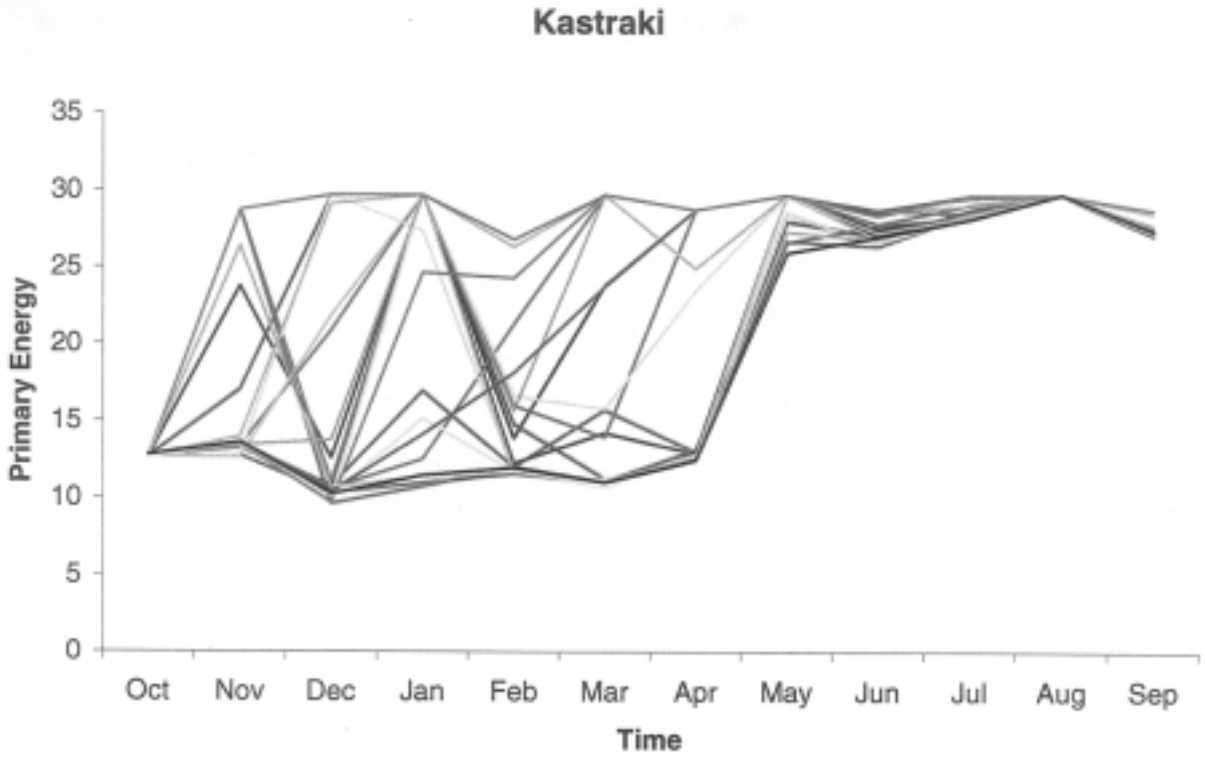

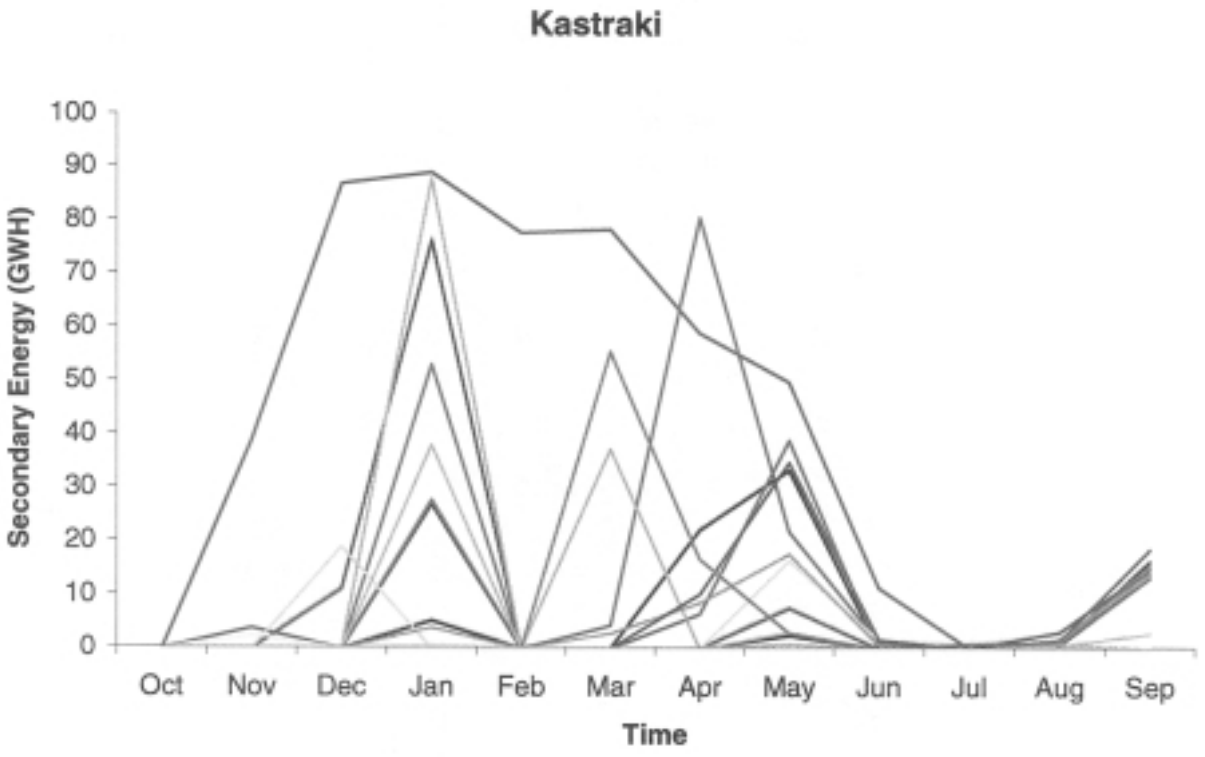

Figure 4.1.8: Kastraki Control Sequences (b)

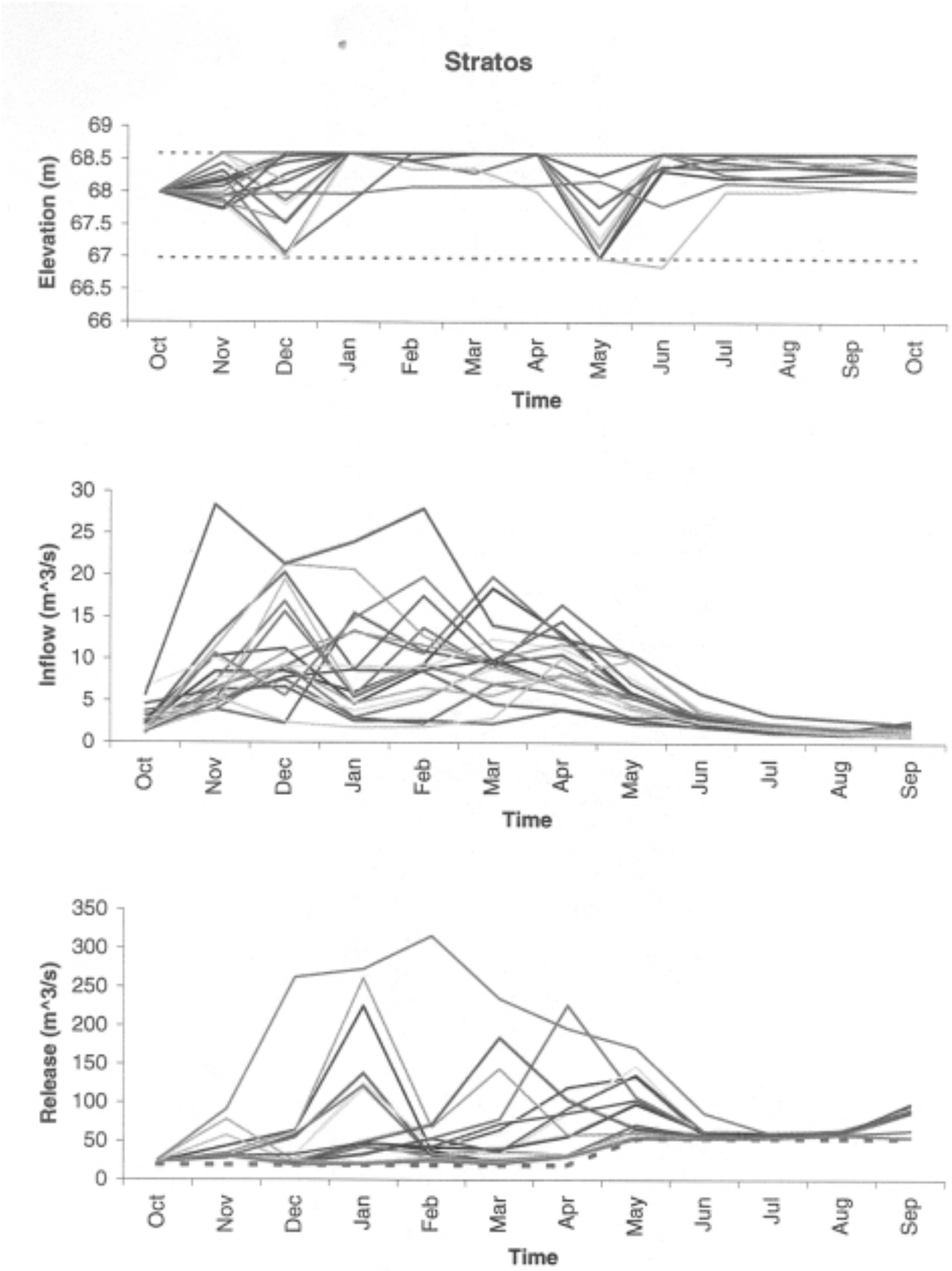

Figure 4.1.9: Stratos Control Sequences (a)

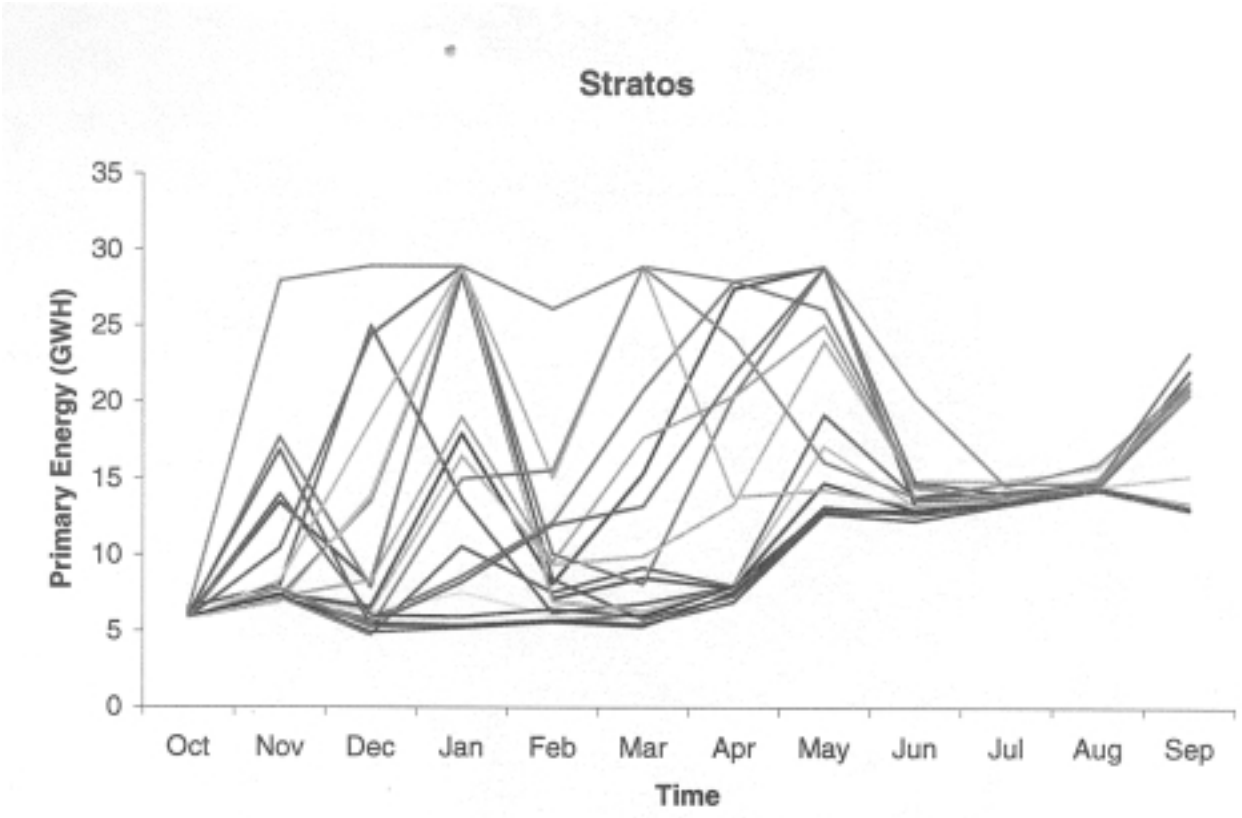

Figure 4.1.10: Stratos Control Sequences (b)

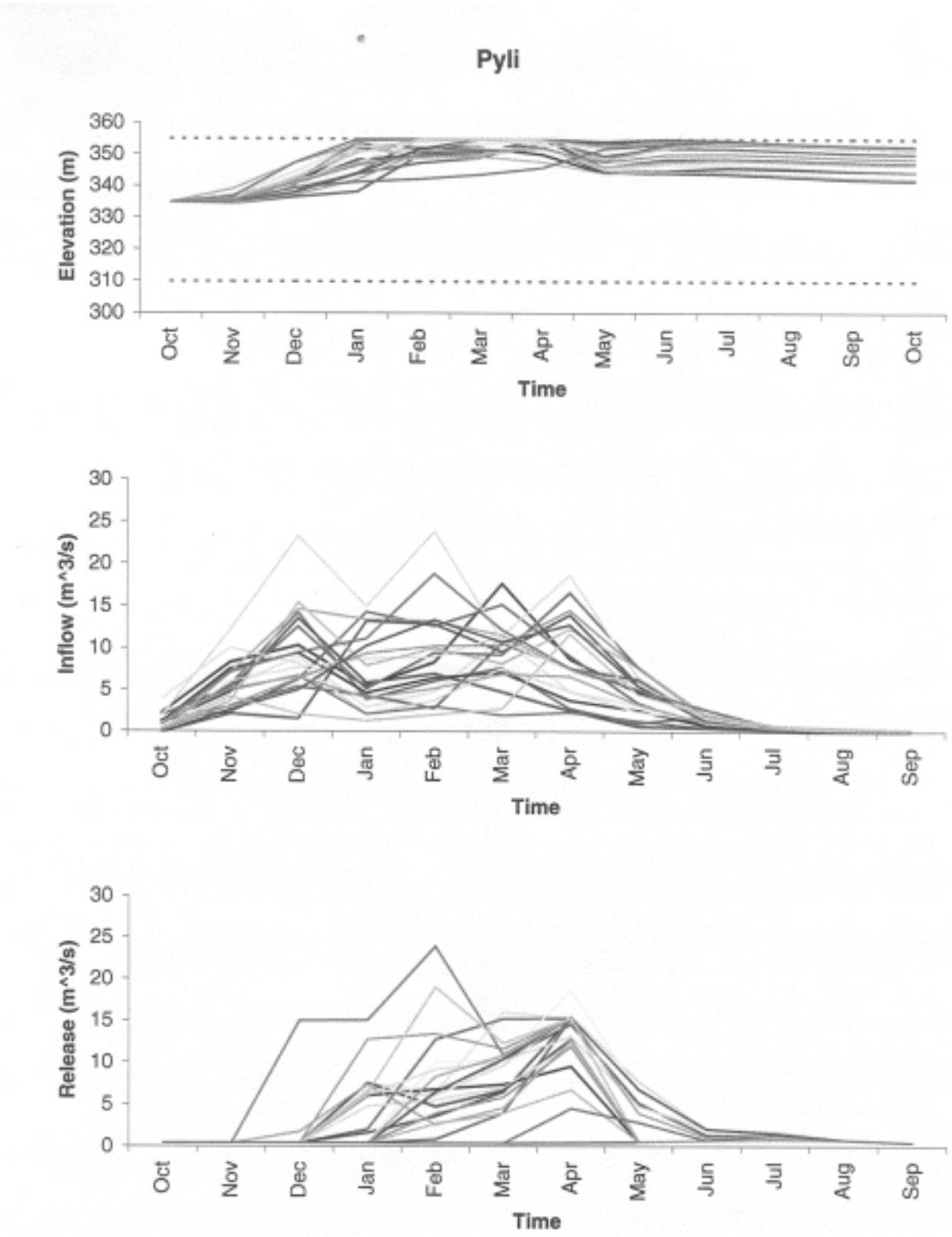

Figure 4.1.11: Pyli Control Sequences

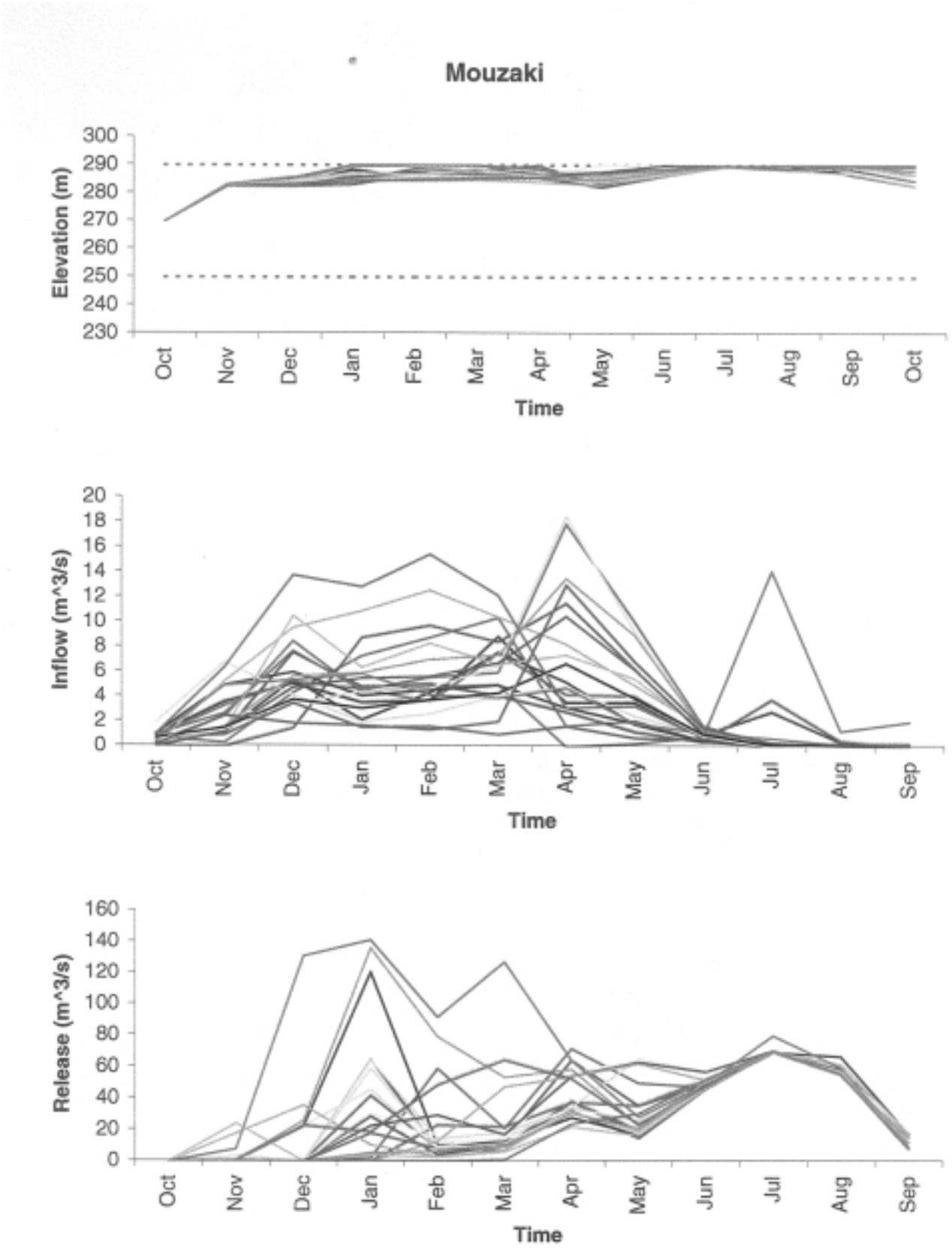

Figure 4.1.12: Mouzaki Control Sequences (a)

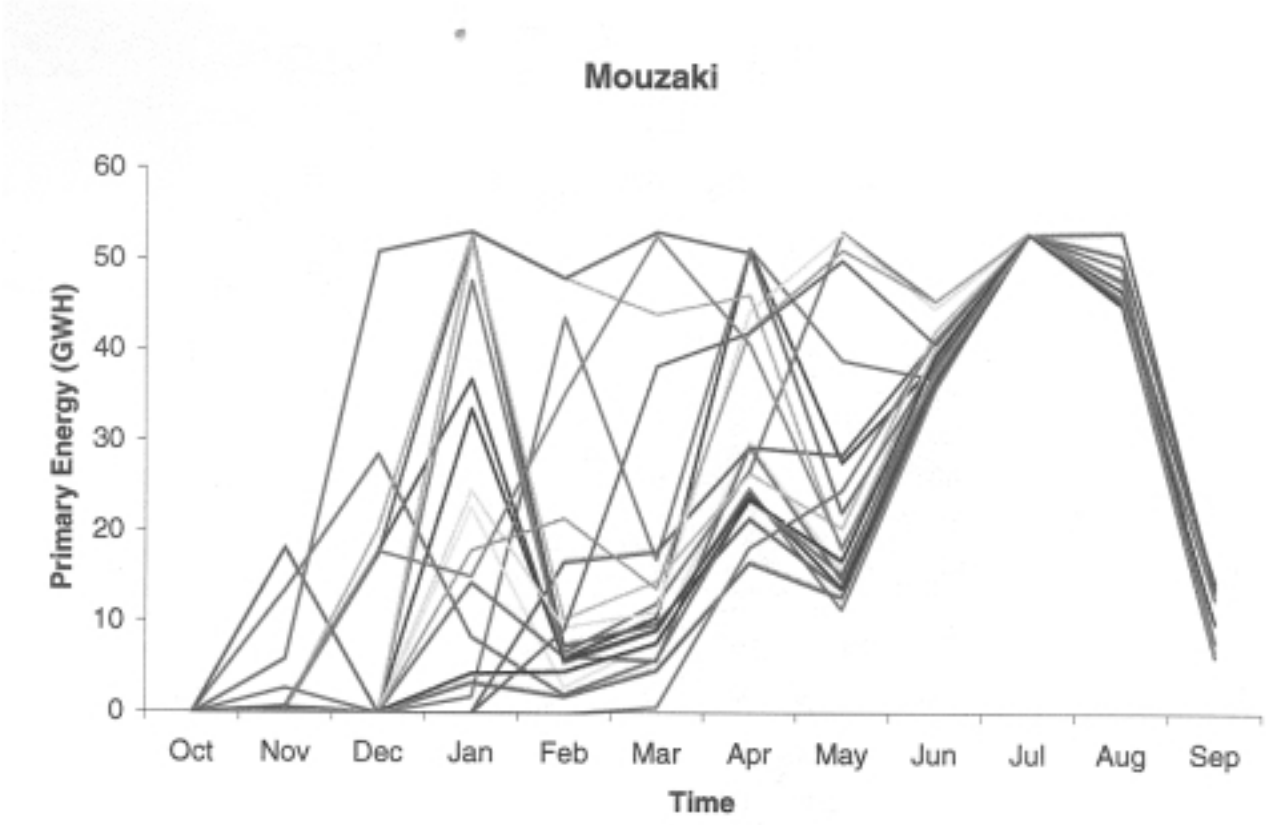

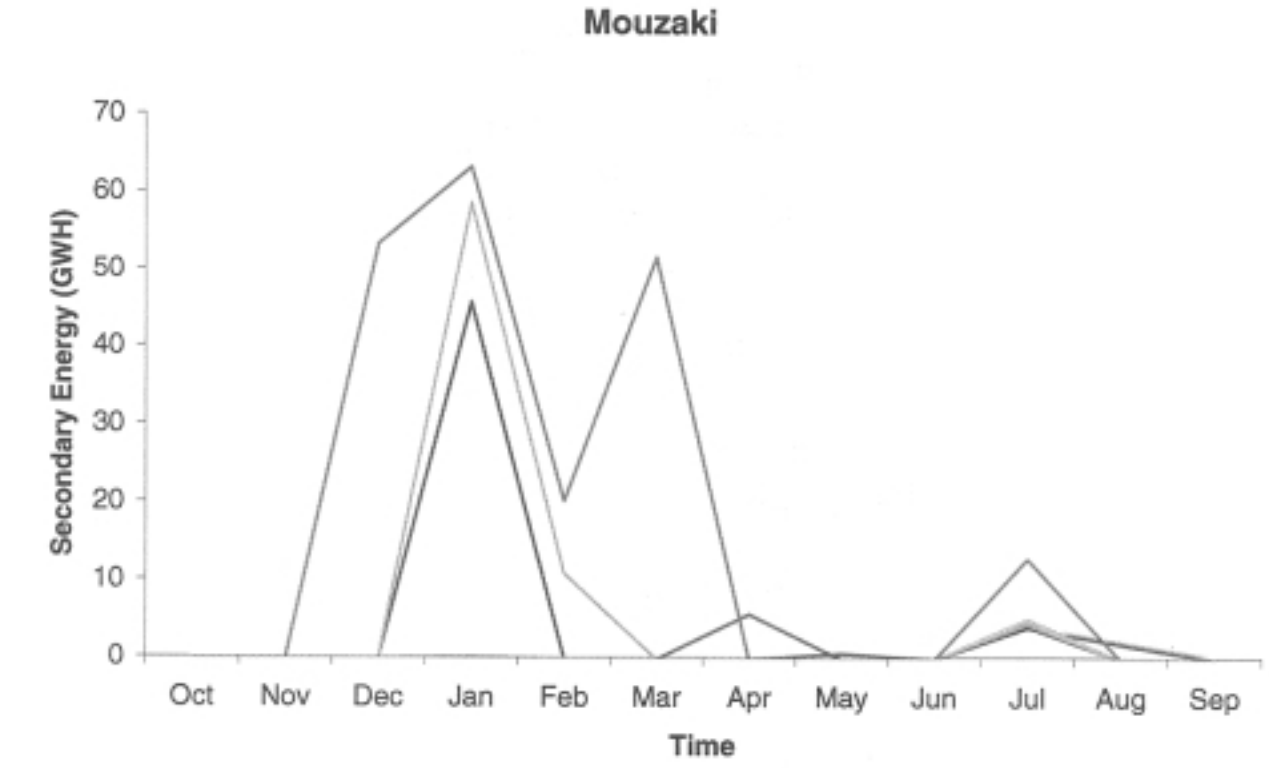

Figure 4.1.13: Mouzaki Control Sequences (b)

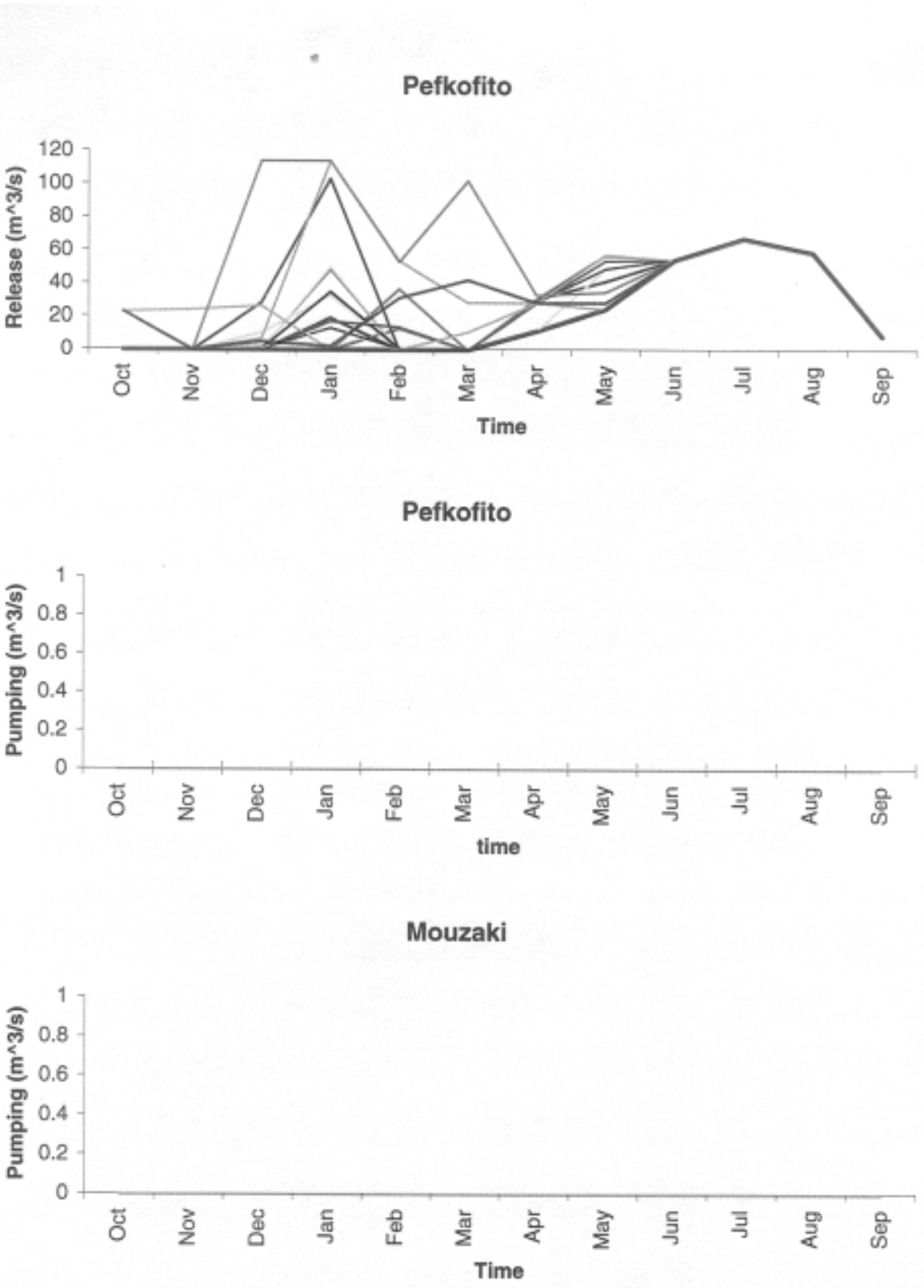

Figure 4.1.14: Pefkofito Control Sequences

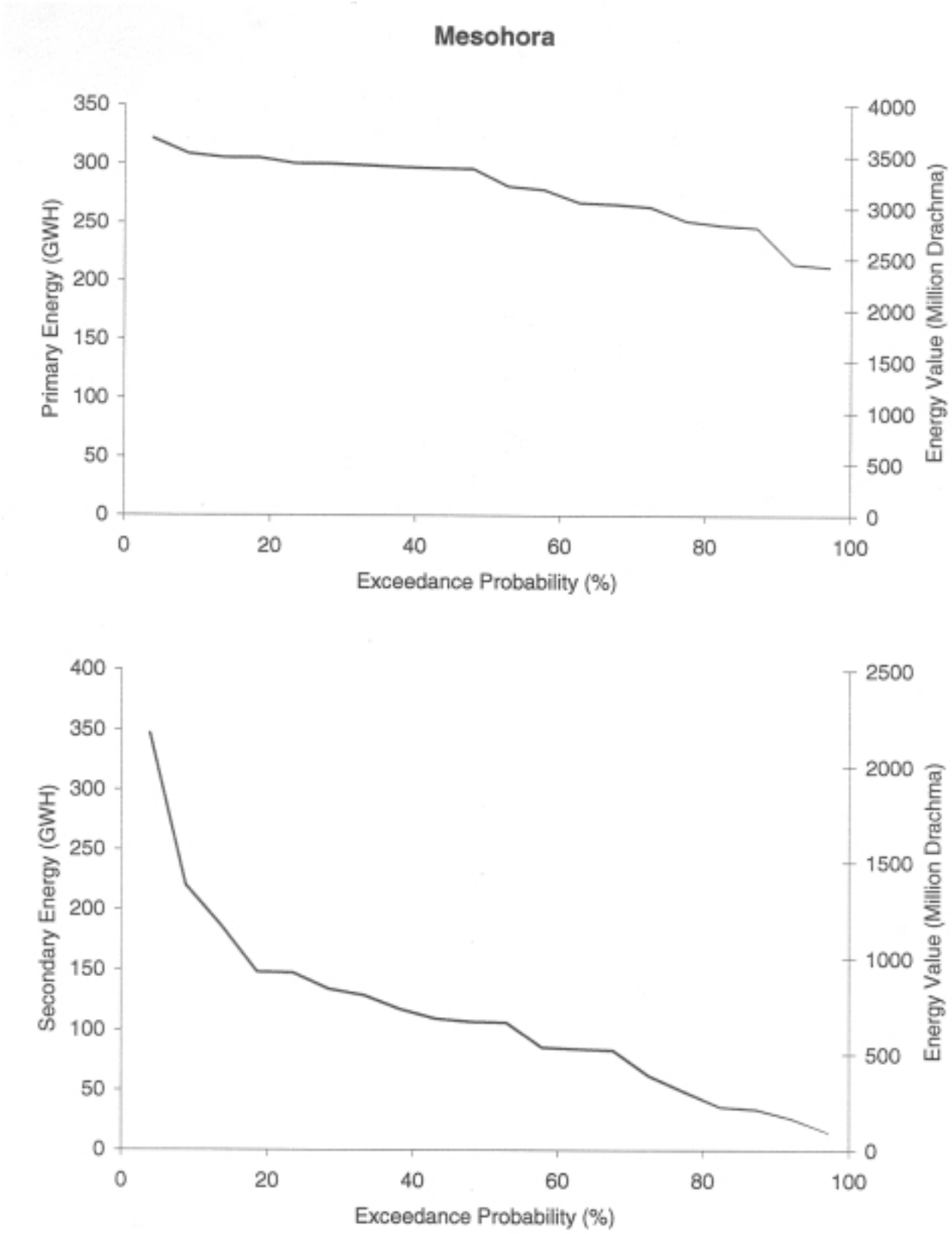

Figure 4.1.15: The exceedance probability curves for Mesohora

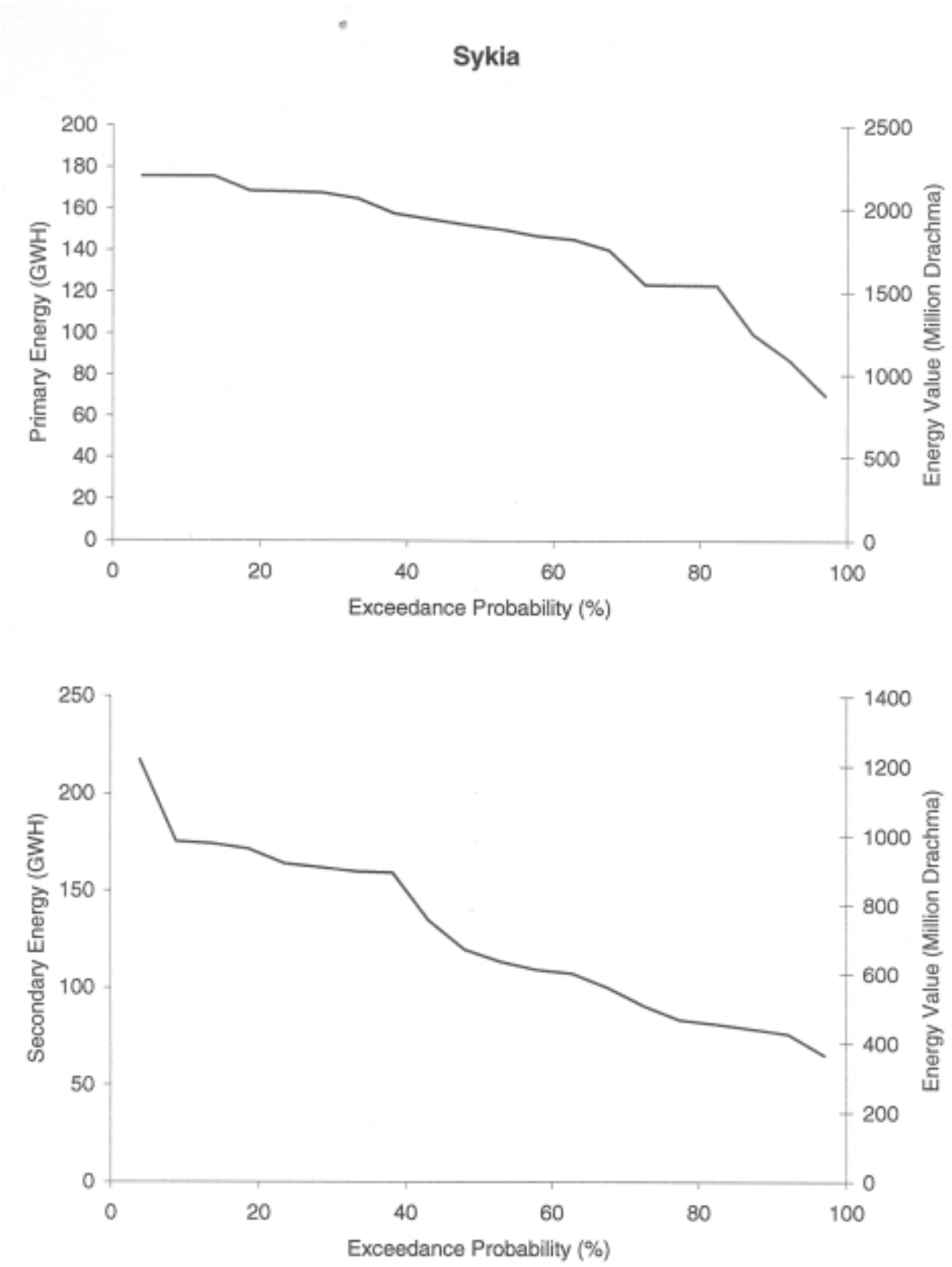

Figure 4.1.16: The exceedance probability curves for Sykia

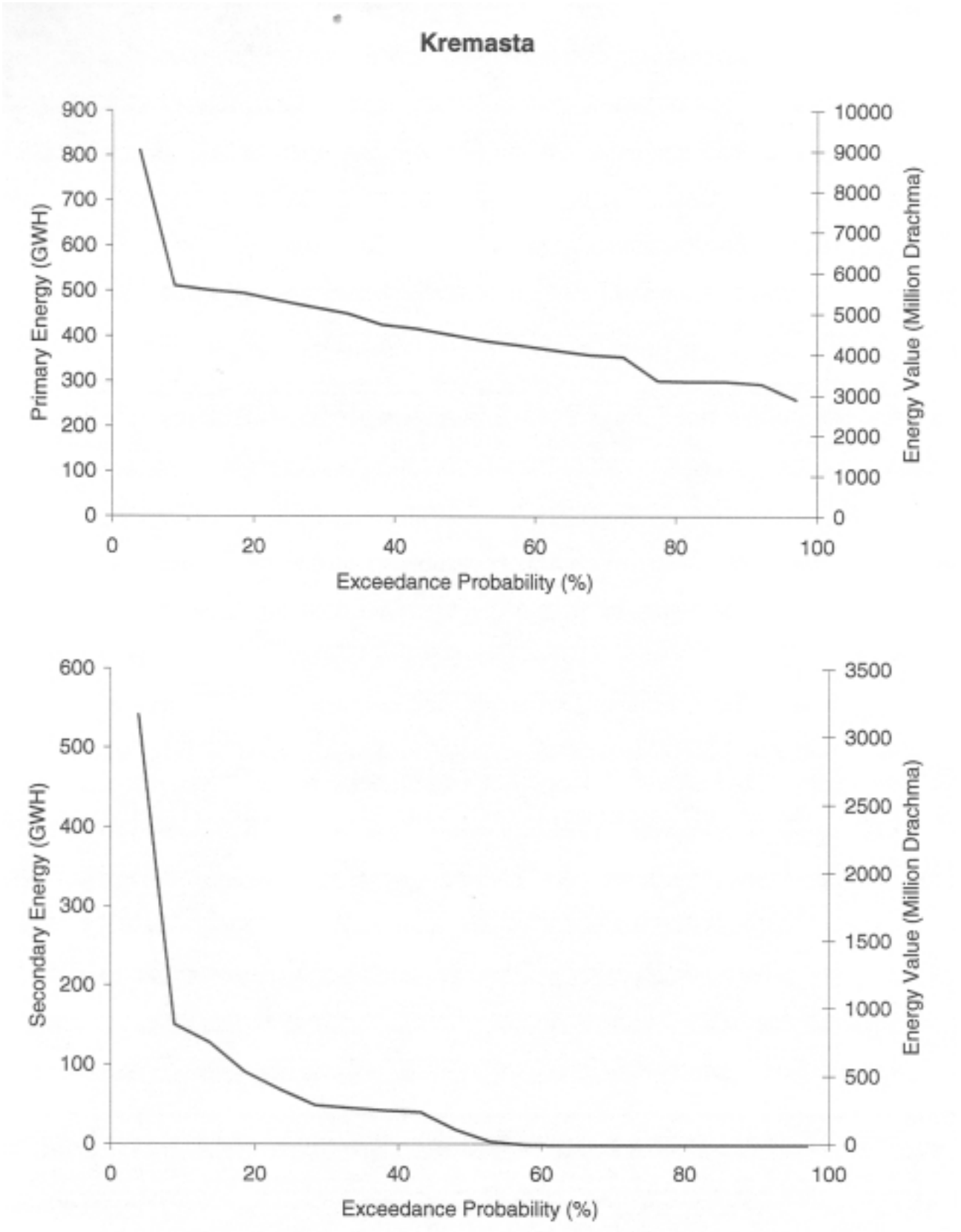

Figure 4.1.17: The exceedance probability curves for Kremasta

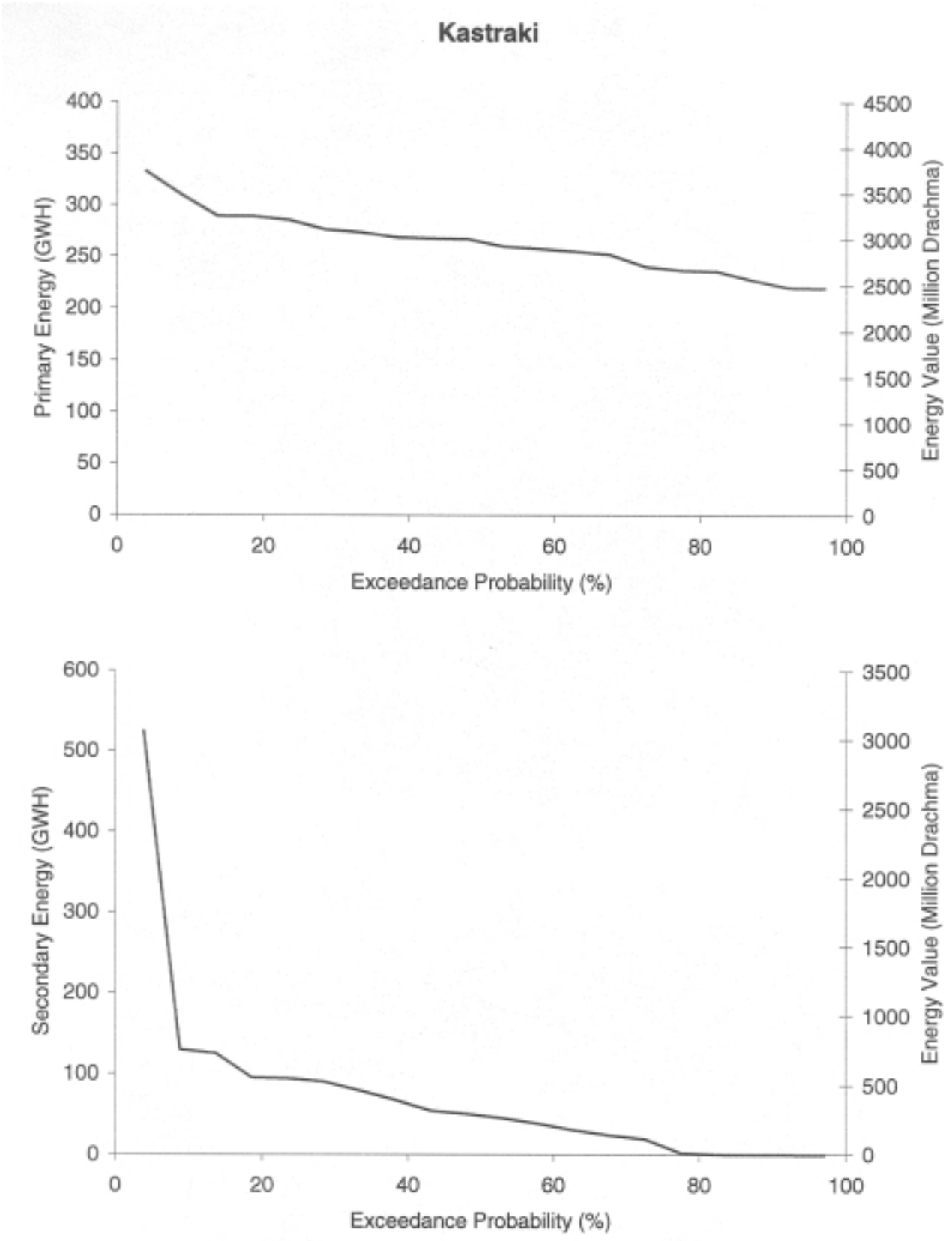

Figure 4.1.18: The exceedance probability curves for Kastraki

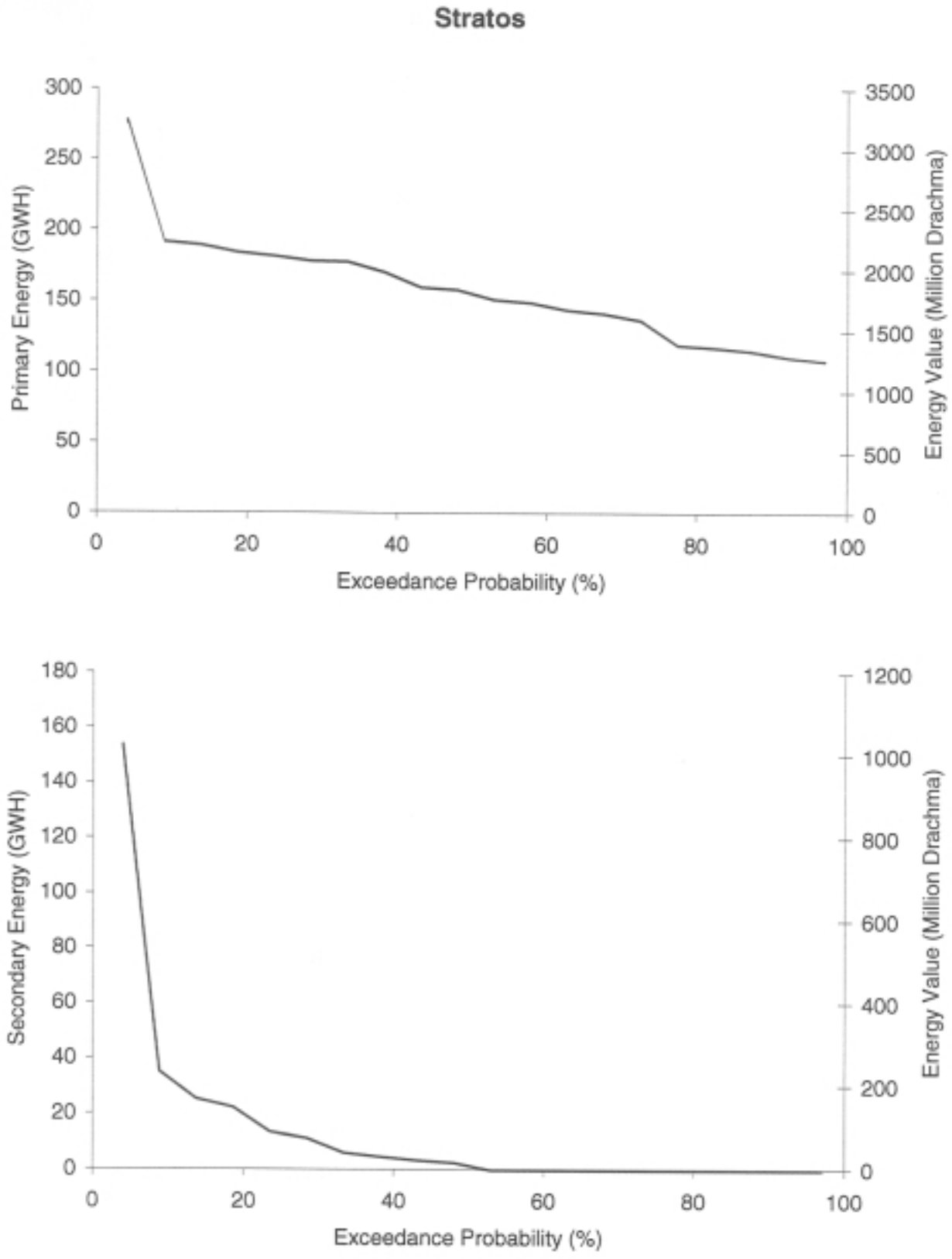

Figure 4.1.19: The exceedance probability curves for Stratos

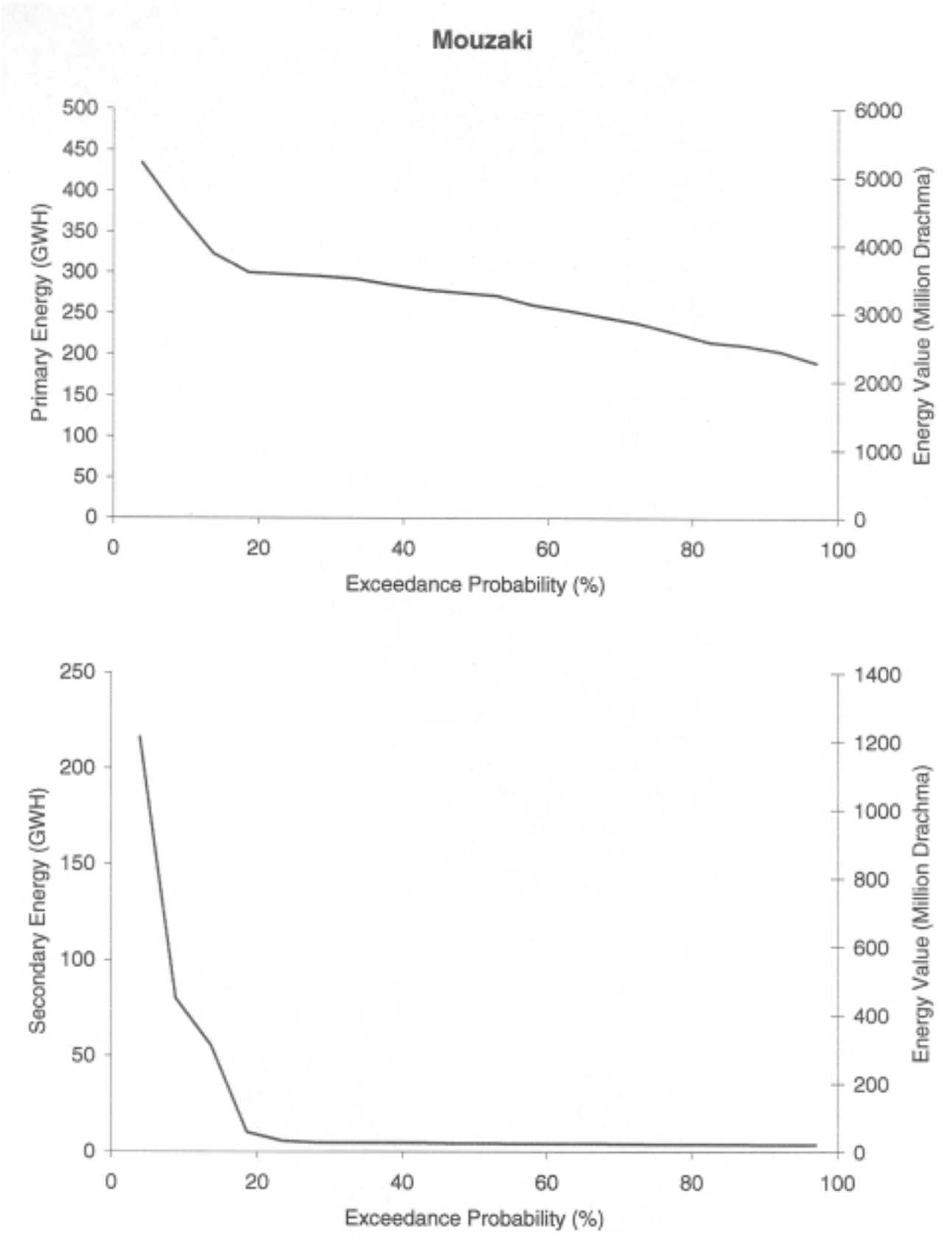

Figure 4.1.20: The exceedance probability curves for Mouzaki

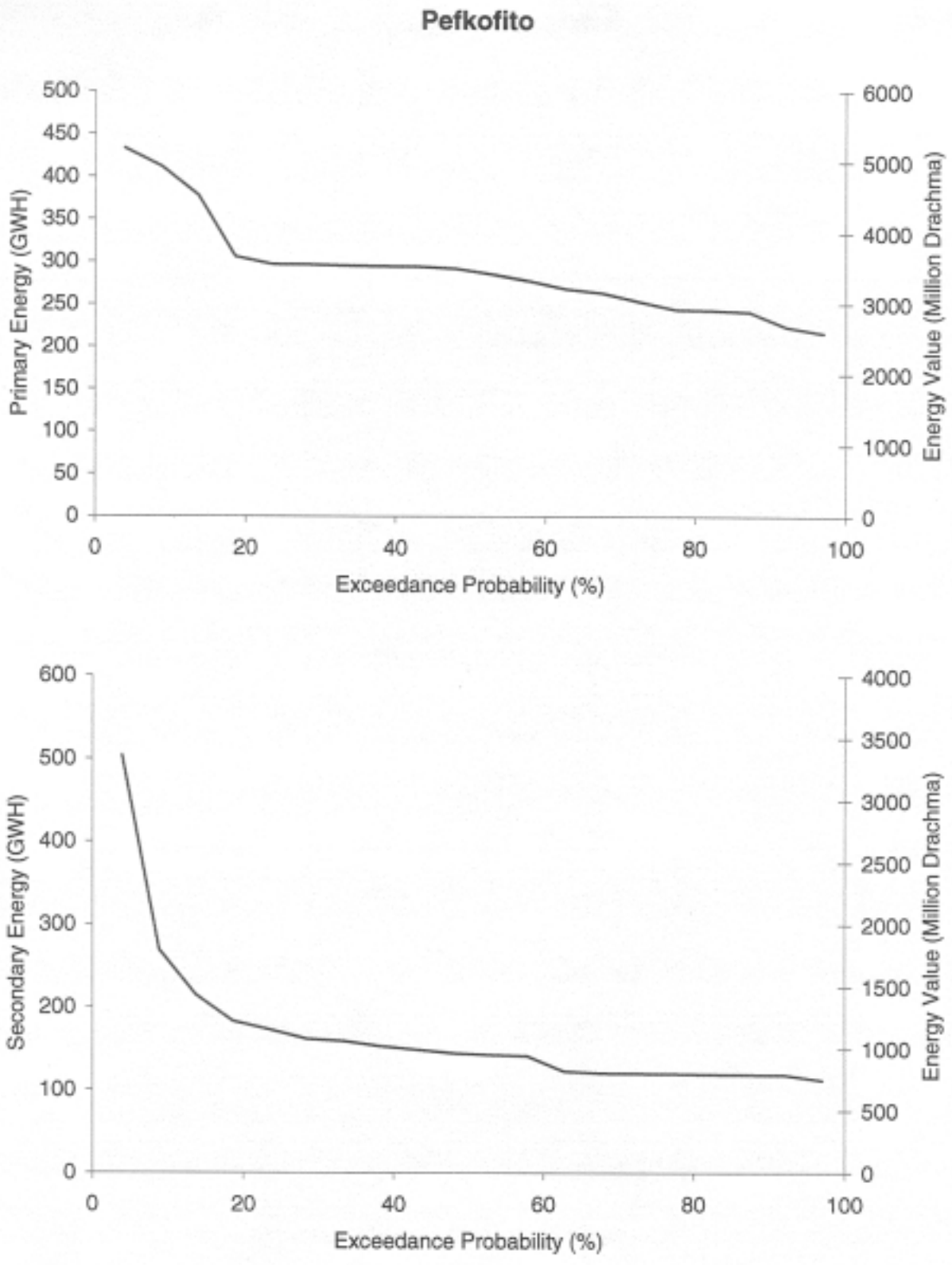

Figure 4.1.21: The exceedance probability curves for Pefkofito

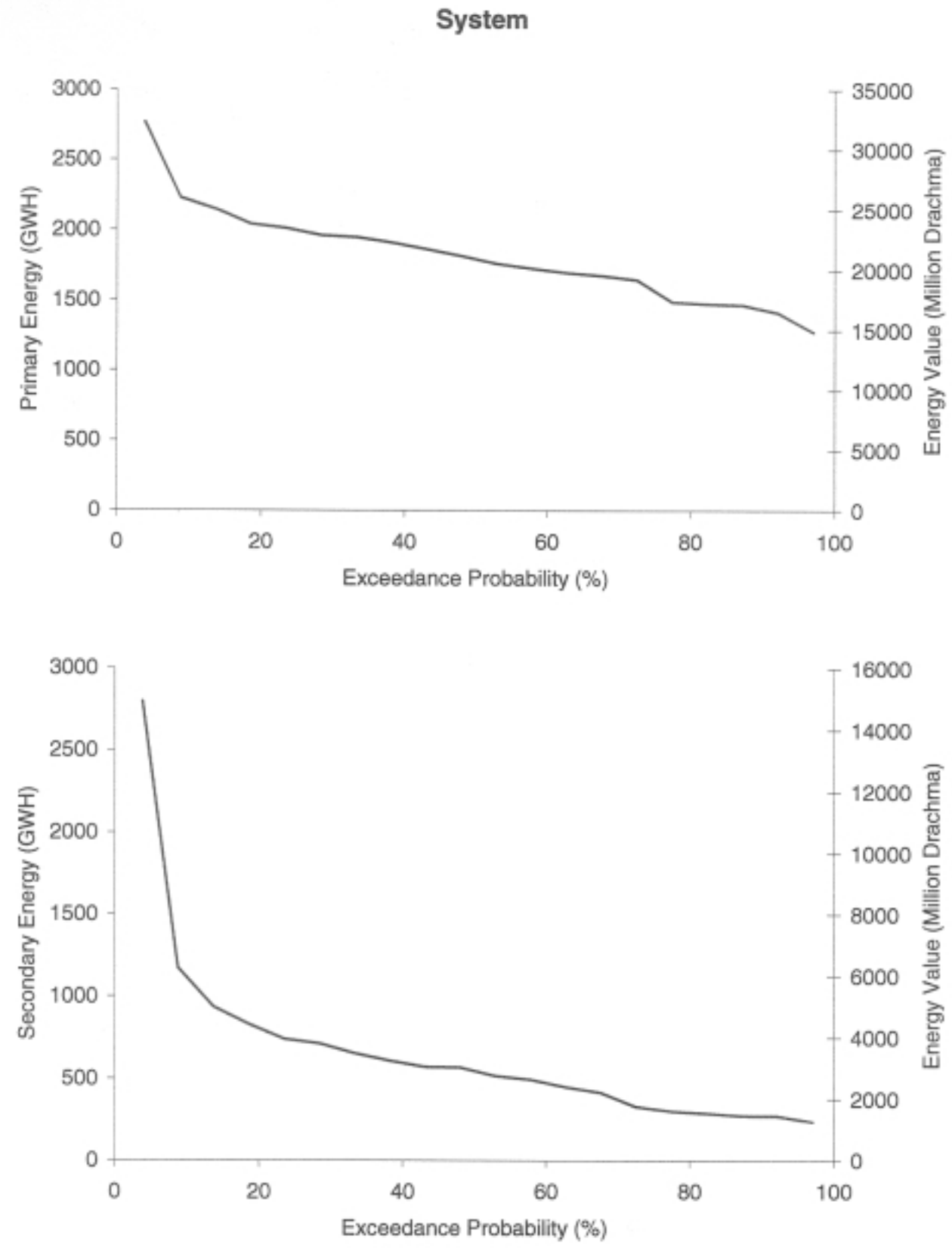

Figure 4.1.22: The exceedance probability curves for the entire system

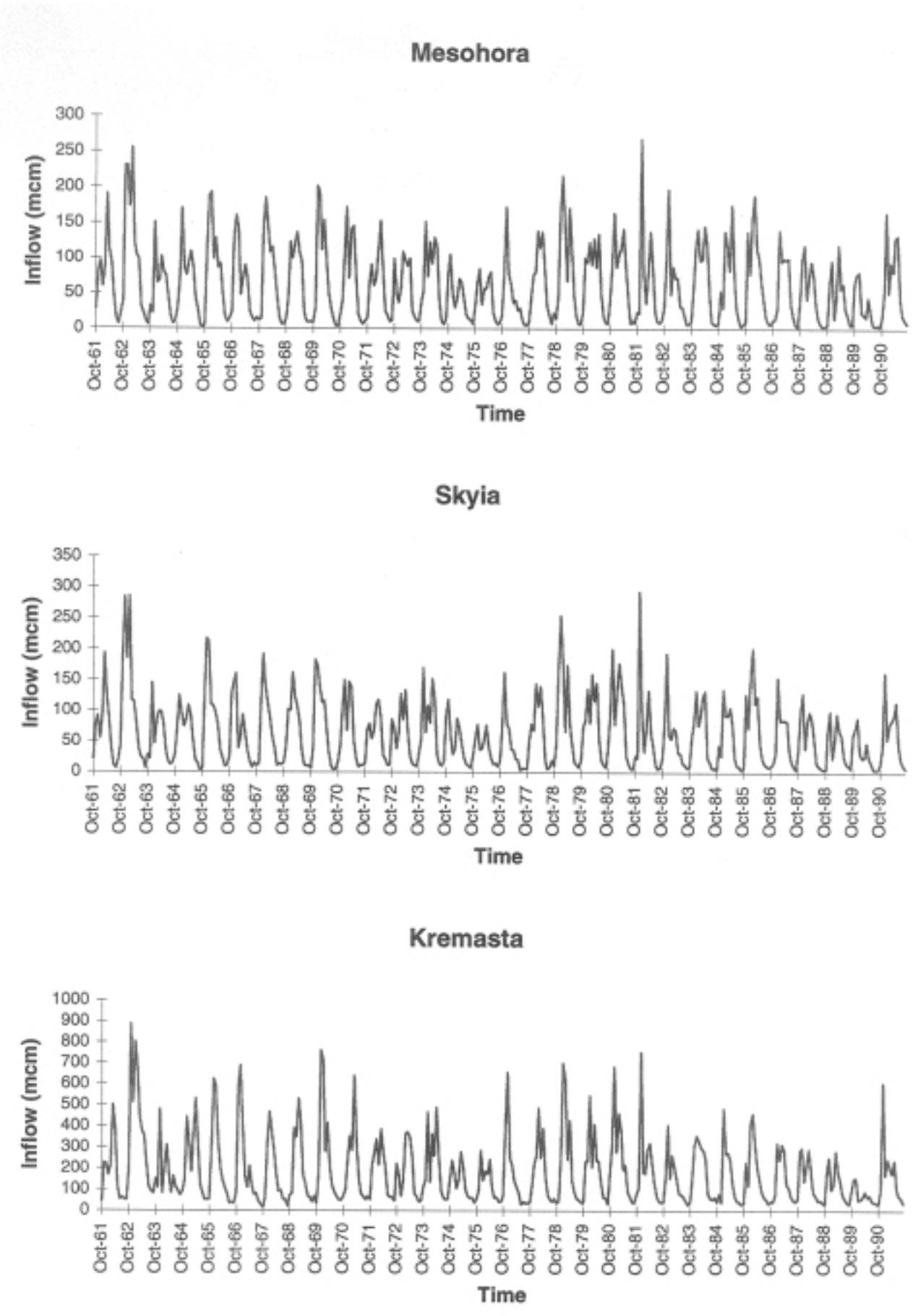

Figure 4.2.1: Historical Inflow Sequences (a)

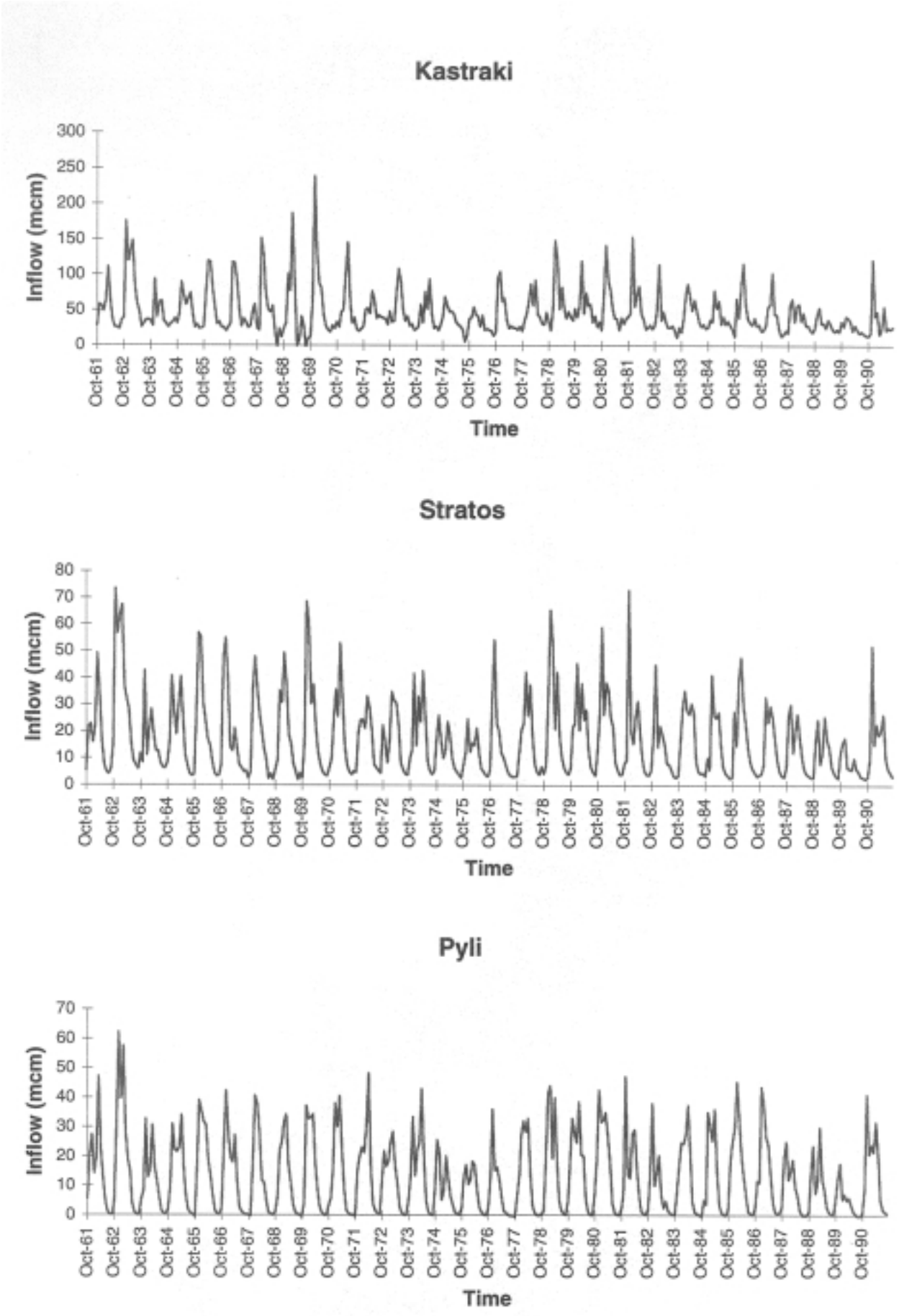

Figure 4.2.2: Historical Inflow Sequences (b)

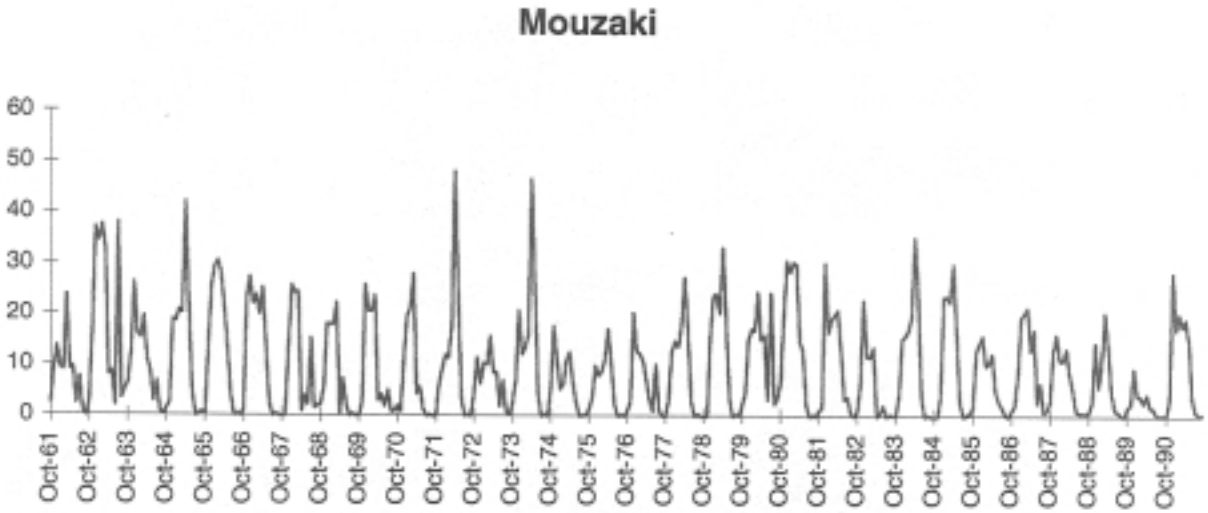

Figure 4.2.3: Historical Inflow Sequences (c)

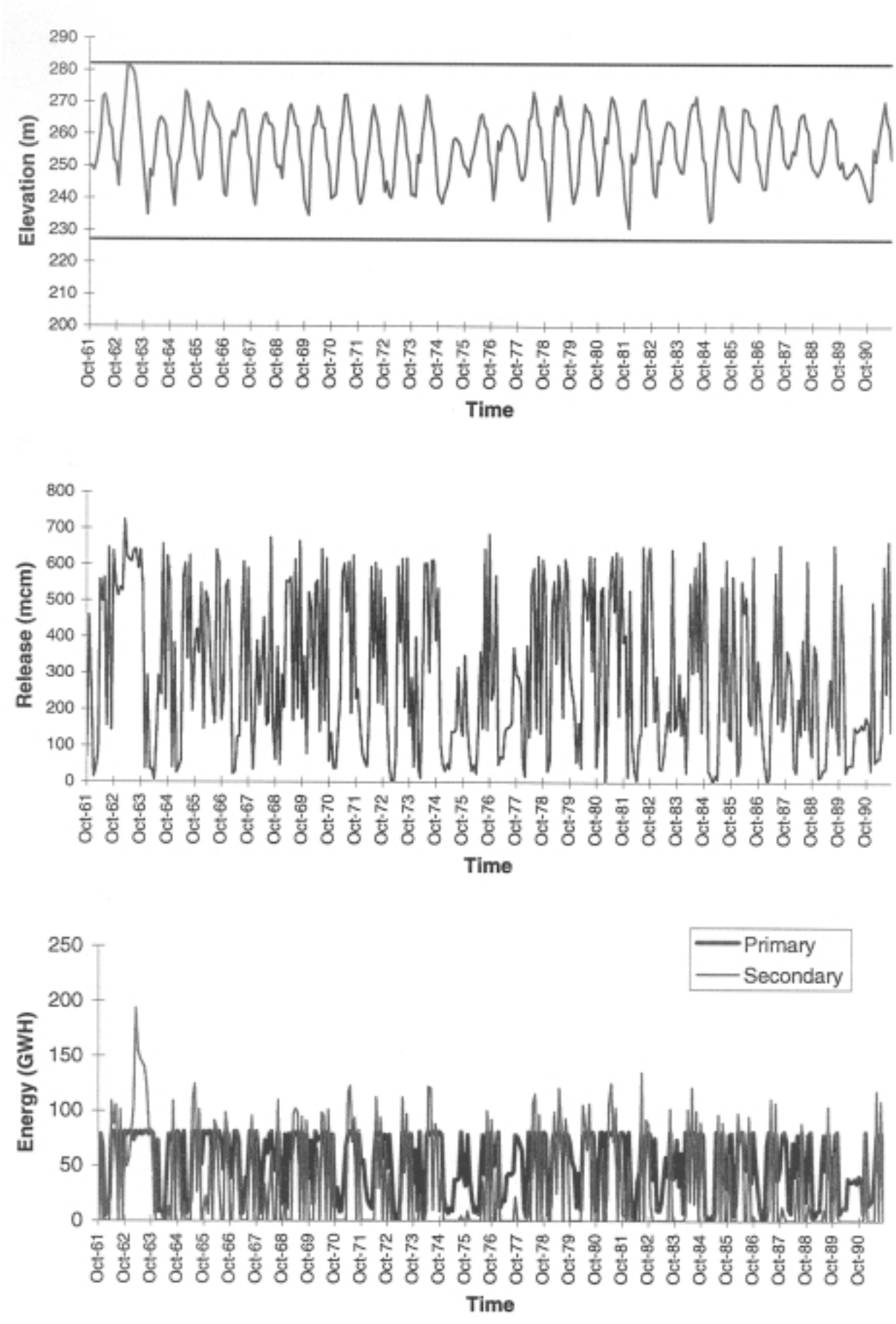

Figure 4.2.4: Kremasta Simulation Sequences; Baseline Case

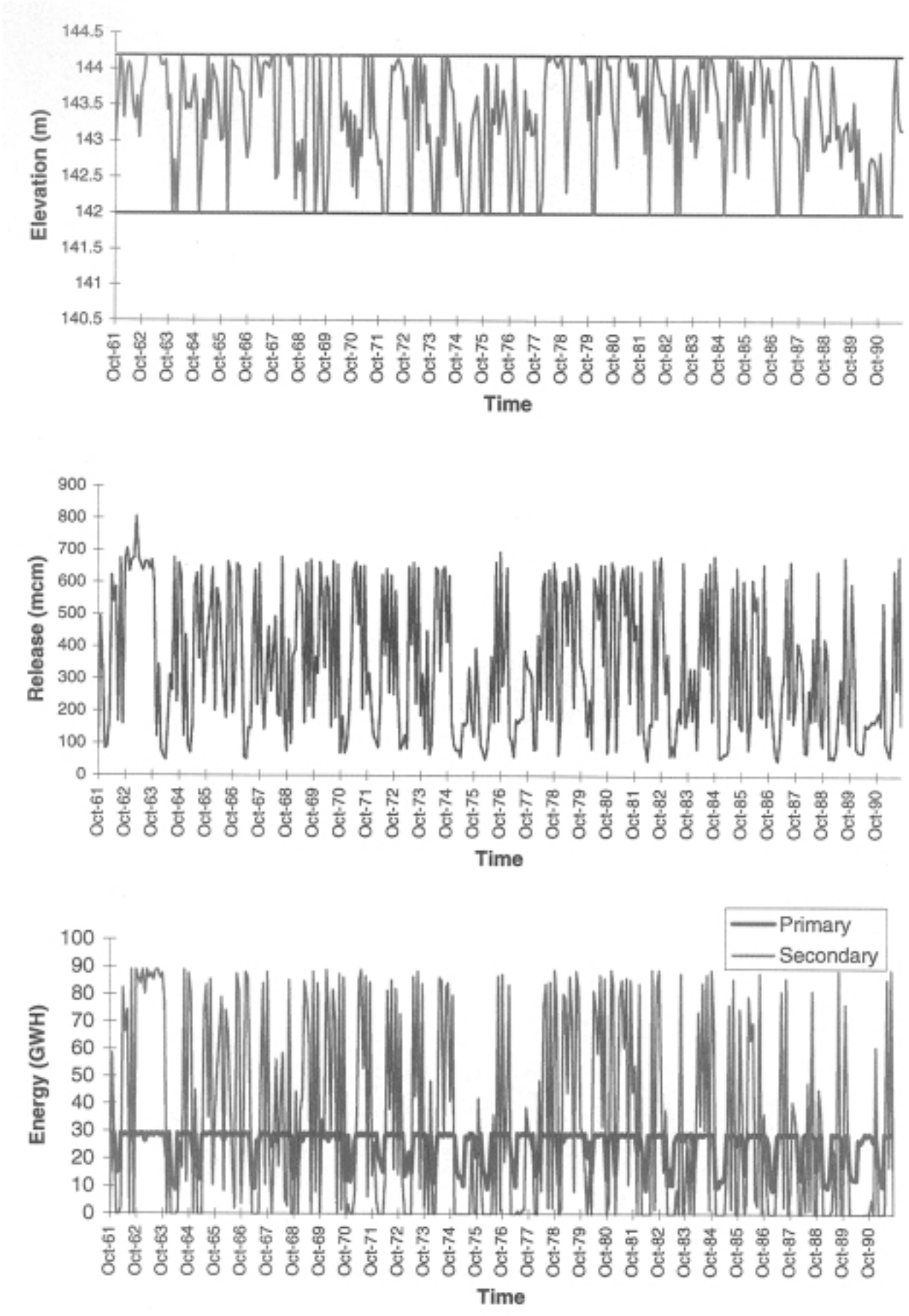

Figure 4.2.5: Kastraki Simulation Sequences; Baseline Case

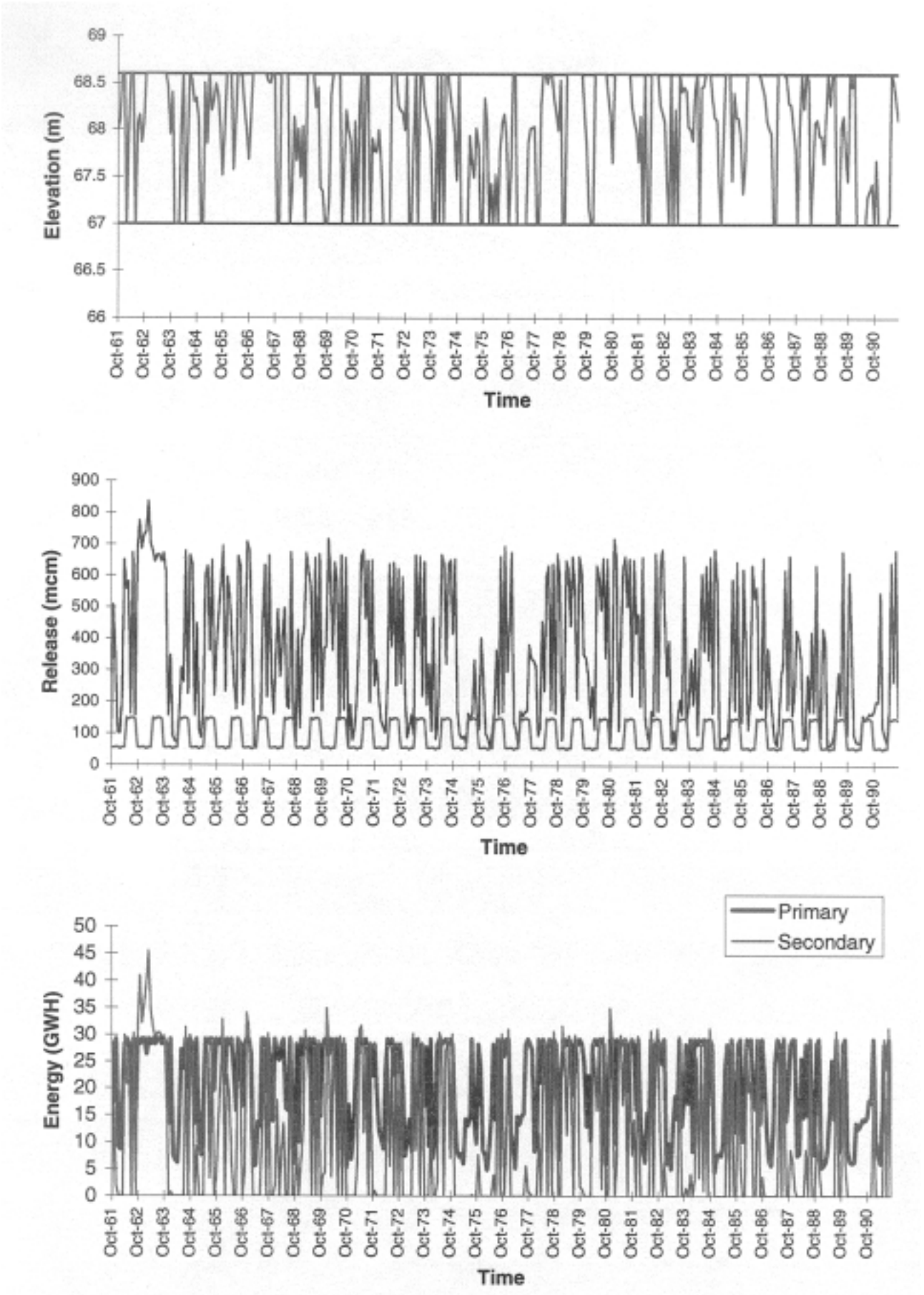

Figure 4.2.6: Stratos Simulation Sequences; Baseline Case

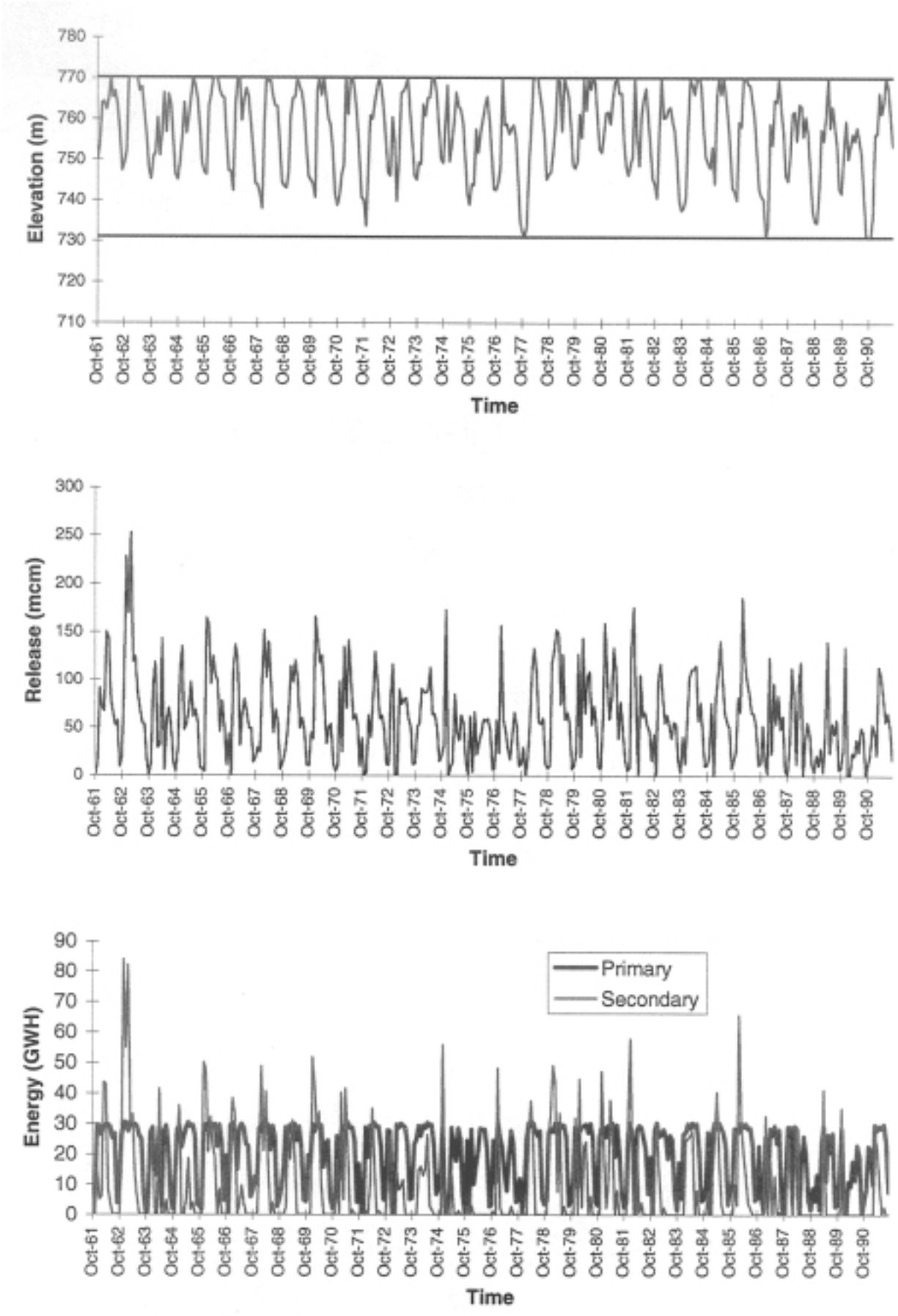

Figure 4.2.7: Mesohora Simulation Sequences; No Pumping

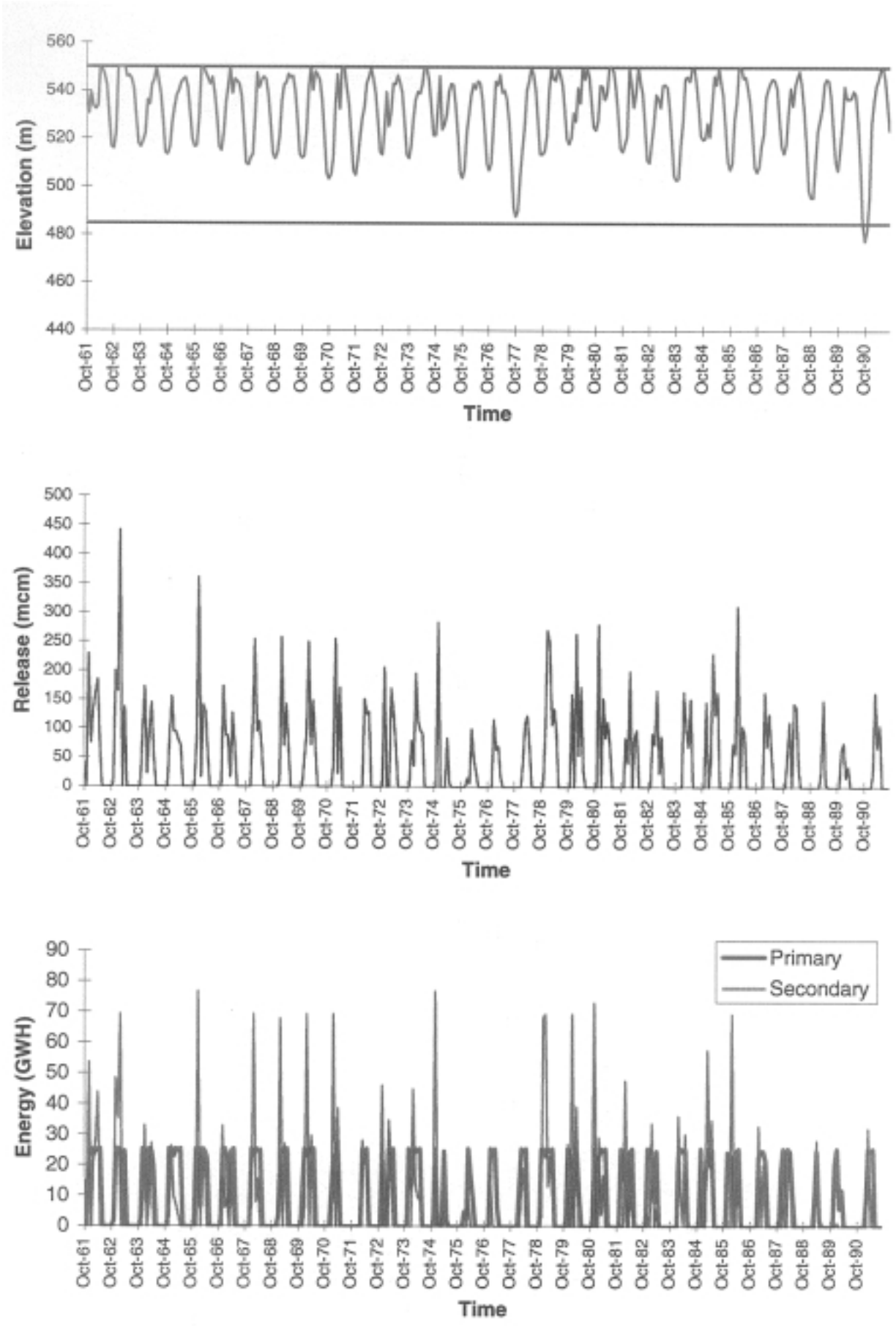

Figure 4.2.8: Sykia Simulation Sequences; No Pumping

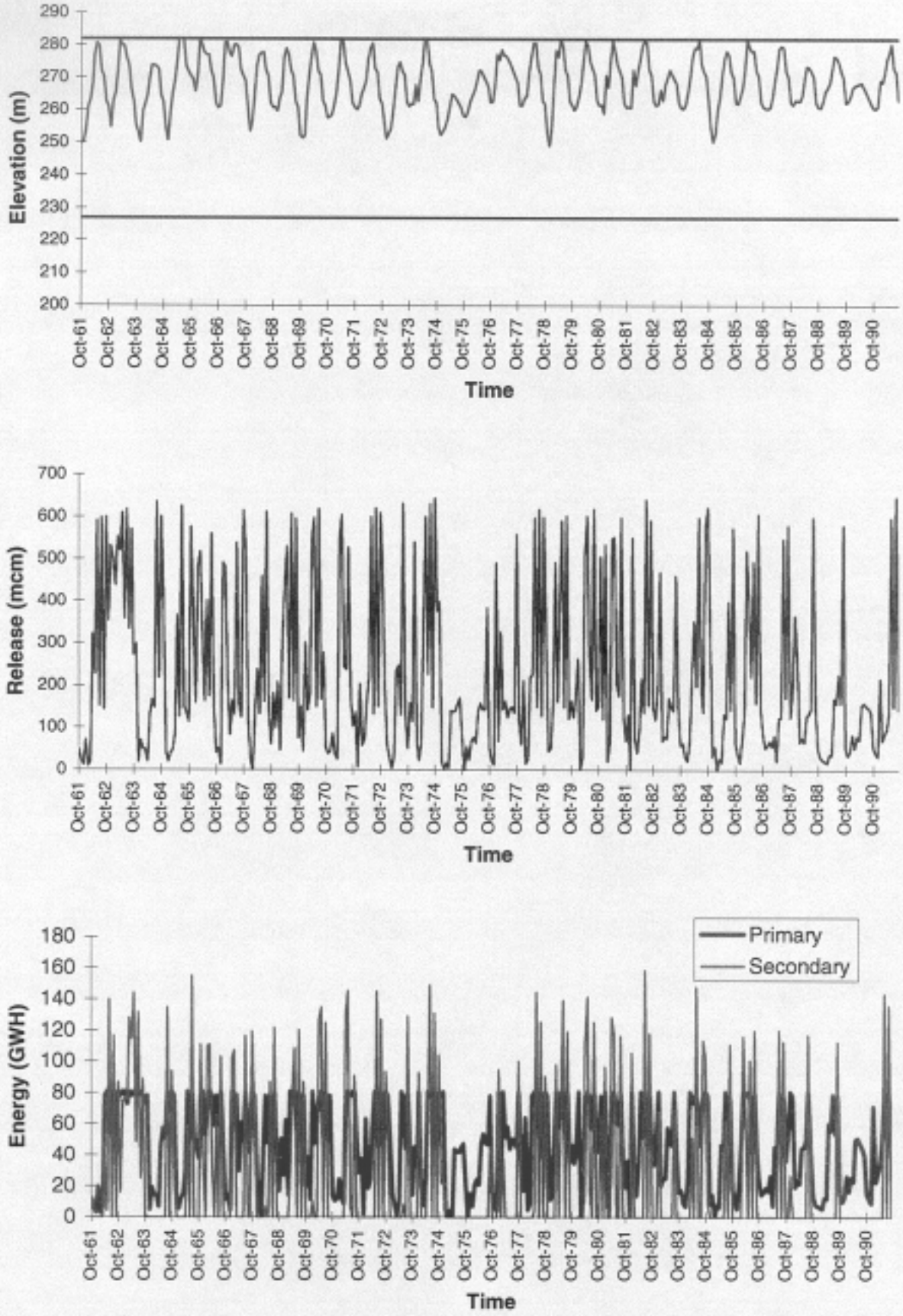

Figure 4.2.9: Kremasta Simulation Sequences; No Pumping

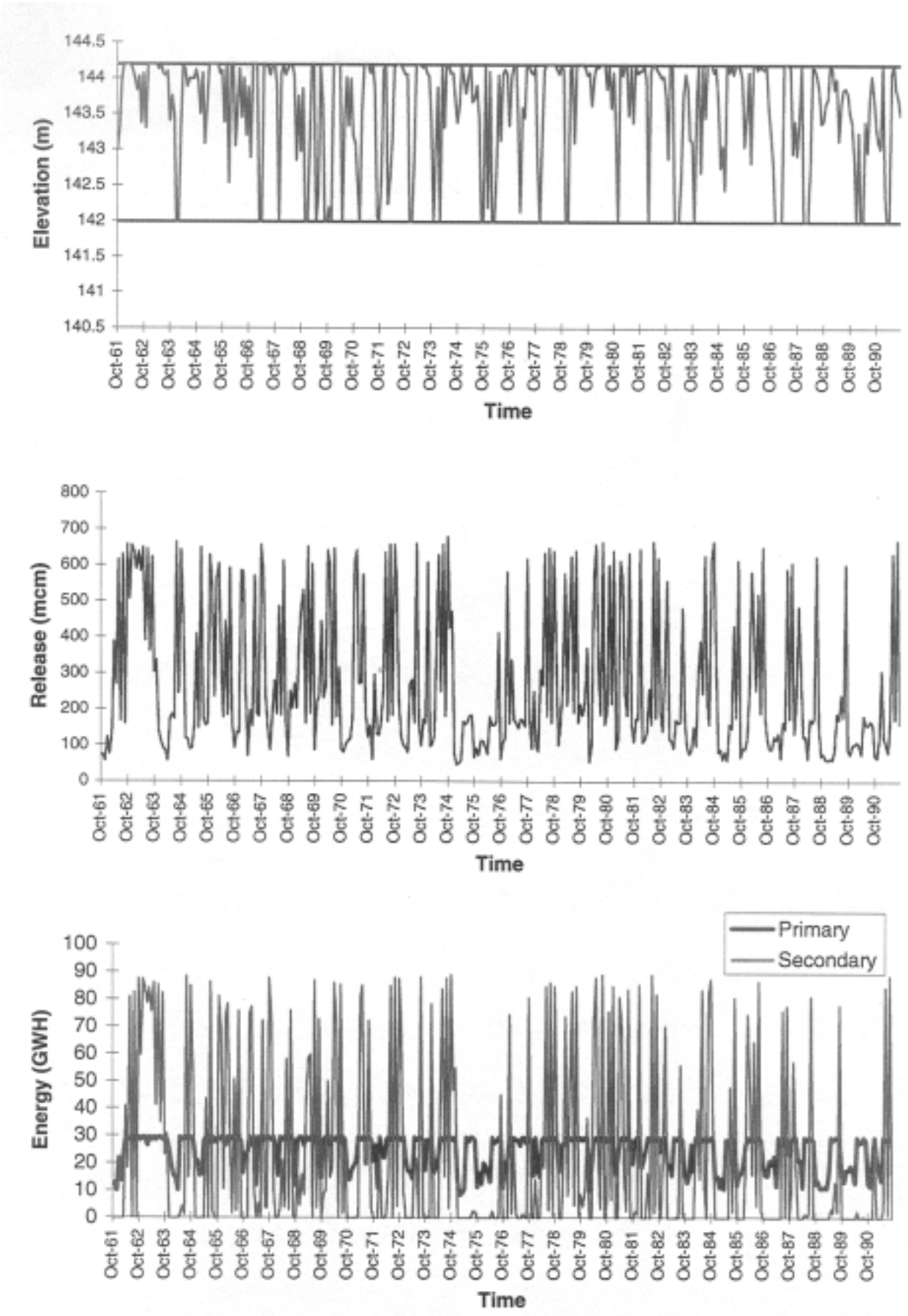

Figure 4.2.10: Kastraki Simulation Sequences; No Pumping

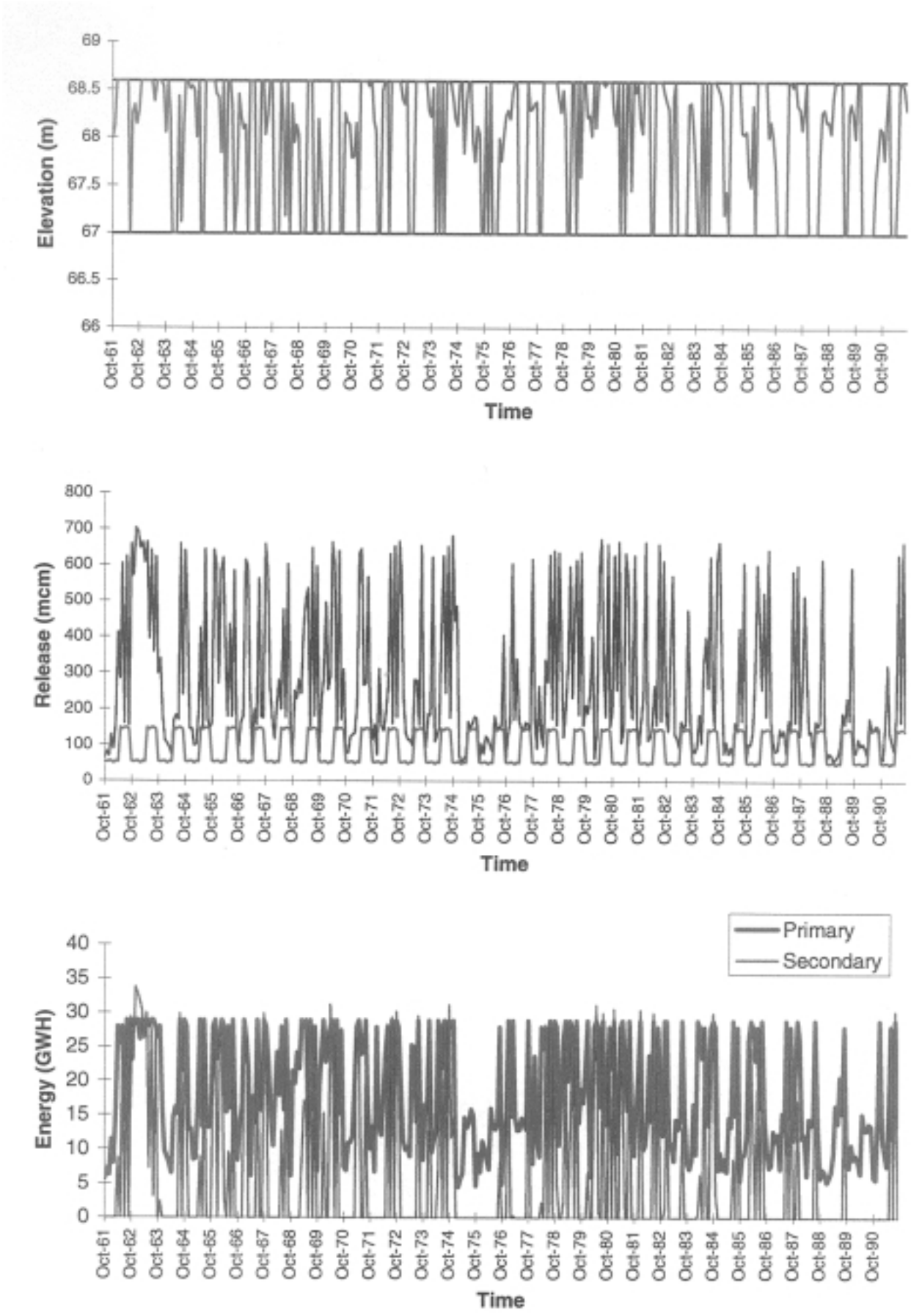

Figure 4.2.11: Srtatos Simulation Sequences; No Pumping

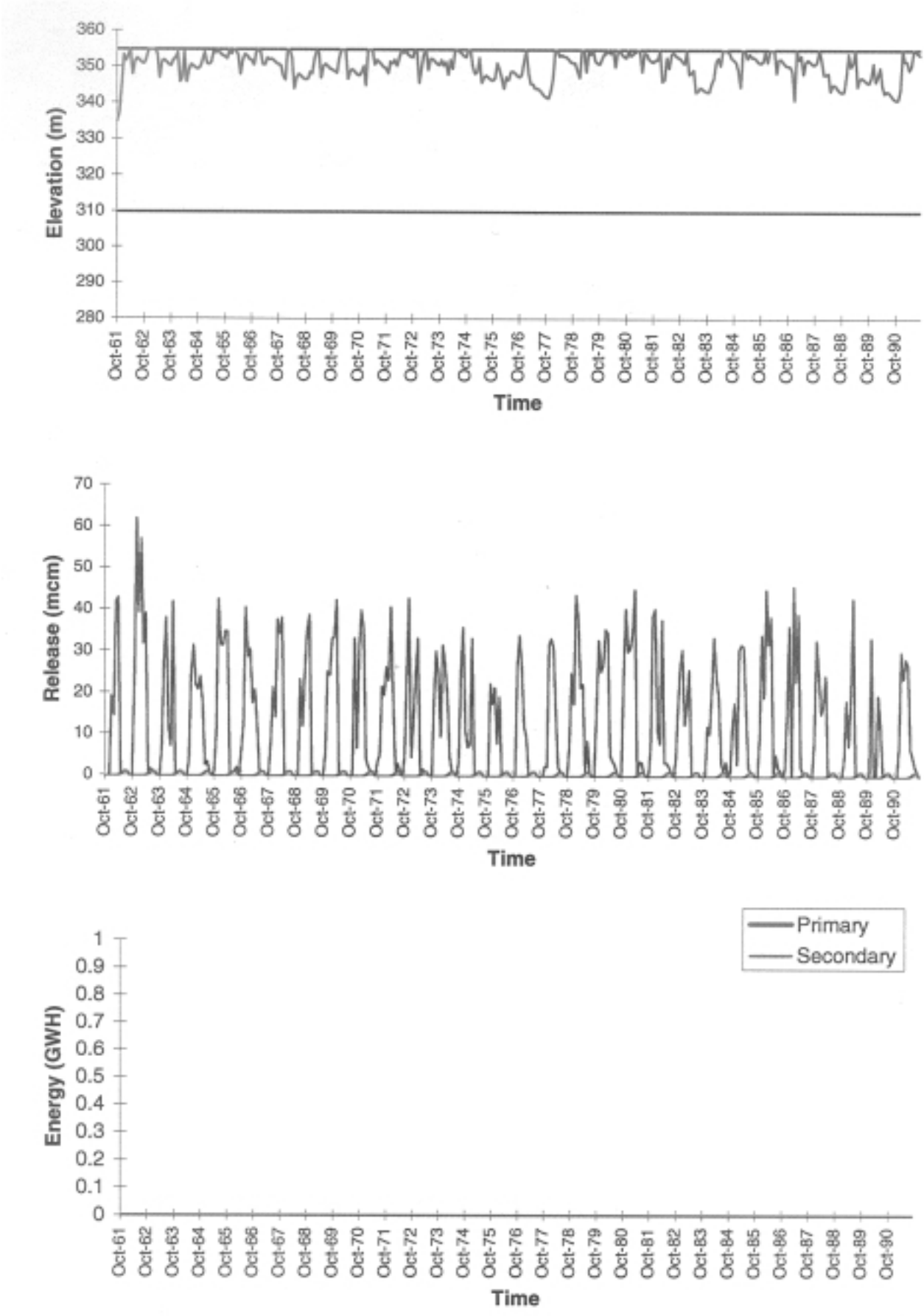

Figure 4.2.12: Pyli Simulation Sequences; No Pumping

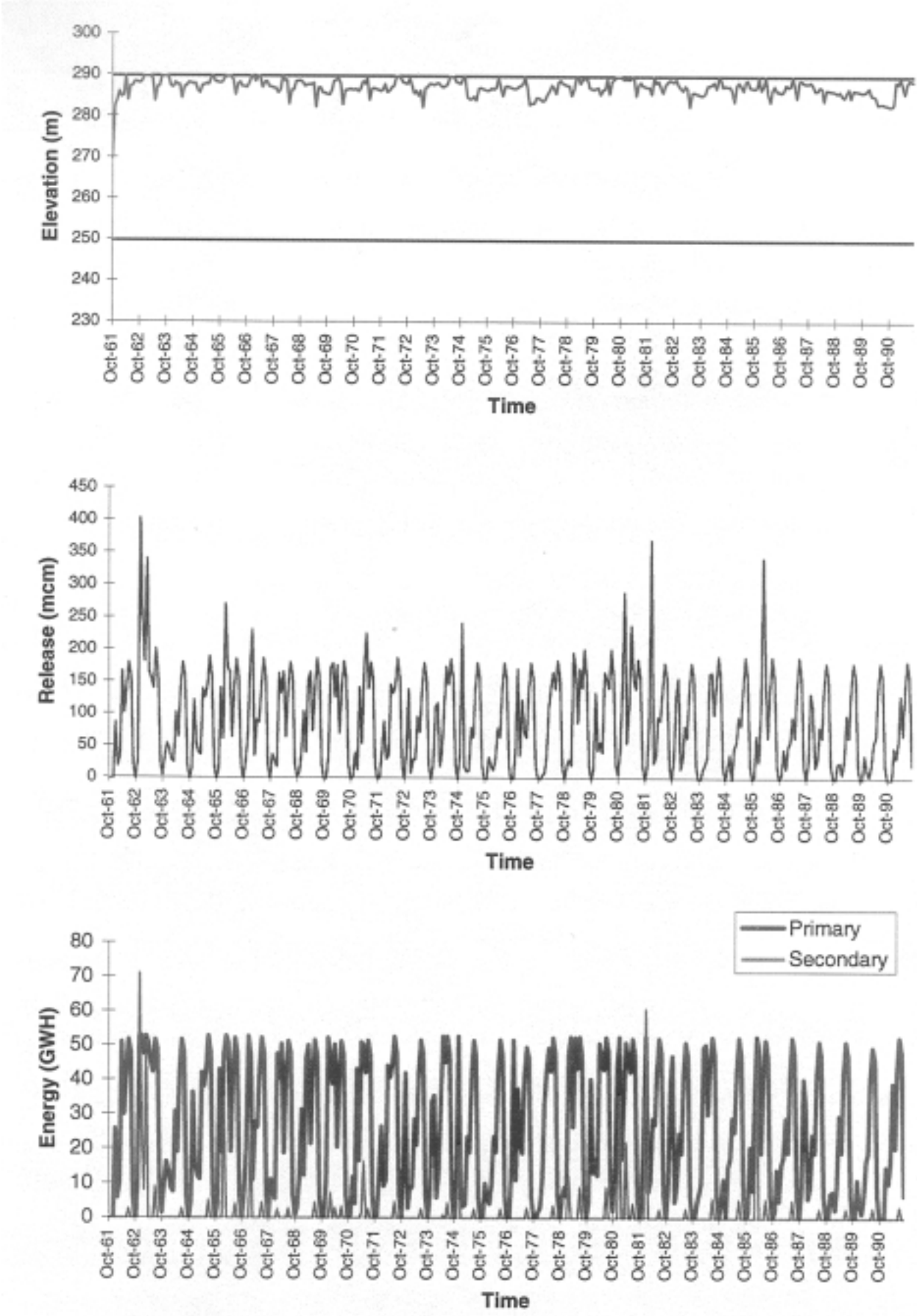

Figure 4.2.13: Mouzaki Simulation Sequences; No Pumping

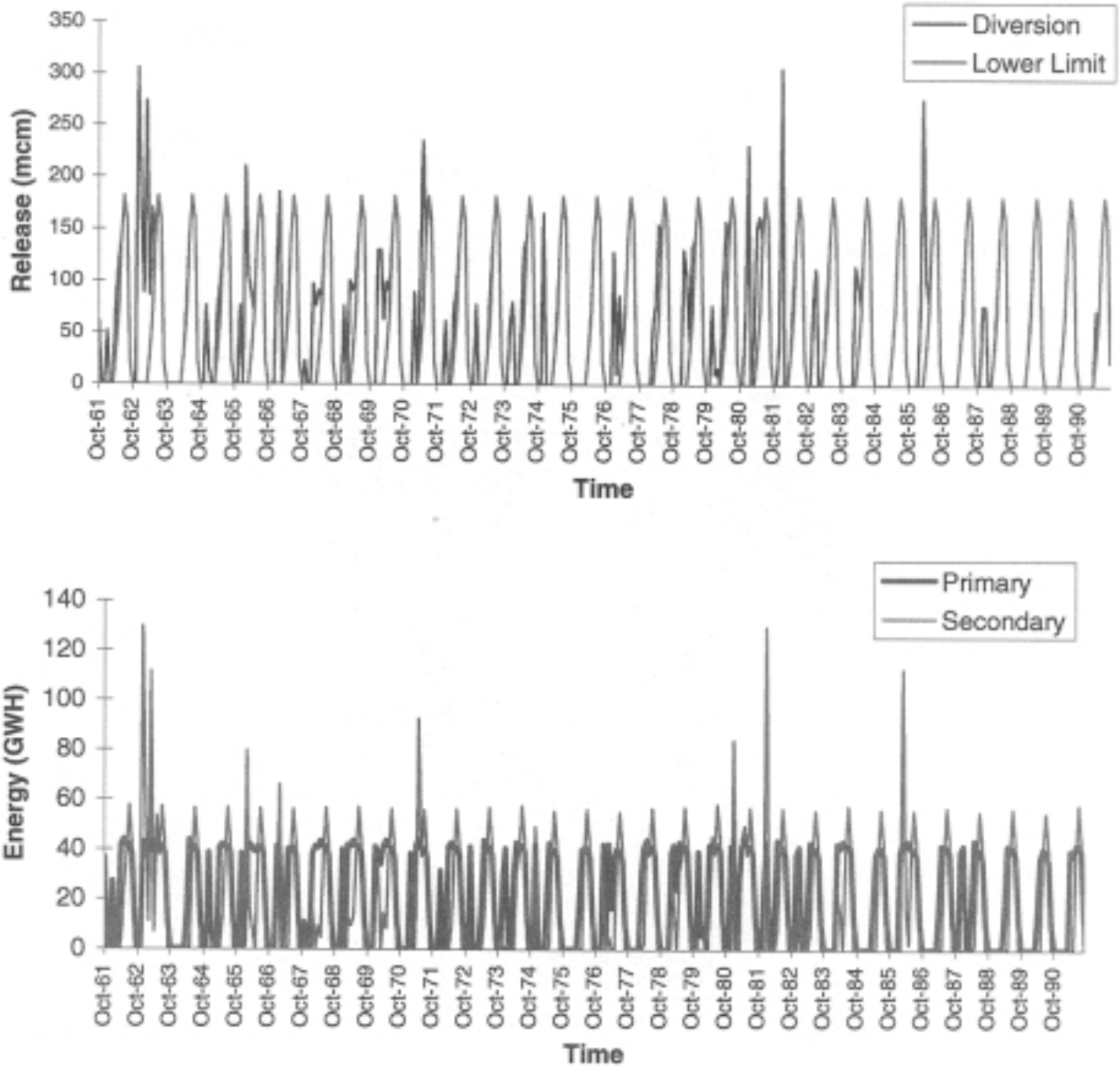

Figure 4.2.14: Pefkofito Simulation Sequences; No Pumping

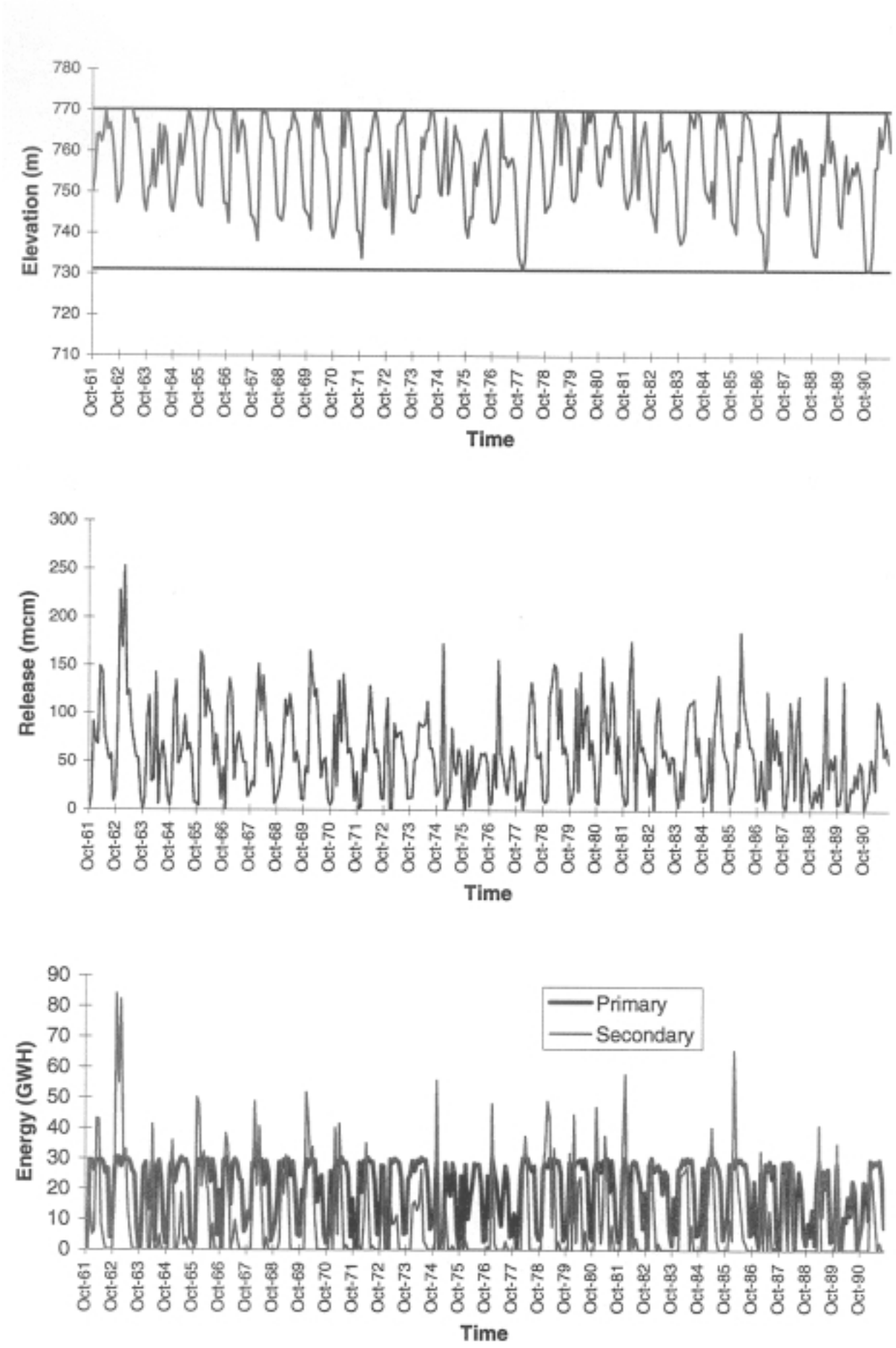

Figure 4.2.15: Mesohora Simulation Sequences: Pumping

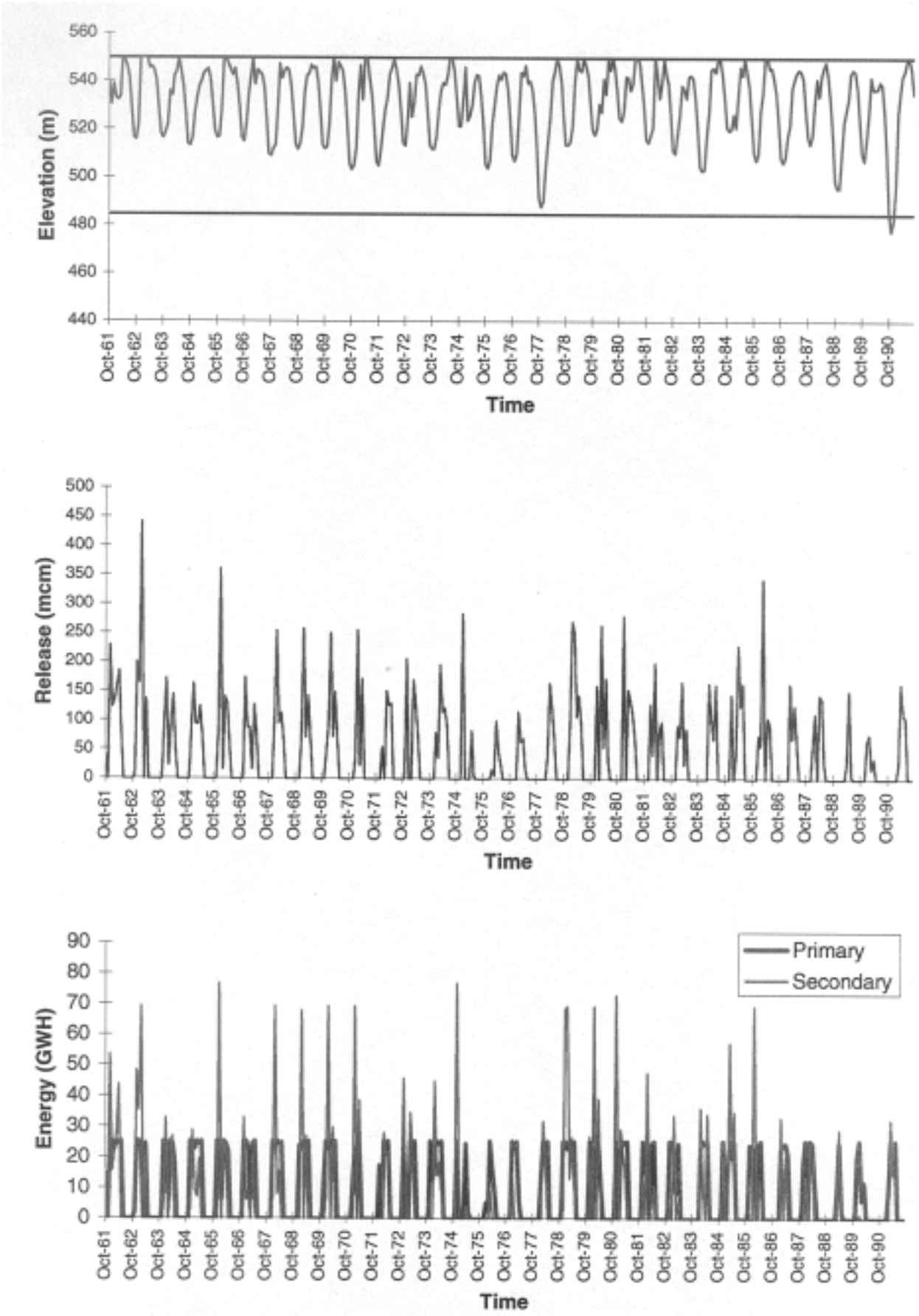

Figure 4.2.16: Sykia Simulation Sequences; Pumping

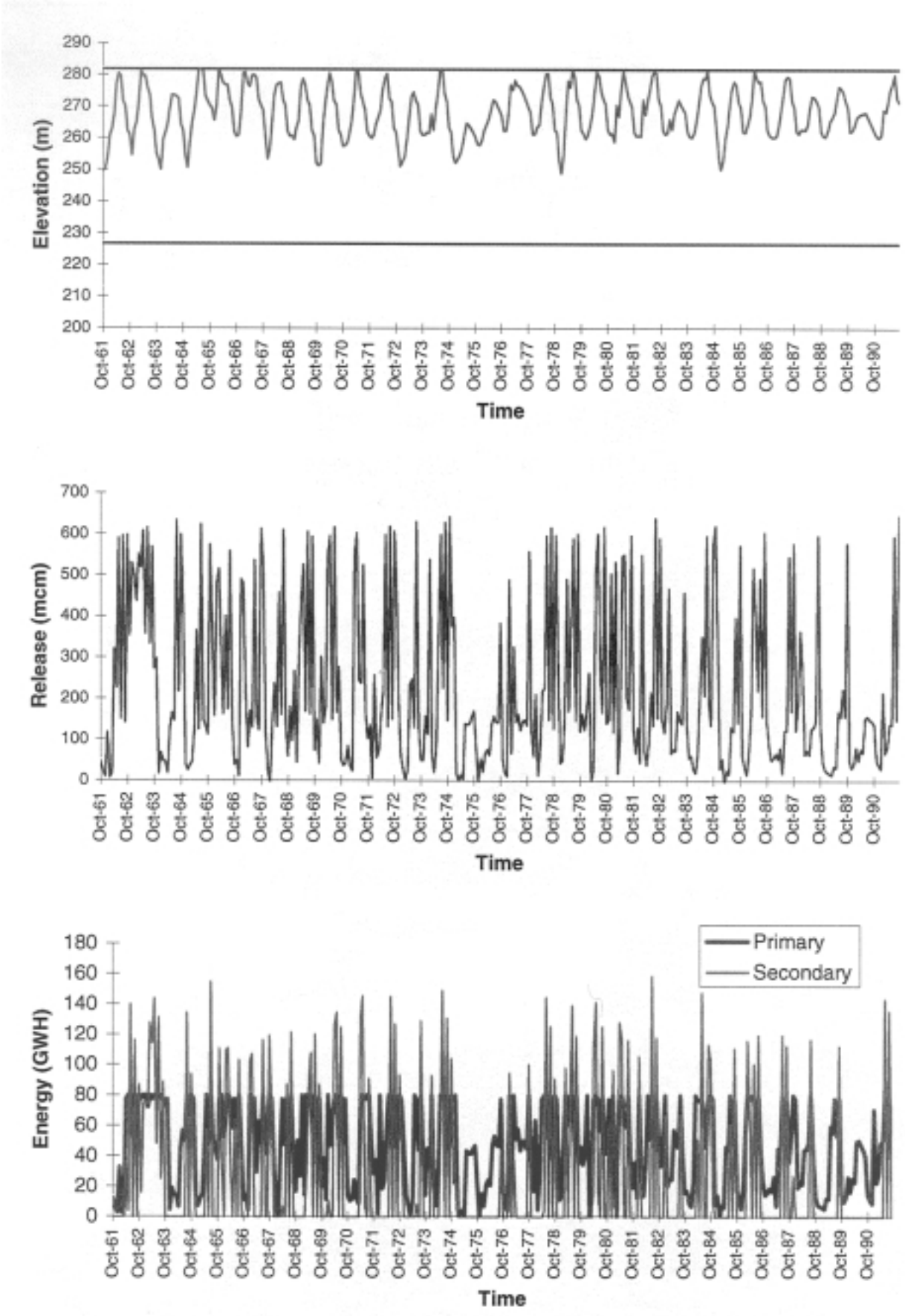

Figure 4.2.17: Kremasta Simulation Sequences; Pumping

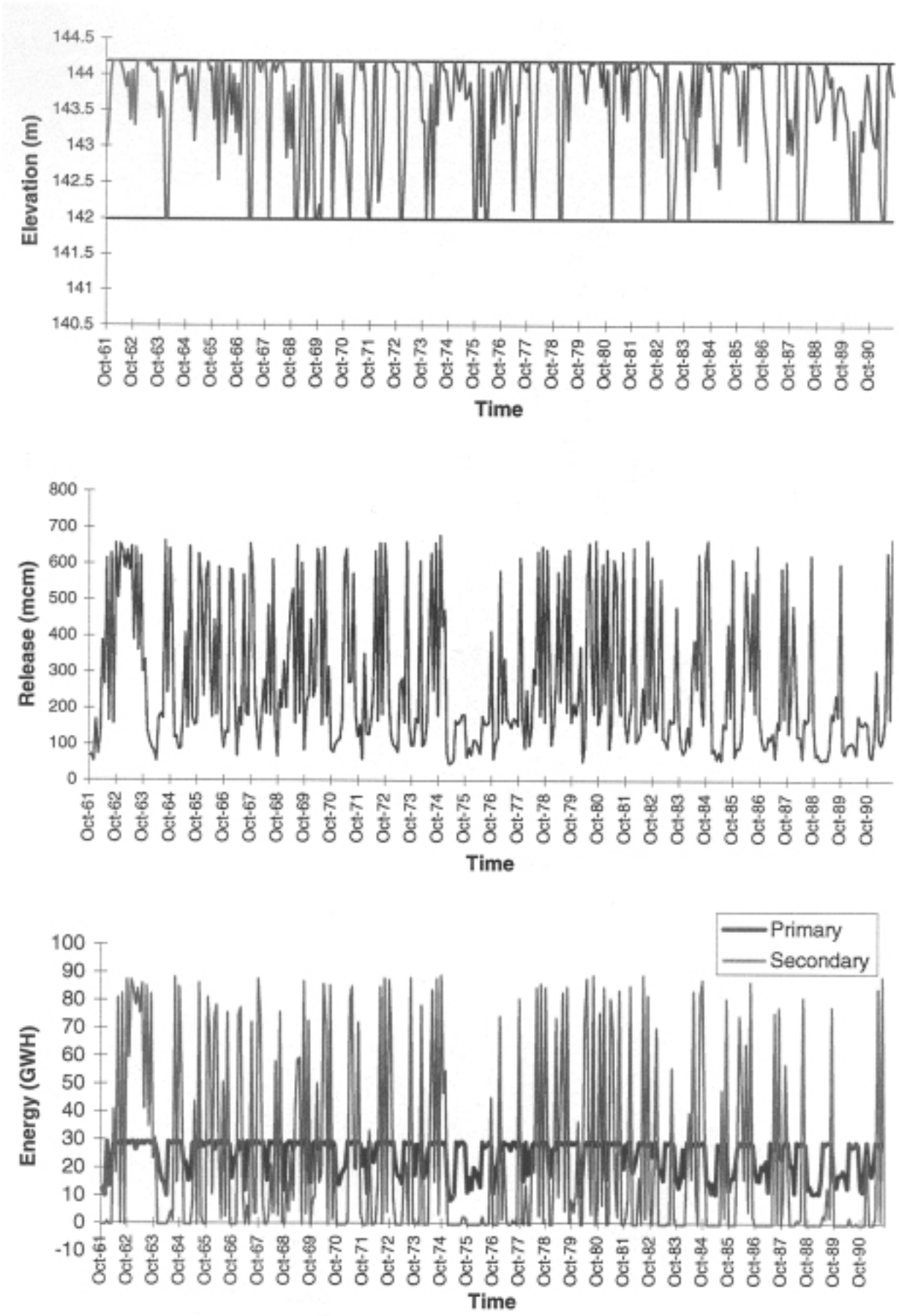

Figure 4.2.18: Kastraki Simulation Sequences; Pumping

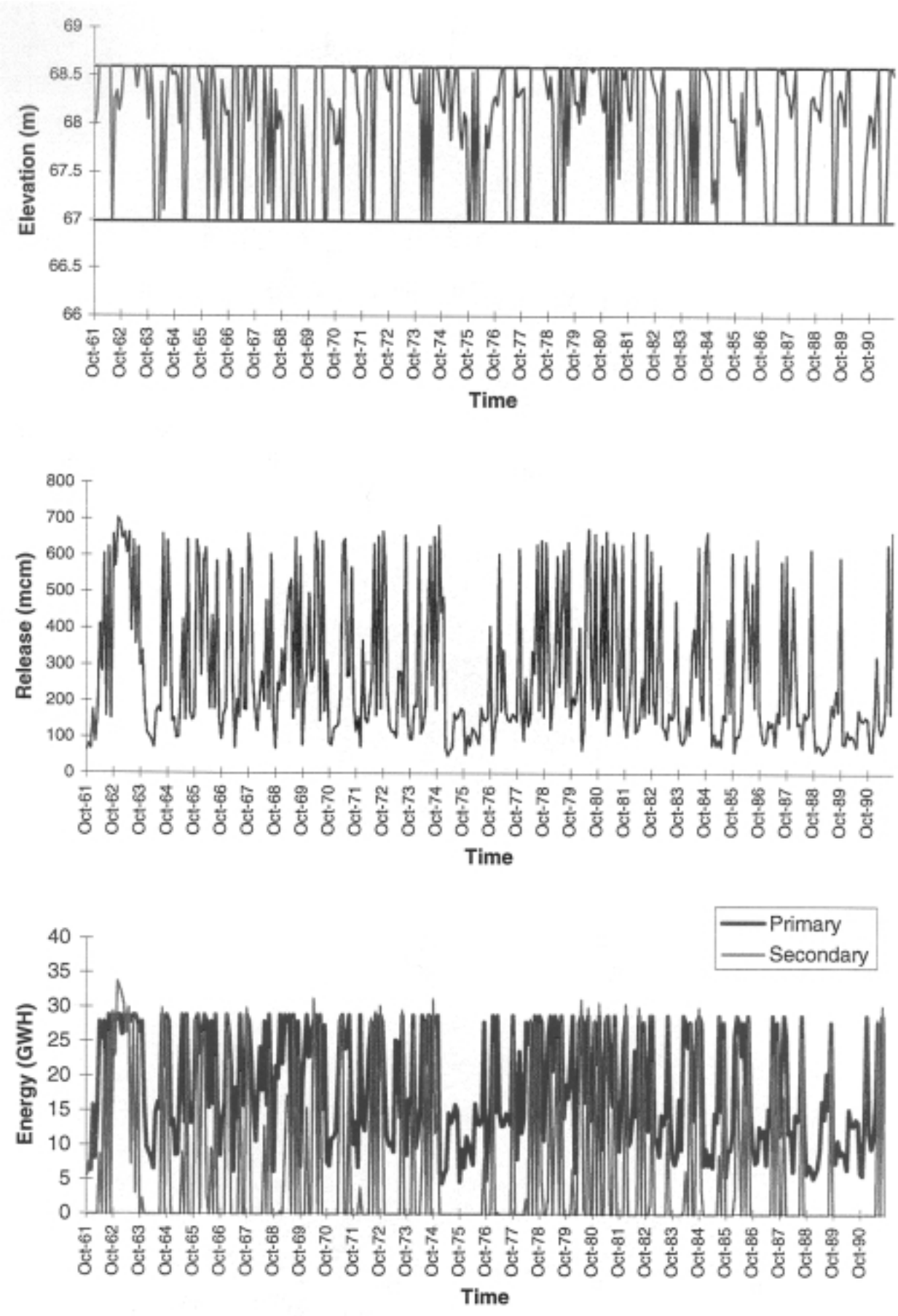

Figure 4.2.19: Stratos Simulation Sequences; Pumping

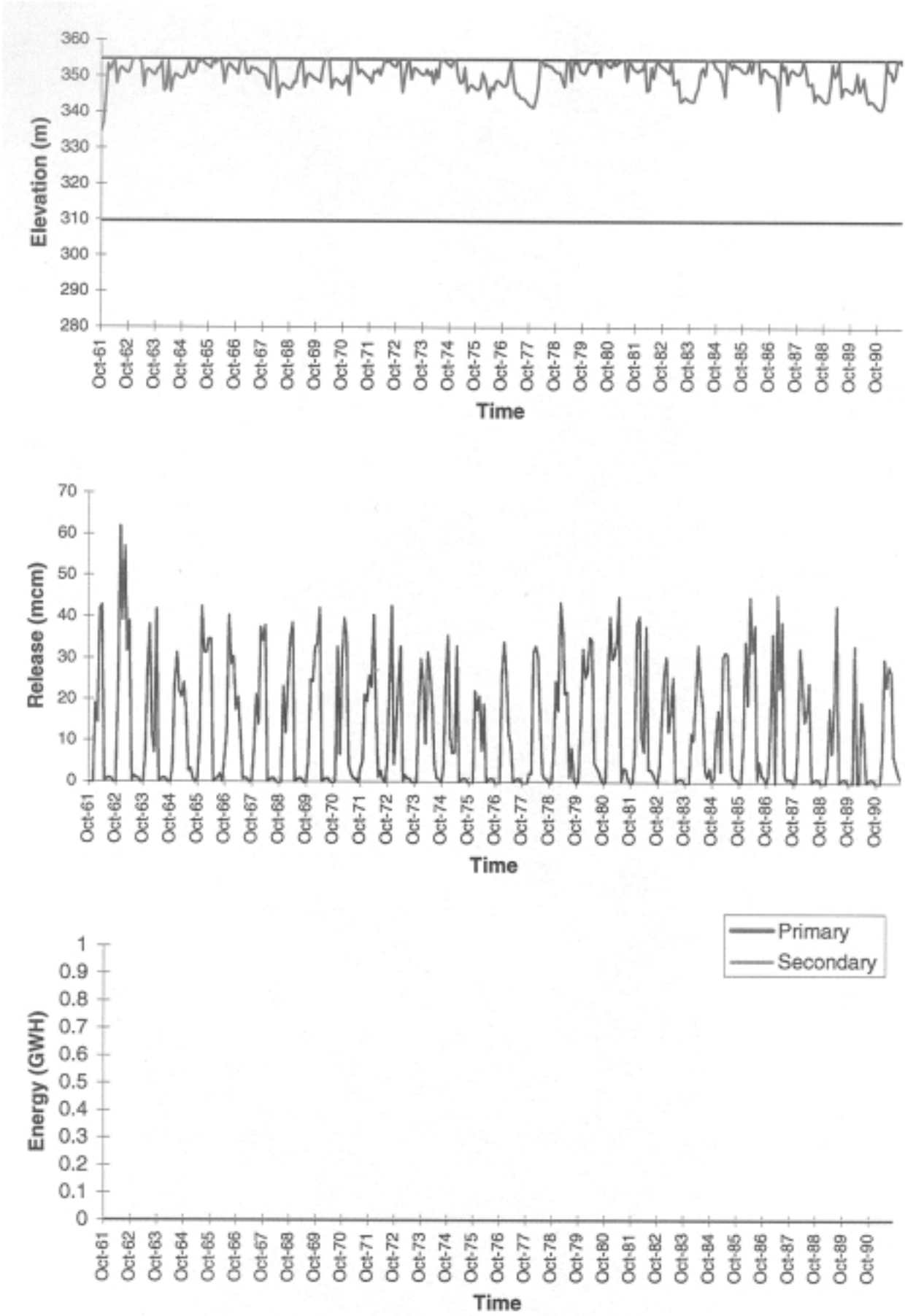

Figure 4.2.20: Pyli Simulation Sequences; Pumping

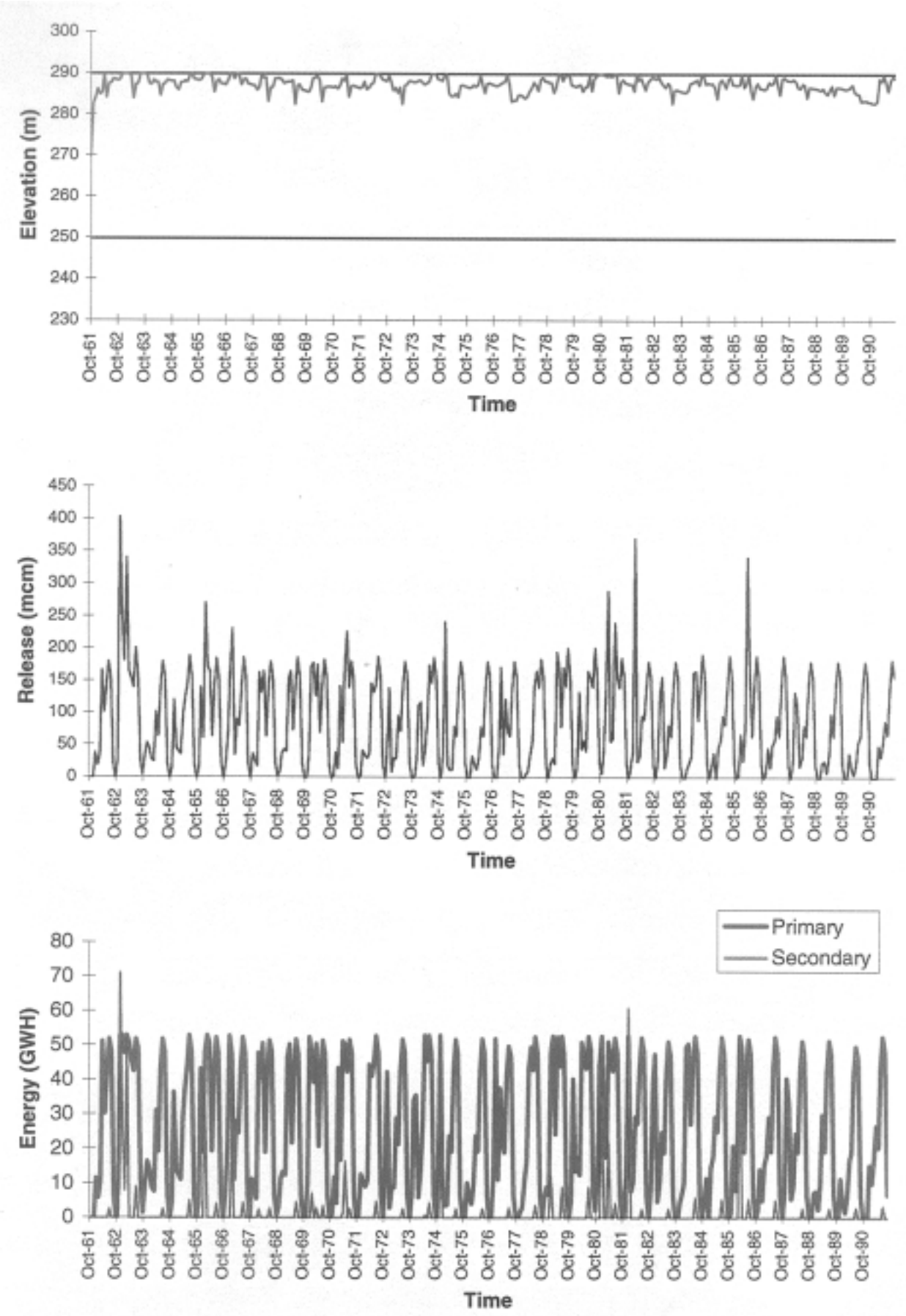

Figure 4.2.21: Mouzaki Simulation Sequences; Pumping

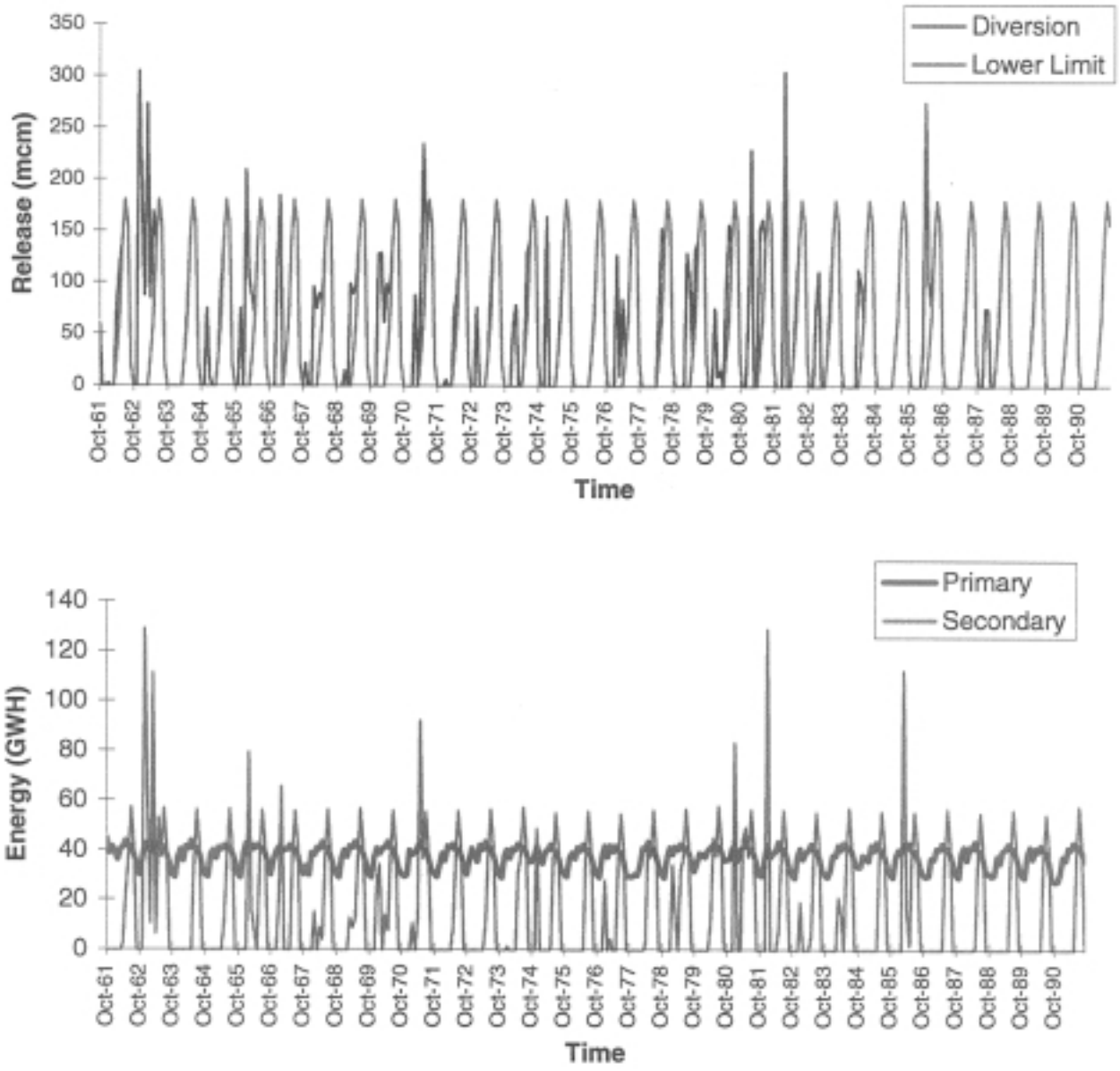

Figure 4.2.22: Pefkofito Simulation Sequences; Pumping

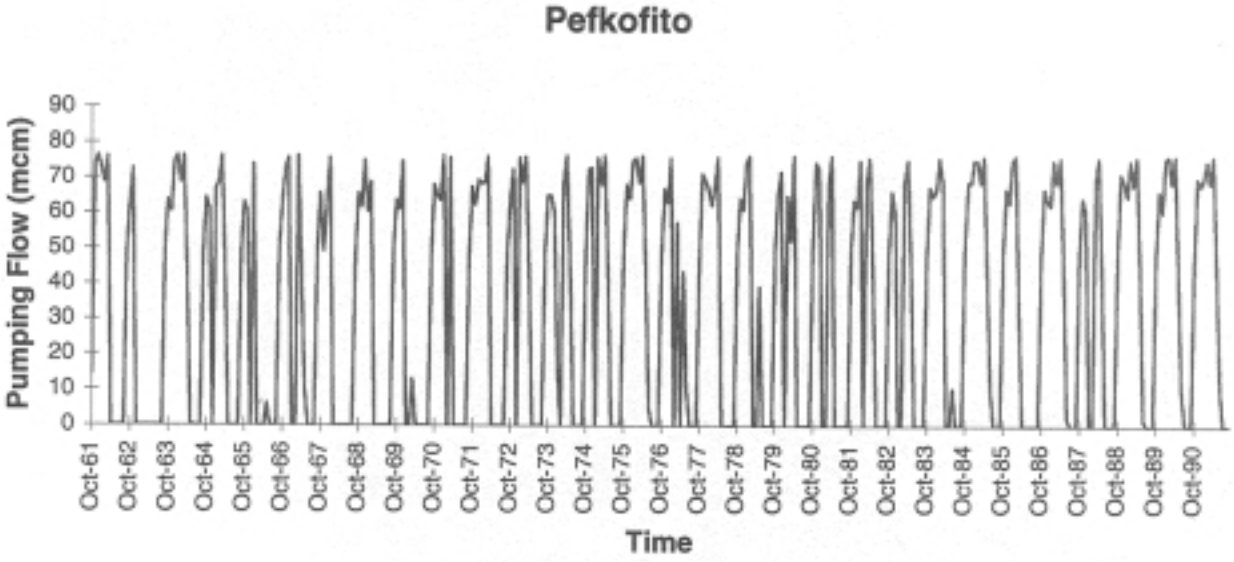

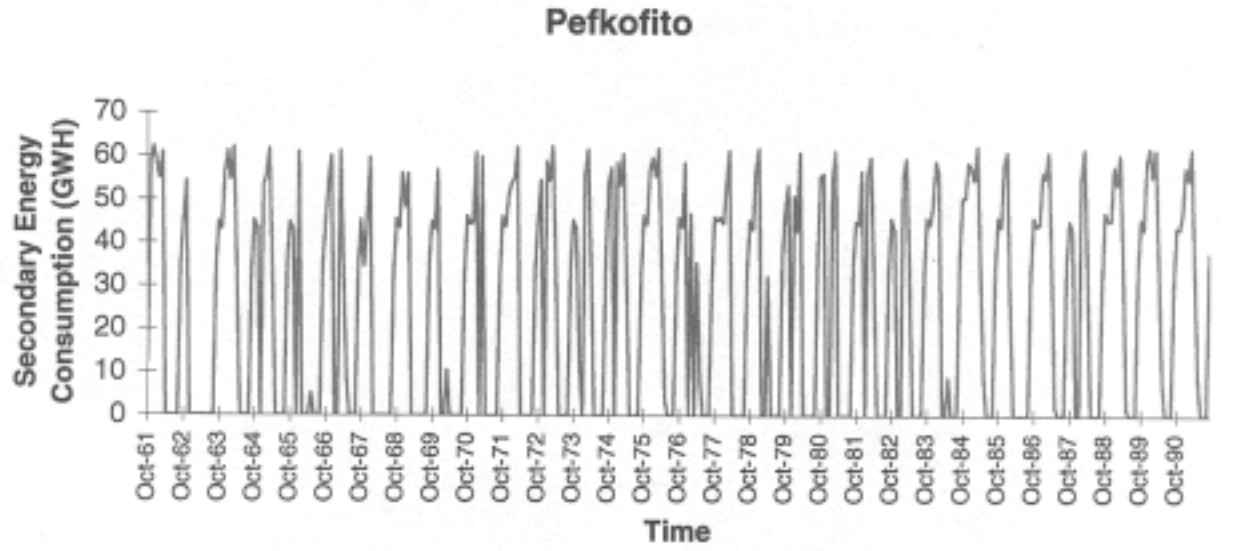

Figure 4.2.23: Pefkofito Pumping Operation Simulation Sequences; Pumping

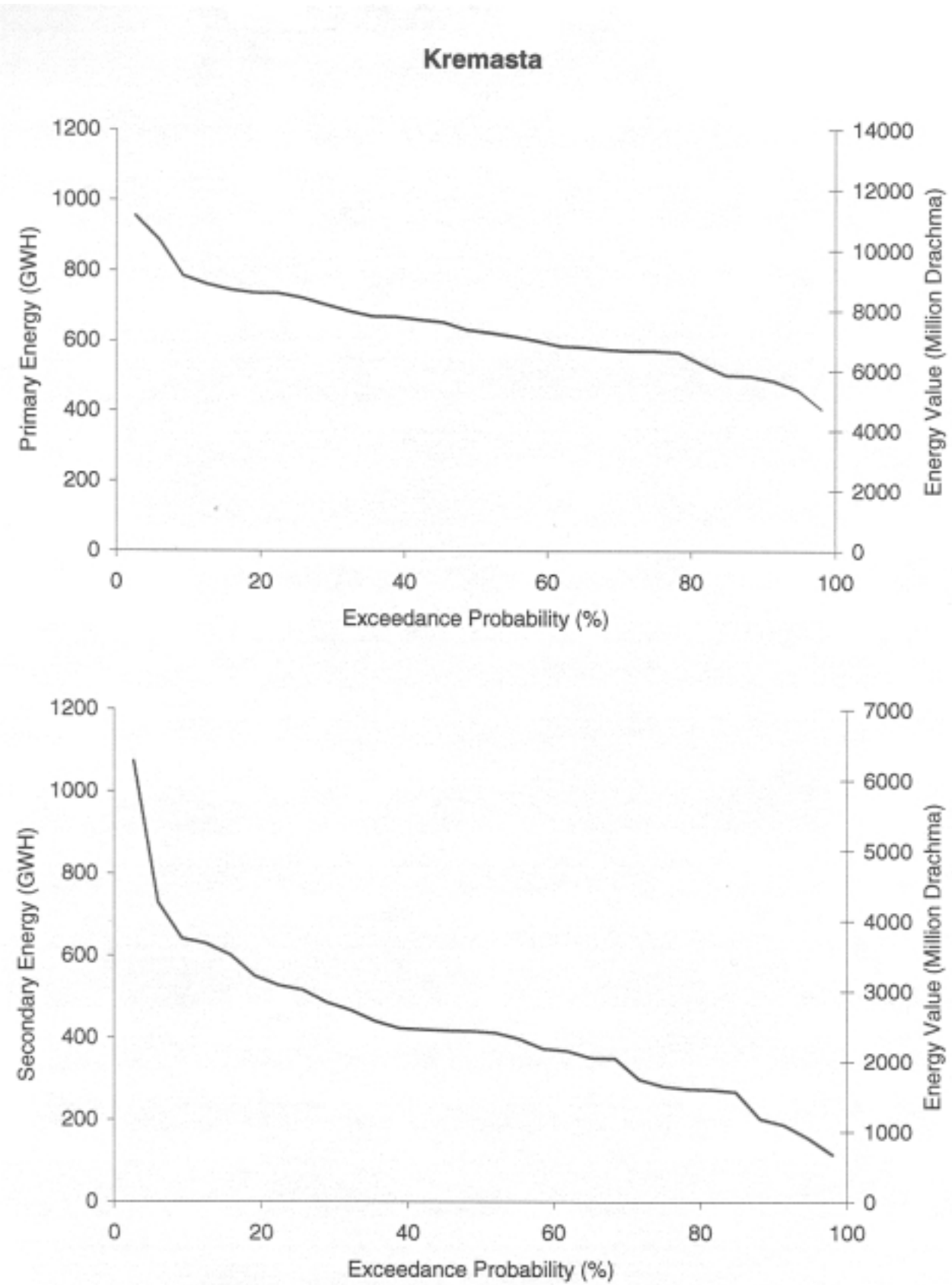

Figure 4.2.24: Energy Probability Exceedance for Kremasta; Baseline case

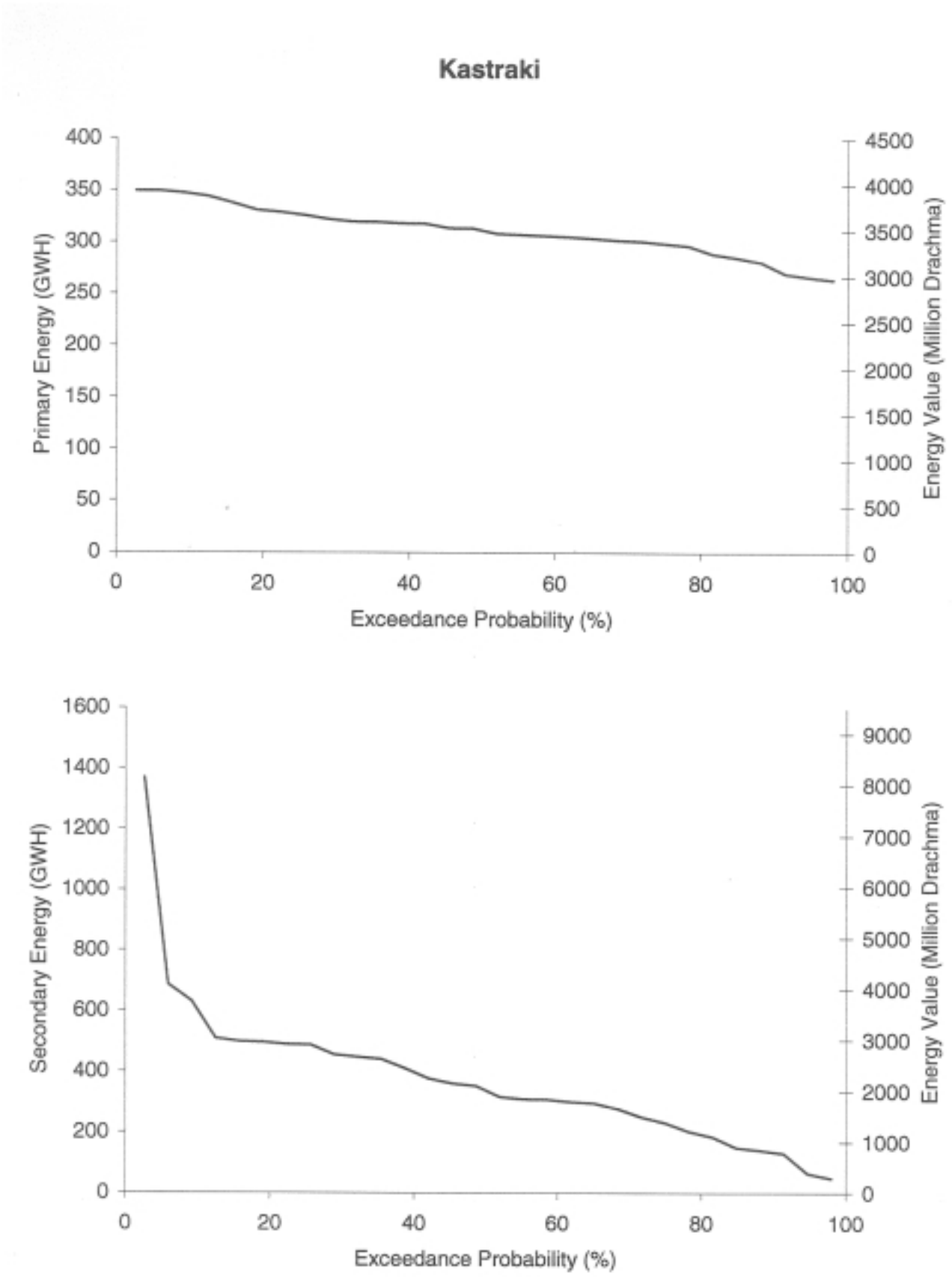

Figure 4.2.25: Energy Probability Exceedance for Kastraki; Baseline case

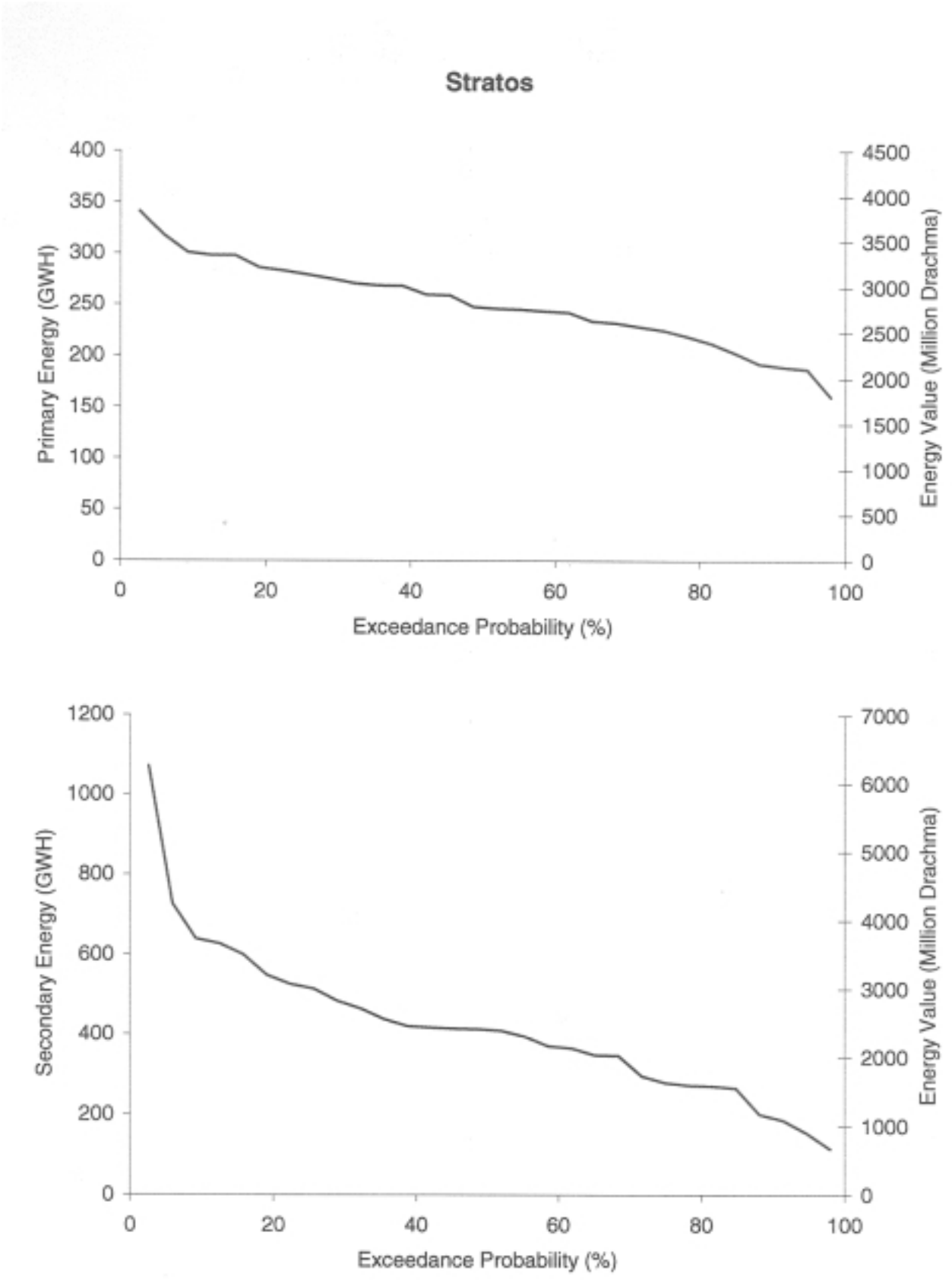

Figure 4.2.26: Energy Probability Exceedance for Stratos; Baseline case

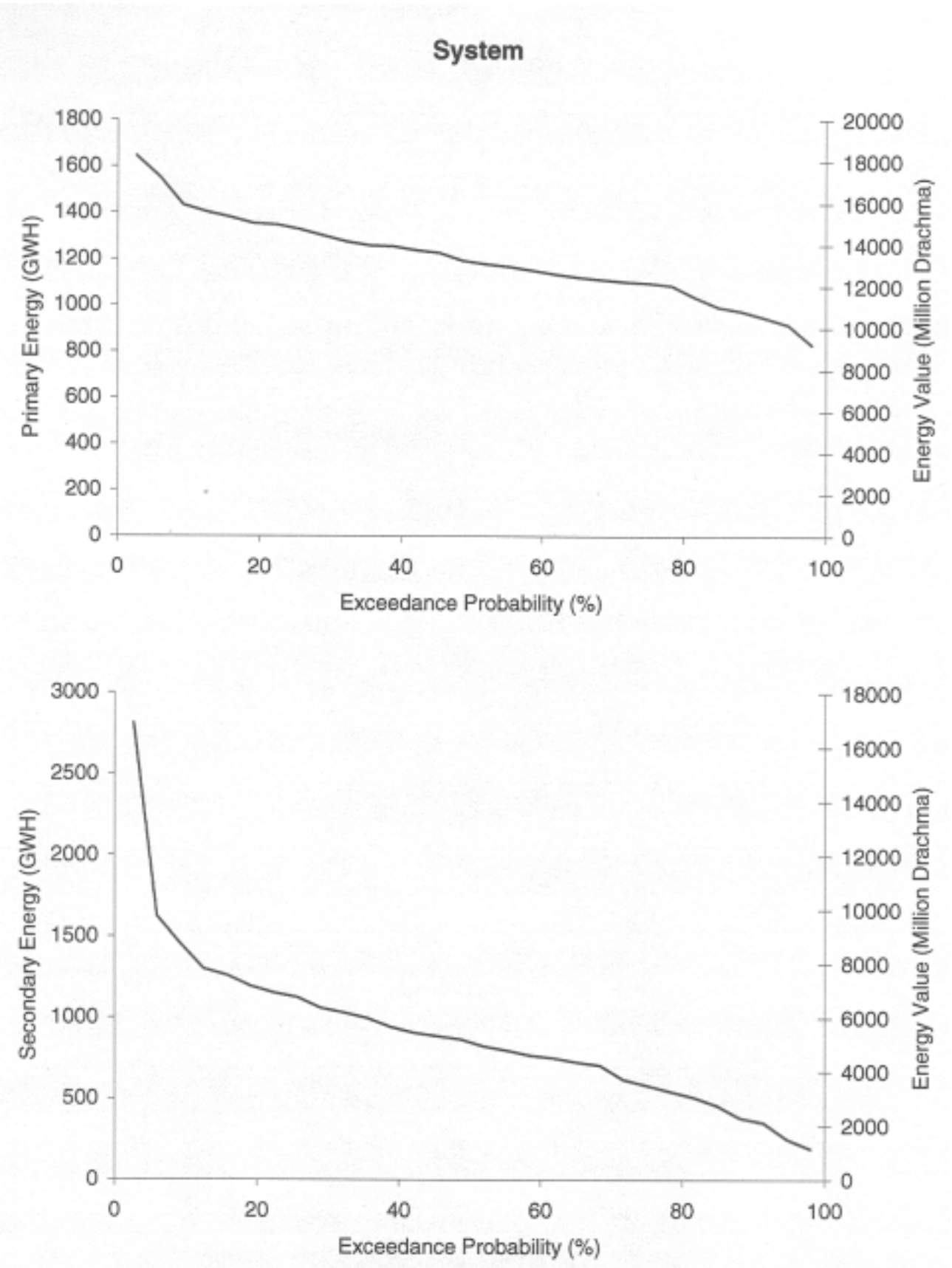

Figure 4.2.27: Energy Probability Exceedance for the System; Baseline case

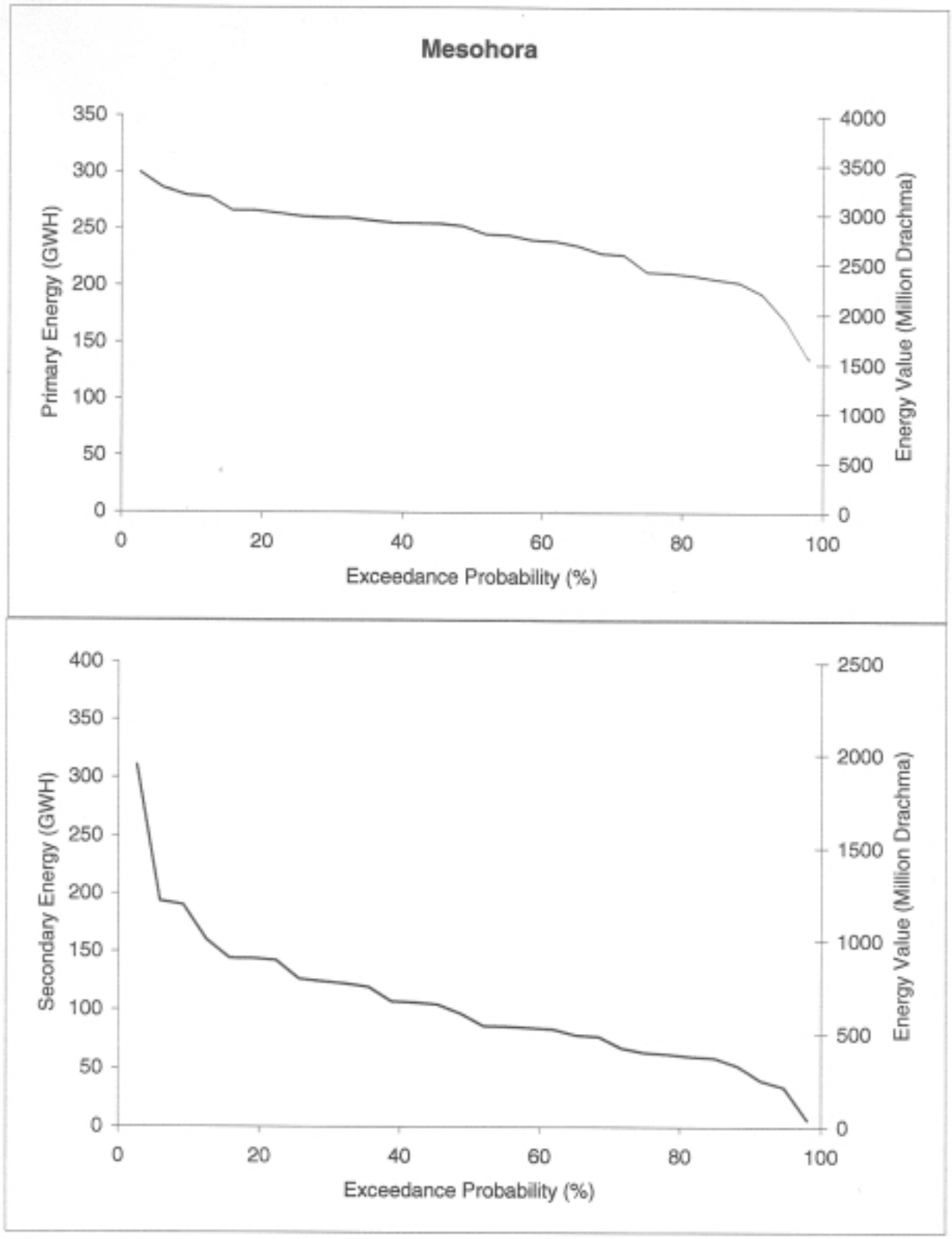

Figure 4.2.28: Energy Probability Exceedance for Mesohora; No Pumping

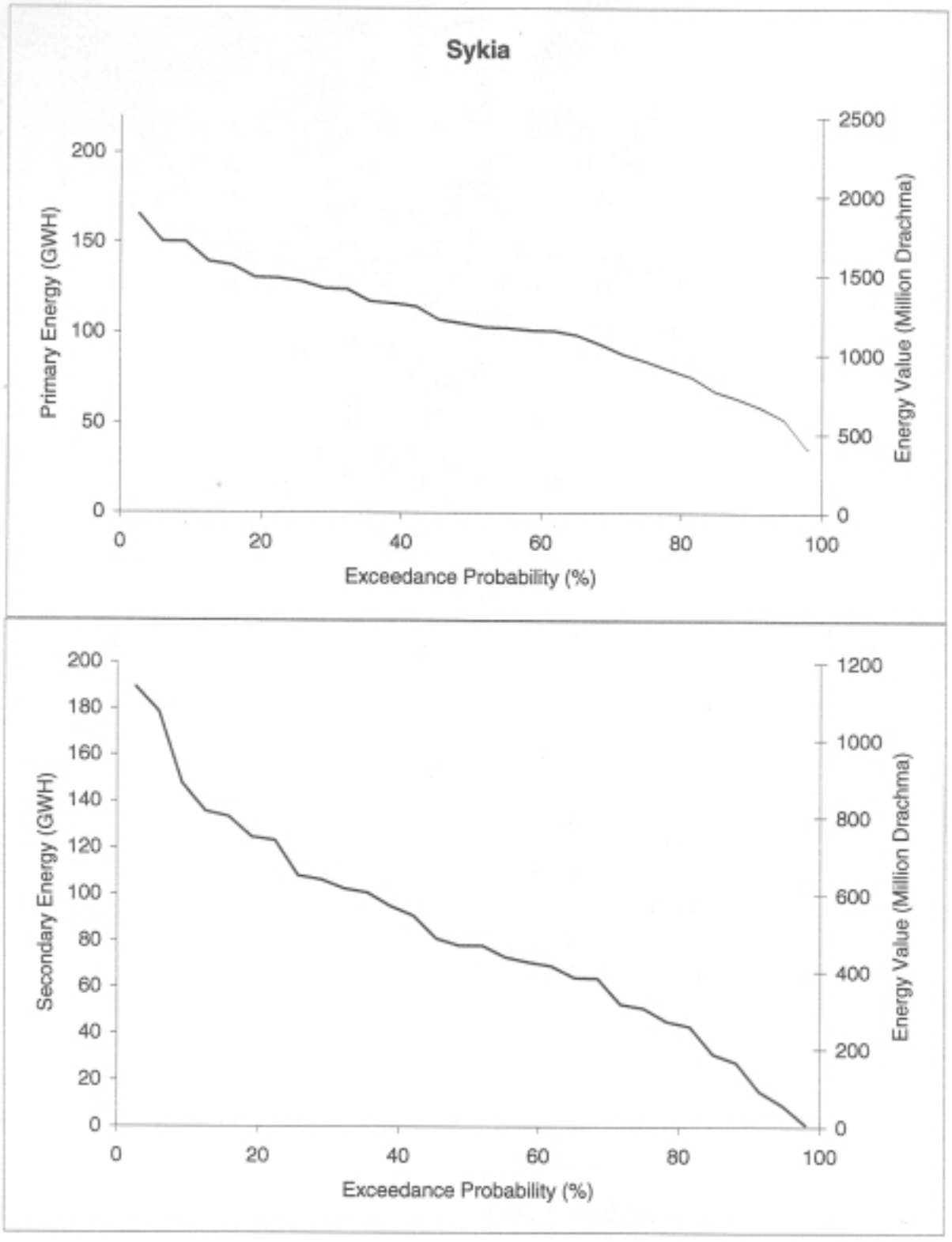

Figure 4.2.29: Energy Probability Exceedance for Sykia; No Pumping

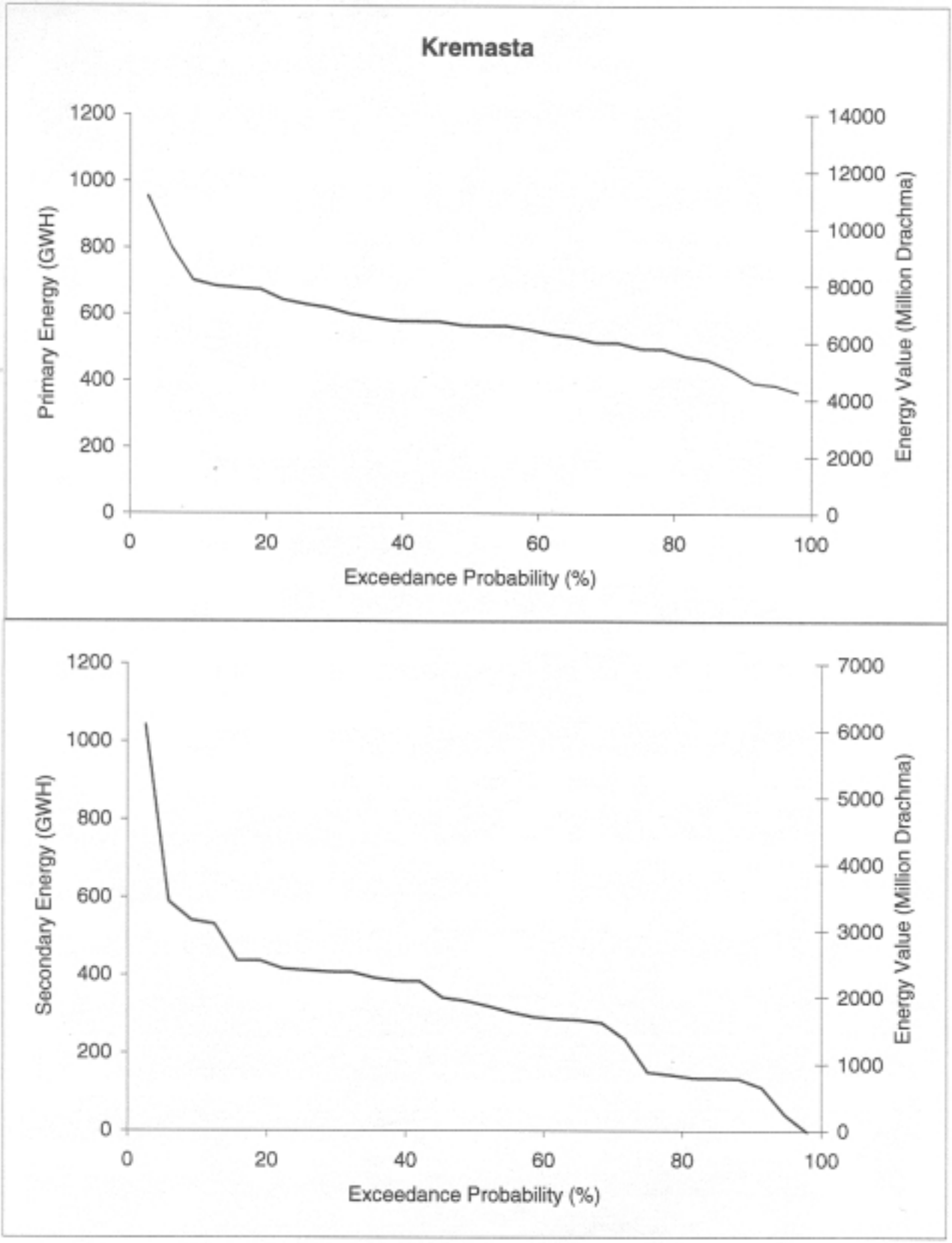

Figure 4.2.30: Energy Probability Exceedance for Kremasta; No Pumping

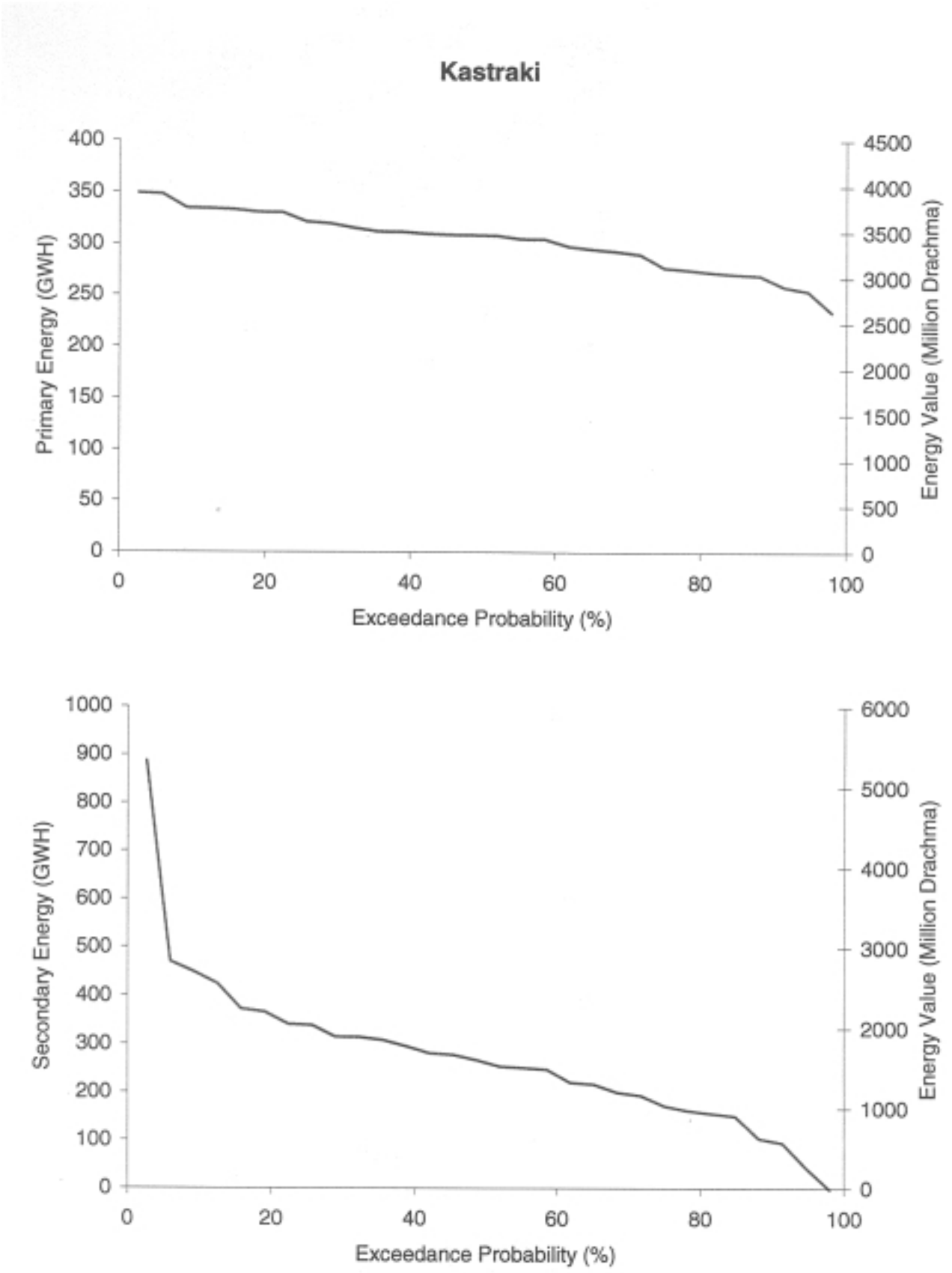

Figure 4.2.31: Energy Probability Exceedance for Kastraki; No Pumping

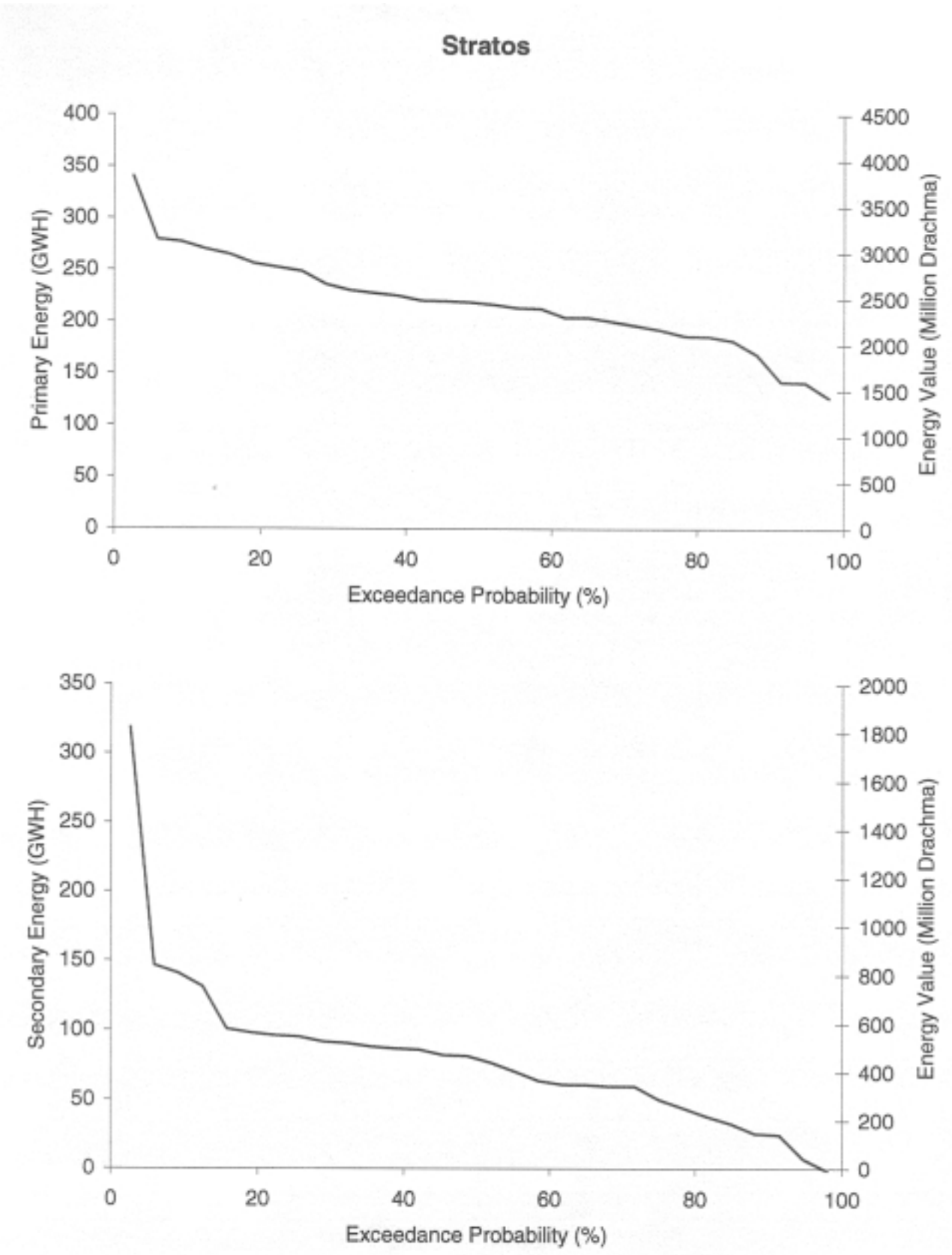

Figure 4.2.32: Energy Probability Exceedance for Stratos; No Pumping

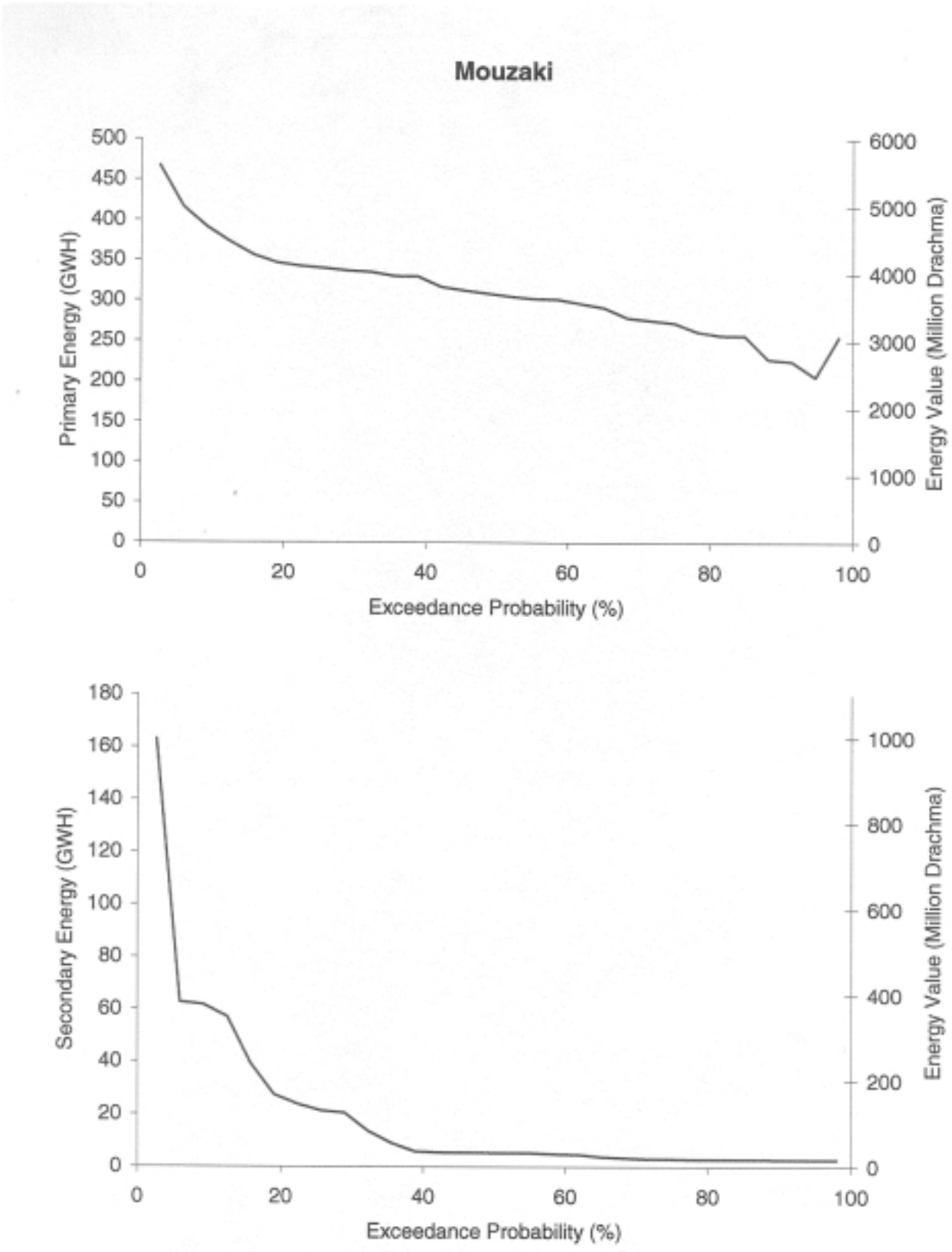

Figure 4.2.33: Energy Probability Exceedance for Mouzaki; No Pumping

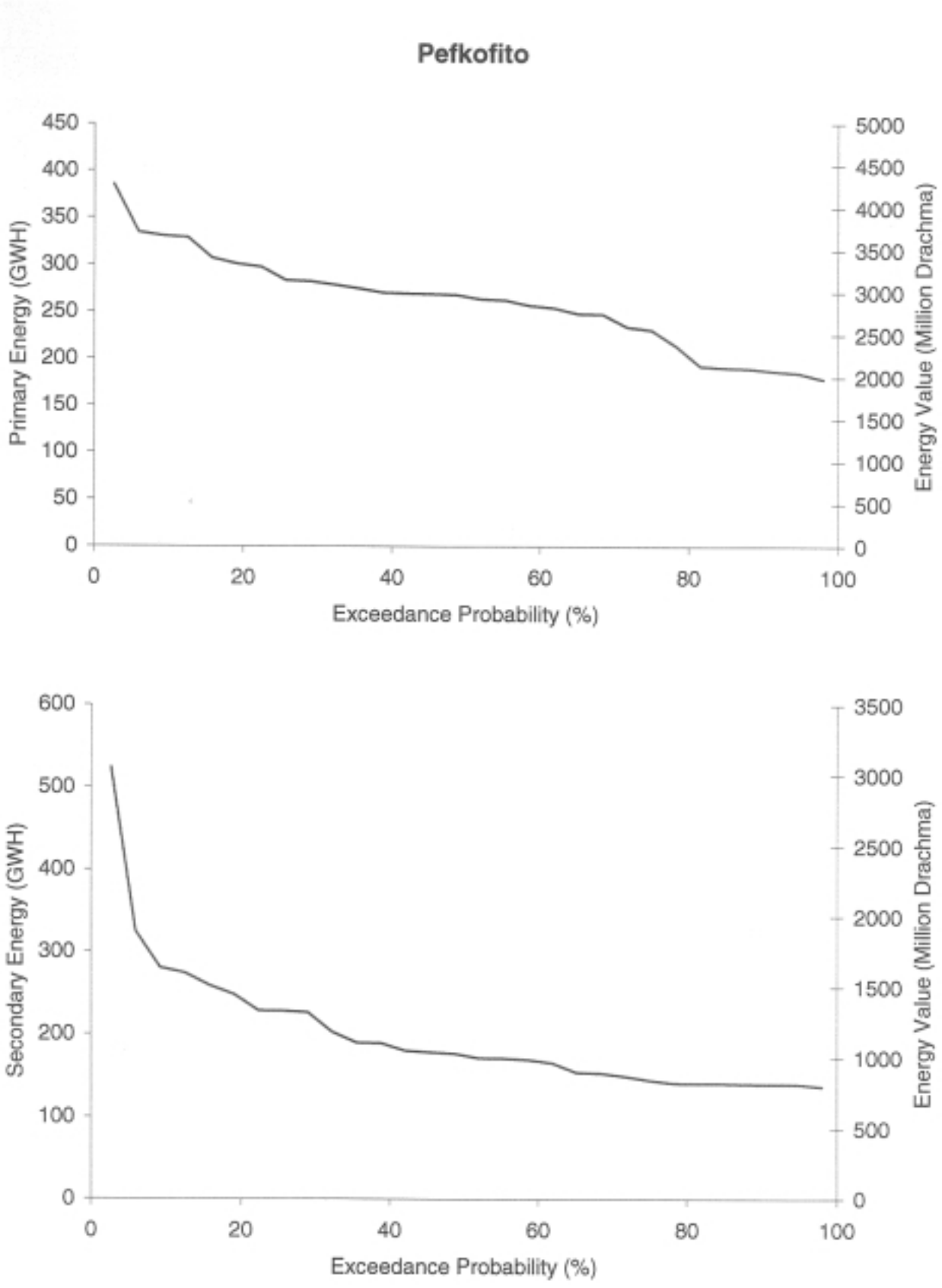

Figure 4.2.34: Energy Probability Exceedance for Pefkofito; No Pumping

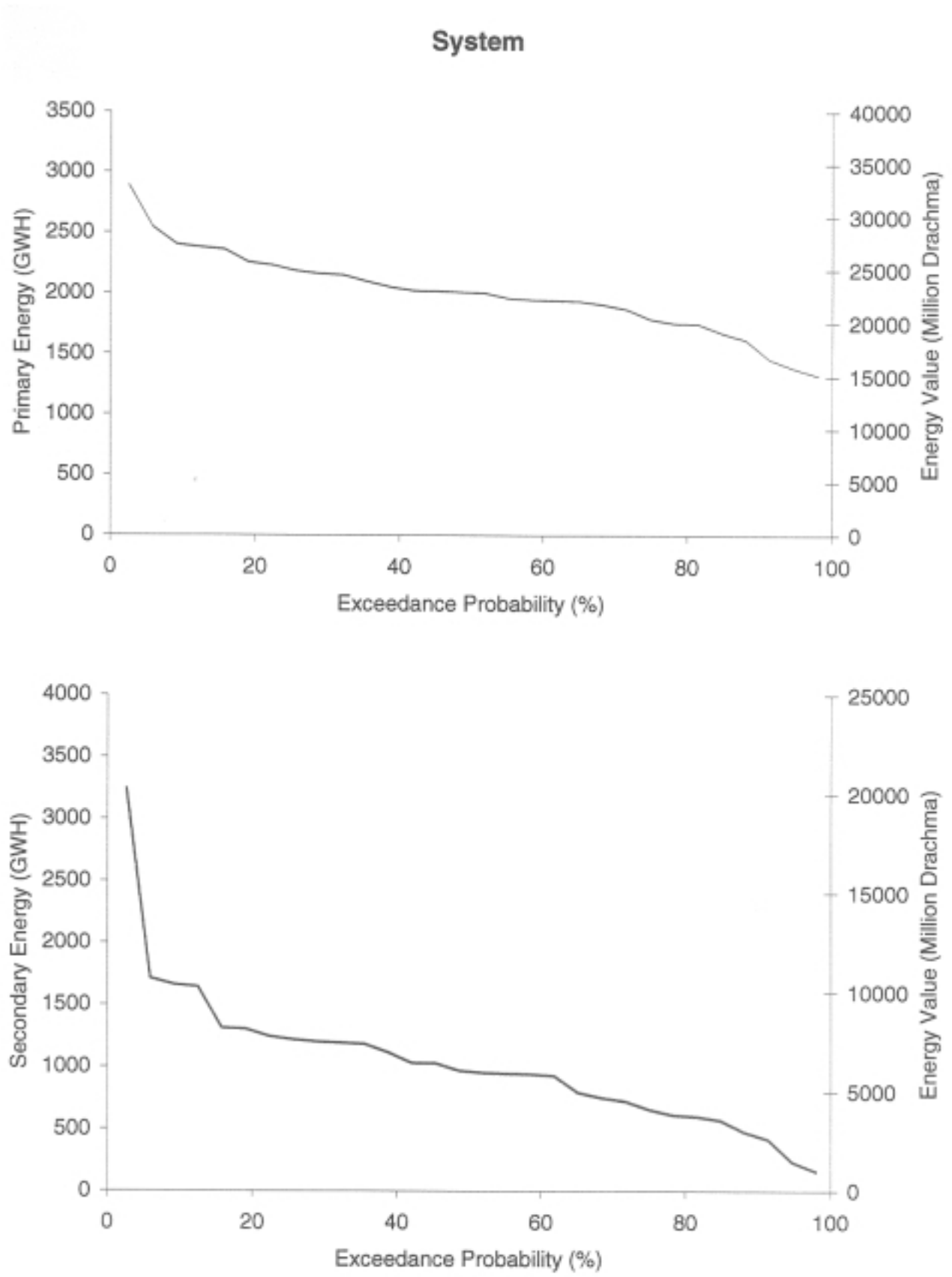

Figure 4.2.35: Energy Probability Exceedance for System; No Pumping

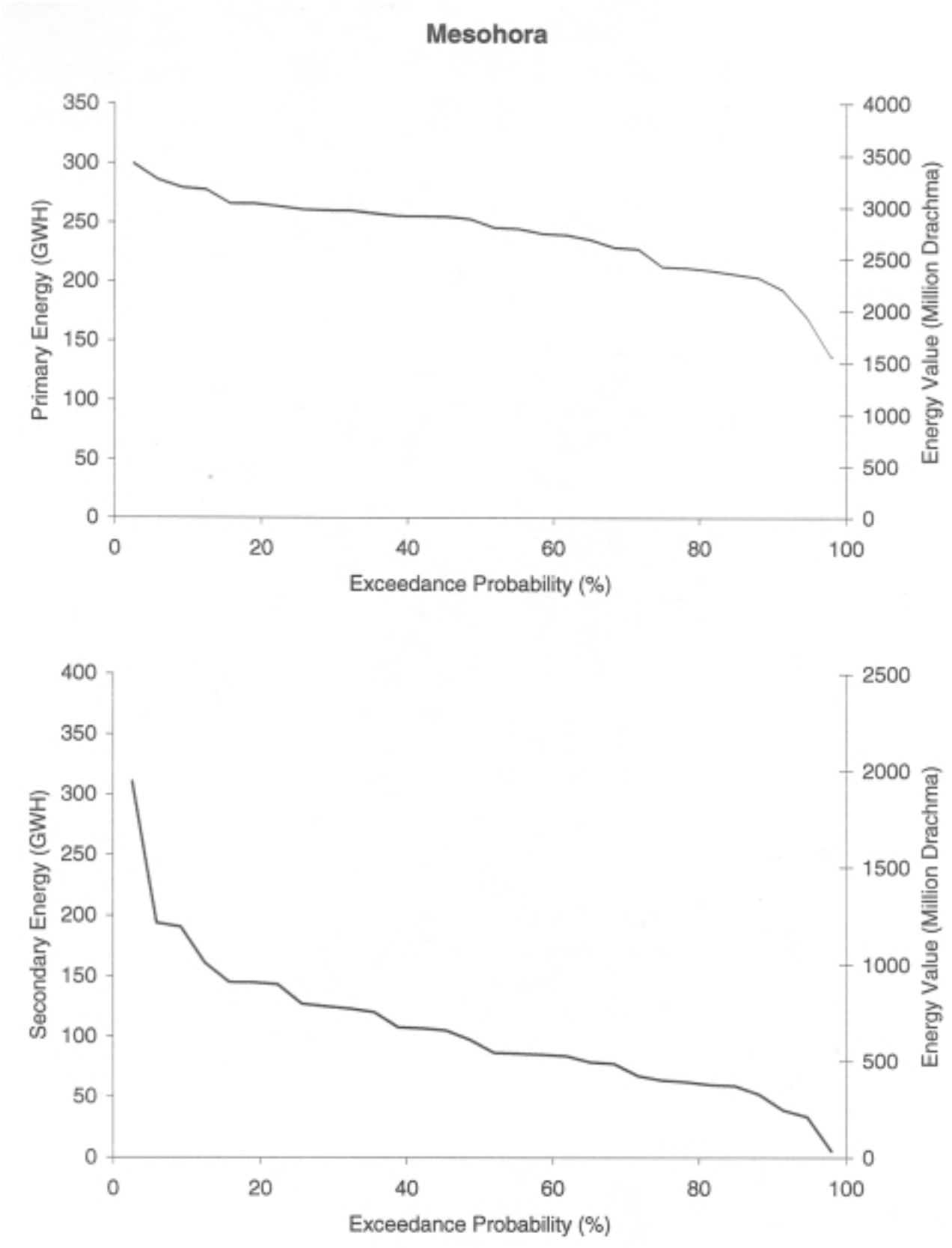

Figure 4.2.36: Energy Probability Exceedance for Mesohora; Pumping

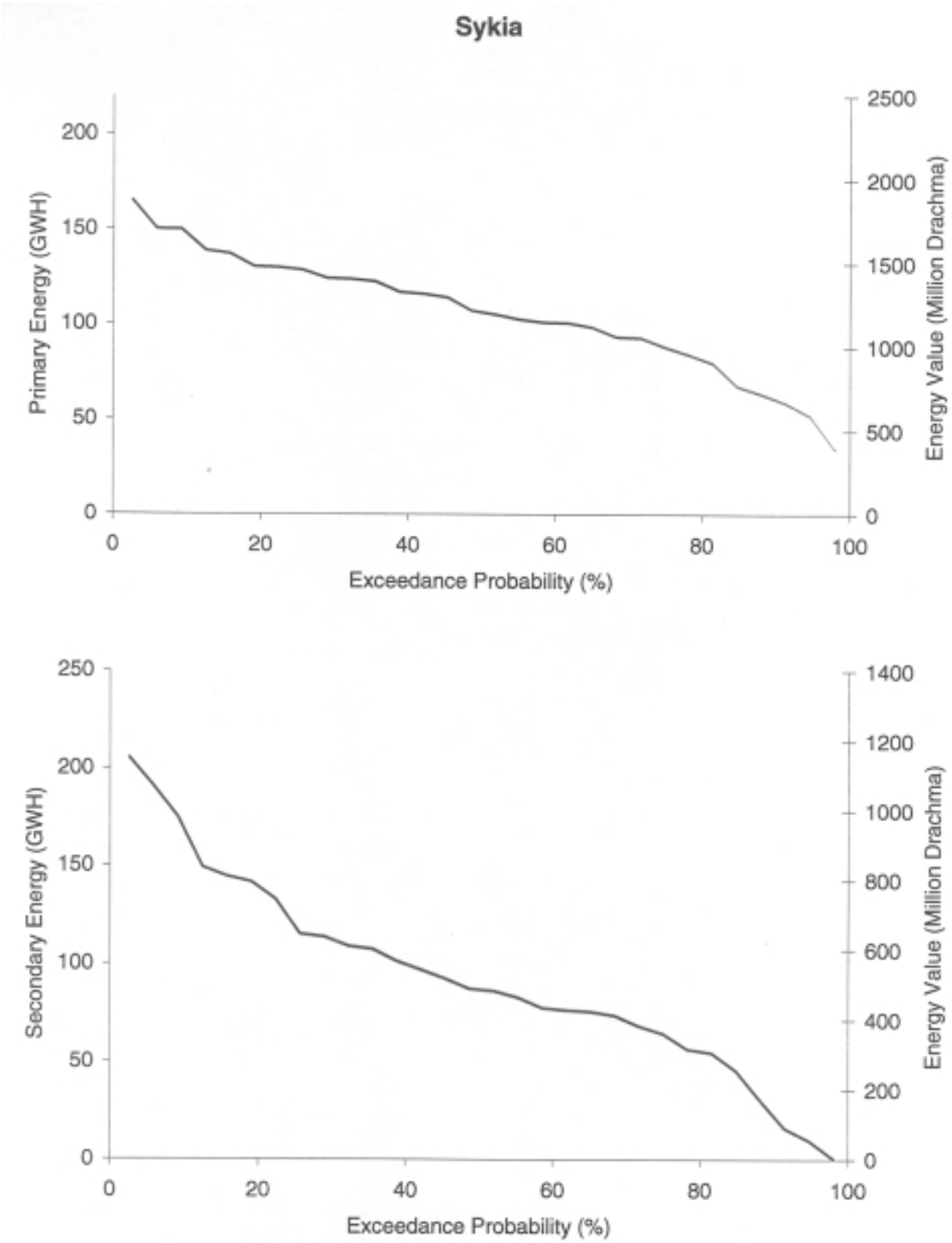

Figure 4.2.37: Energy Probability Exceedance for Sykia; Pumping

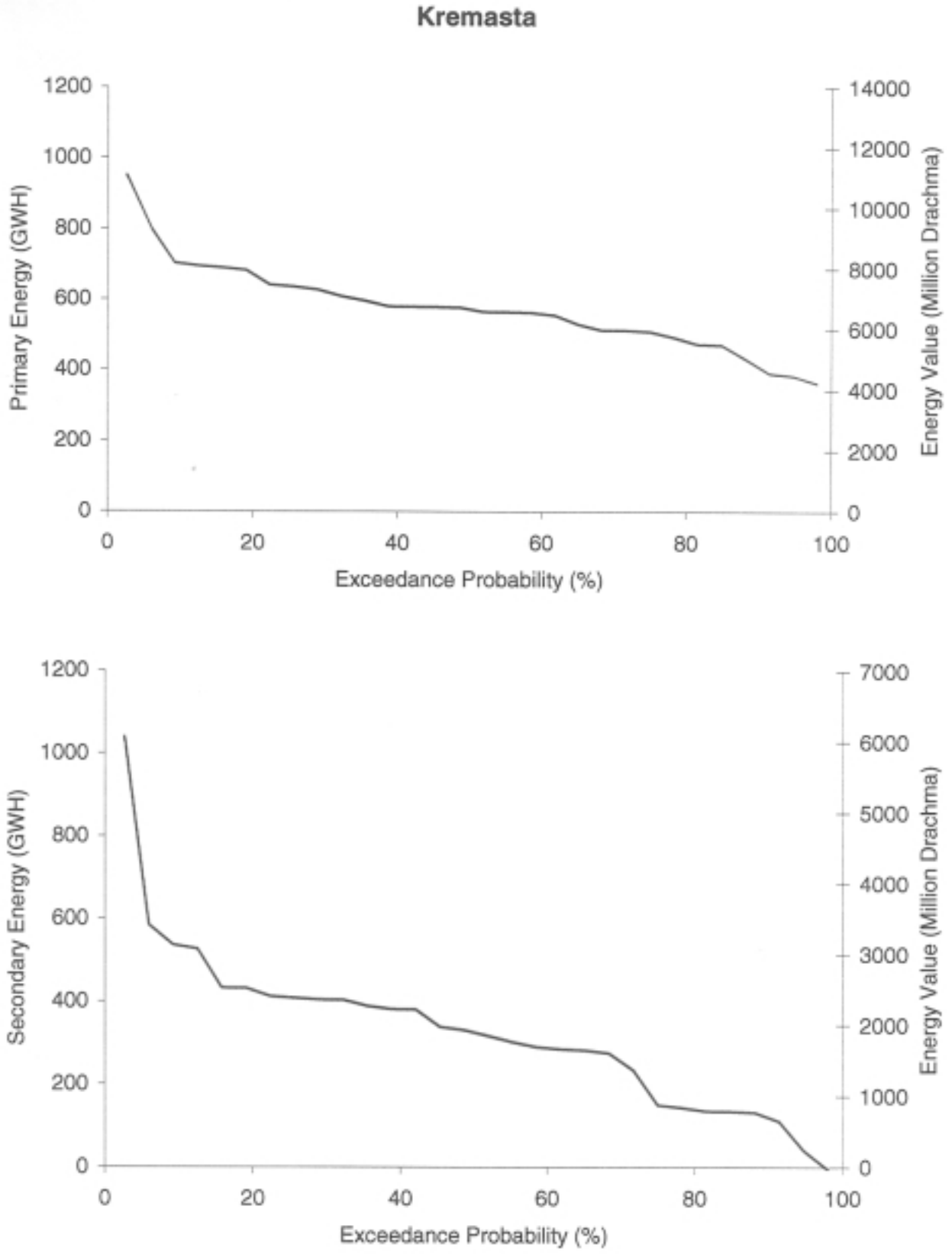

Figure 4.2.38: Energy Probability Exceedance for Kremasta; Pumping

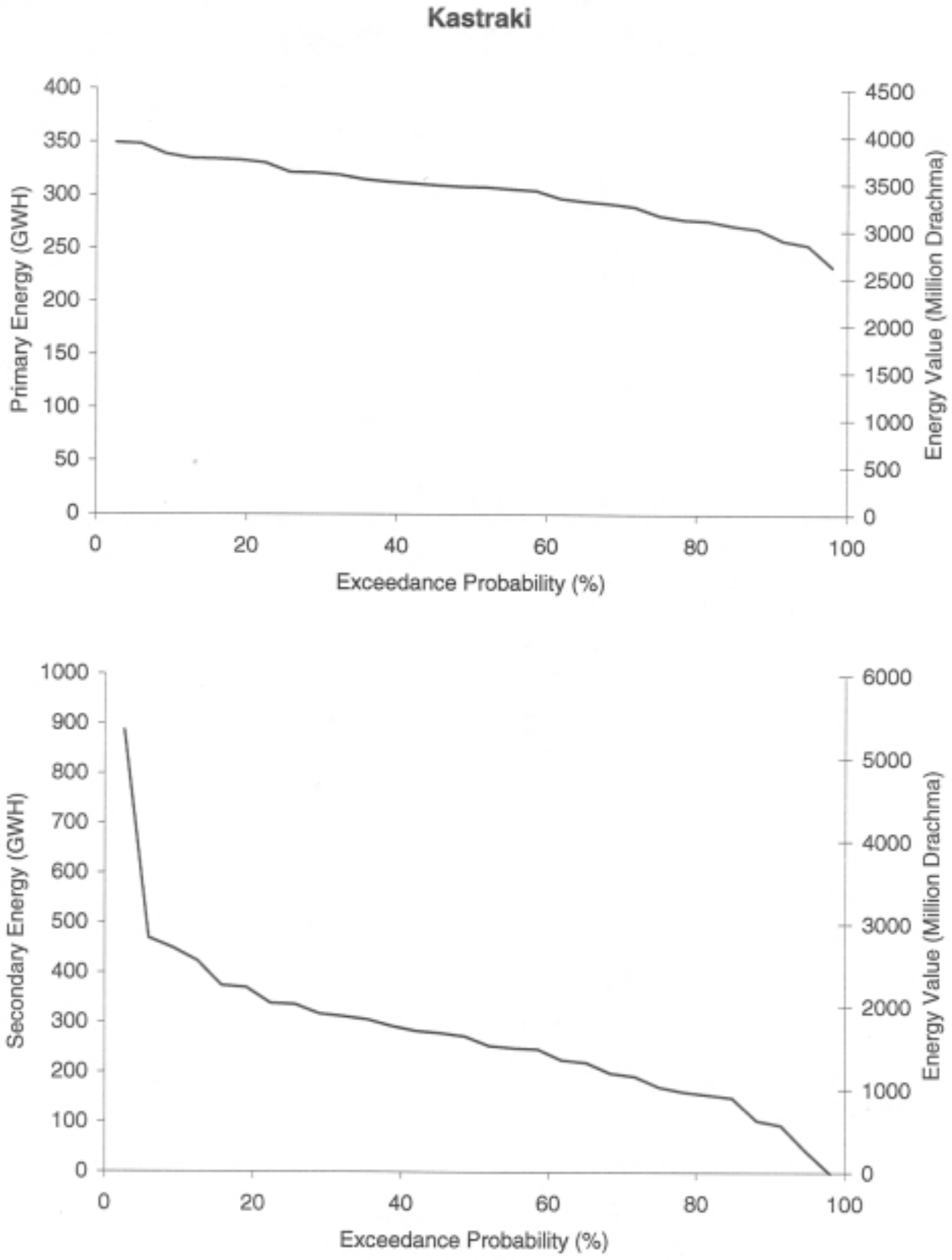

Figure 4.2.39: Energy Probability Exceedance for Kastraki; Pumping

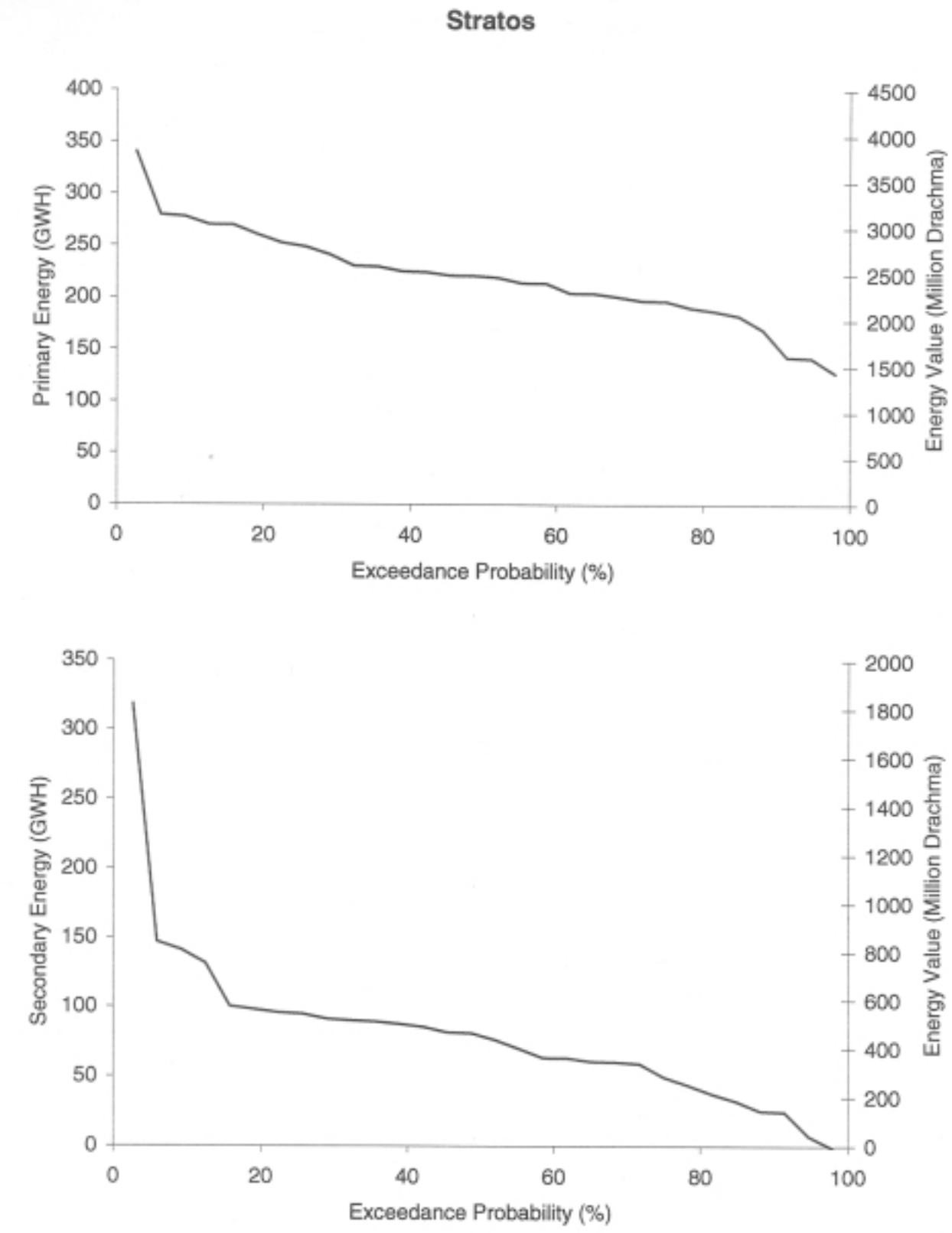

Figure 4.2.40: Energy Probability Exceedance for Stratos; Pumping

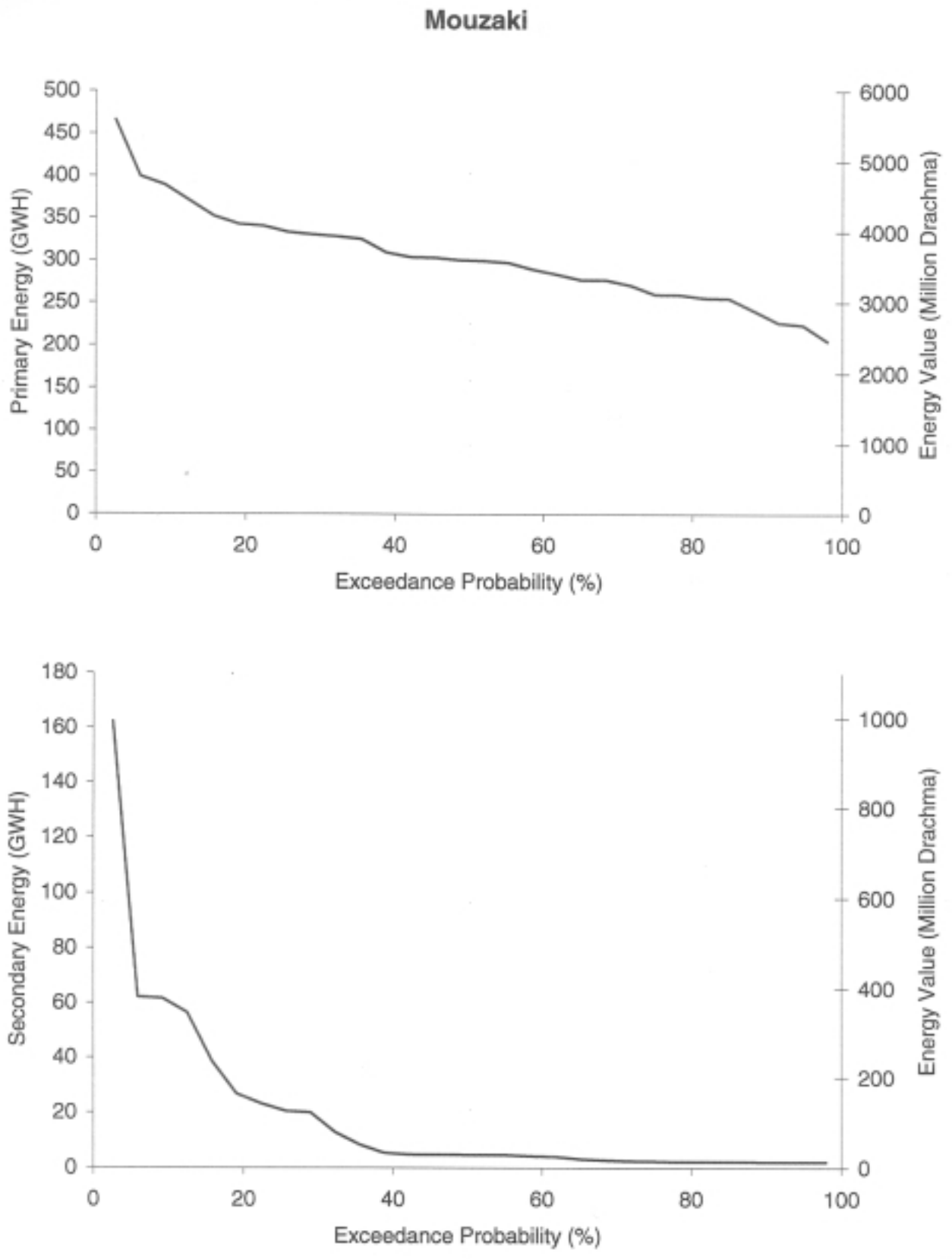

Figure 4.4.41: Energy Probability Exceedance for Mouzaki; Pumping

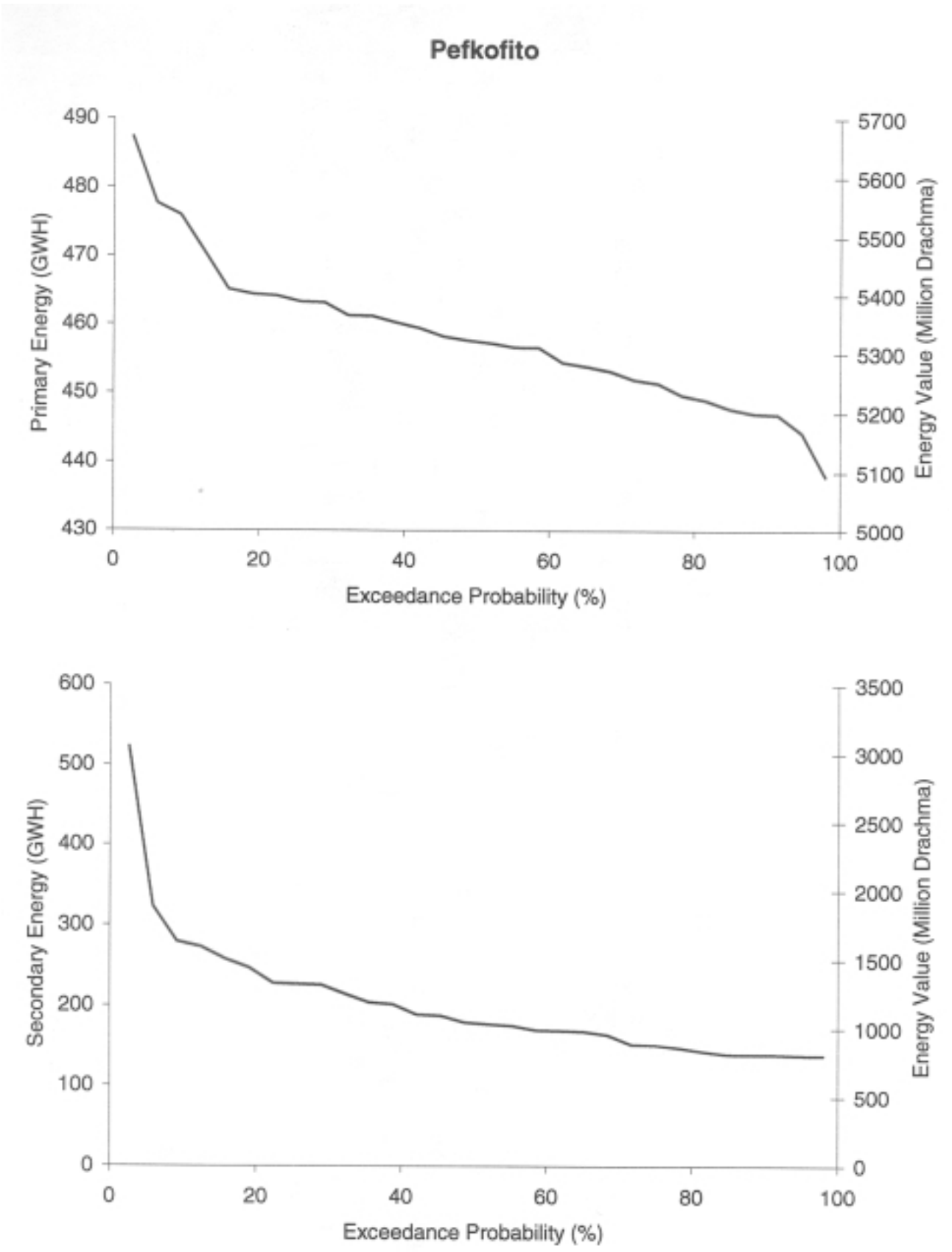

Figure 4.2.42: Energy Probability Exceedance for Pefkofito; Pumping

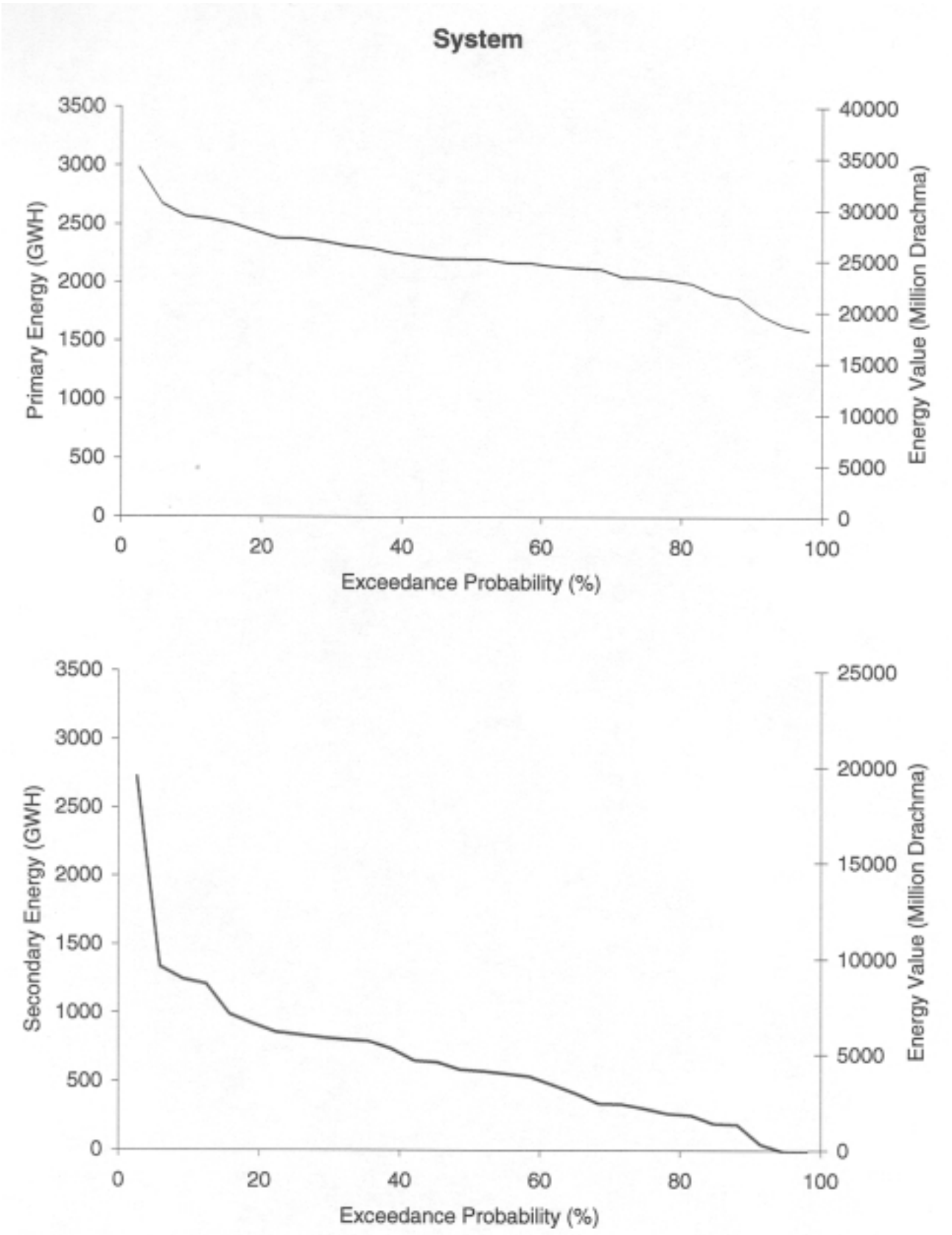

Figure 4.2.43: Energy Probability Exceedance for Entire System; Pumping

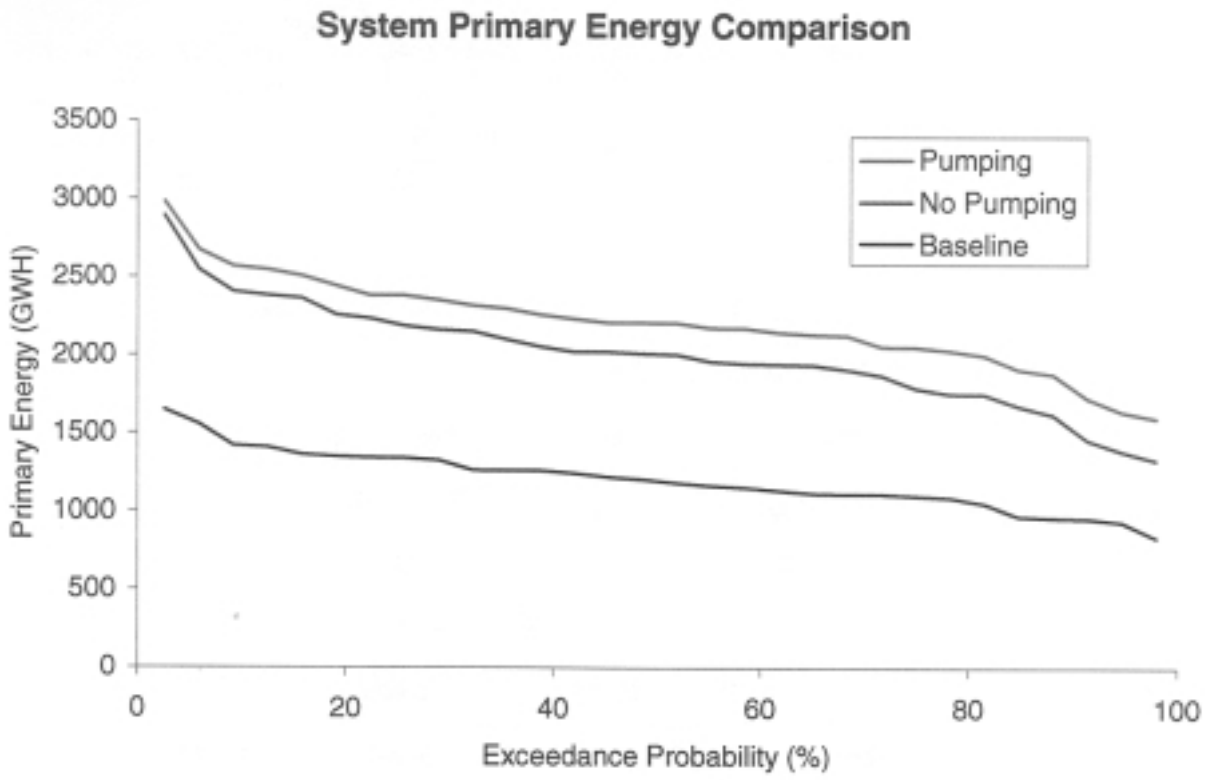

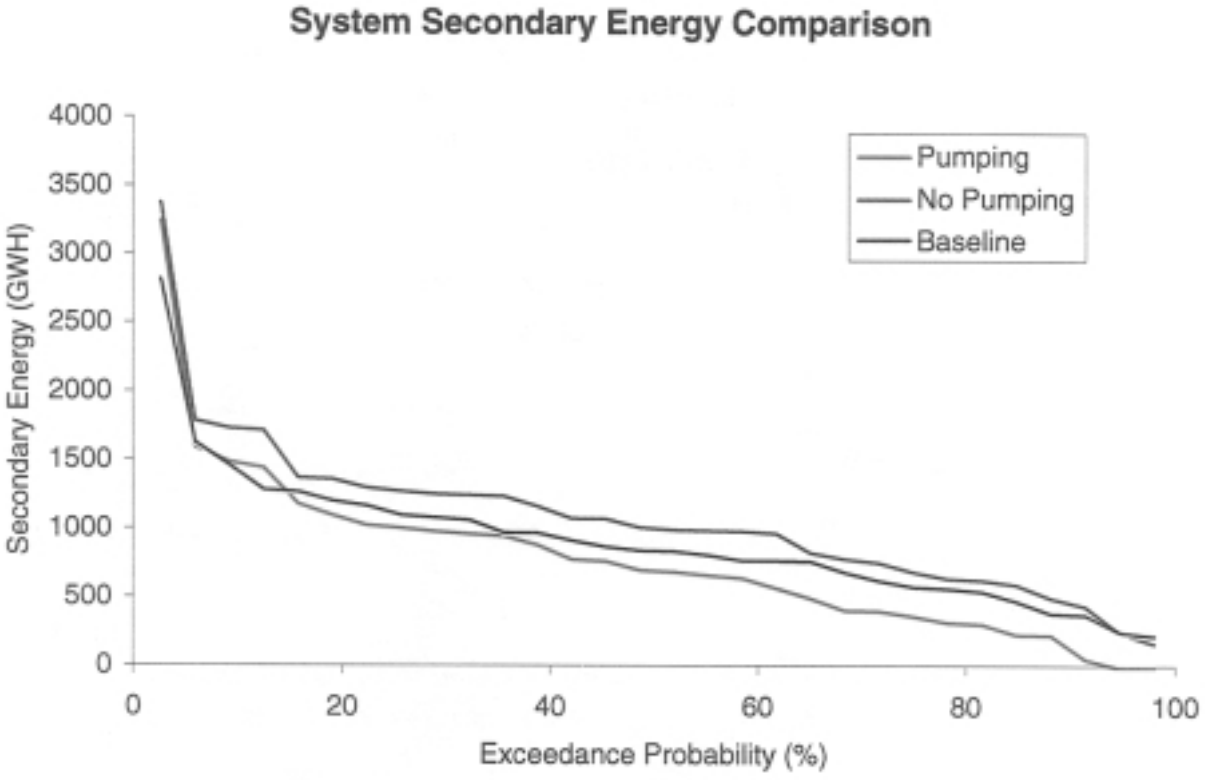

Figure 4.2.44: System Energy Probability Exceedance Comparison

CHAPTER 5

CONCLUSIONS AND FURTHER INVESTIGATIONS

The contributions of the work effort described herein fall in two categories: First, is the development of an integrated decision model for the planning and management of the Acheloos-Thessalia reservoir system. And second, is the use of this model to assess the impacts of the proposed water diversion and performance of various associated system configurations.

The reservoir control model is based on a new adaptation of the dynamic programming optimization methodology that circumvents the well-known "dimensionality" limitations. The new approach represents all system reservoirs in an optimal fashion, models their hydropower operations (both conventional and pumping) as well as their water use requirements, and develops feedback policies that optimize the system in a fully uncertain operational framework.

To assess the impacts of the water transfer from the Acheloos Basin to the Thessalia Region, a forecast-control-simulation model was also developed and is a part of the decision support system. Noteworthy findings of the investigations described herein (Chapter 4) are as follows:

- With reference to the existing hydropower facilities in the Acheloos River (namely, Kremasta, Kastraki, and Stratos), an annual diversion of 600 million cubic meters of water to Thessalia is expected to decrease annual energy generation by about 16% (from approximately 2,107 GWH per year to 1,766 GWH per year). However, considering the additional hydropower facilities that will be constructed to facilitate the diversion (depicted in Figure 1.1), energy generation is expected to increase by 47% (to 3,097 GWH annually). Assuming that peak and off-peak power is respectively valued at 11.5 and 6 drachma per KWH, this hydropower increase implies an annual economic benefit of 10.5 billion drachma per year (from 19.2 billion to 29.7 billion drachma).

- Pumping operations are profitable only when the price difference between peak and off-

peak power is significant. Specifically, at a price of 8 drachma/off-peak KWH, pumping operations cannot produce additional revenues. On the other hand, if off-peak power costs 6 dr/KWH, pumping at Pefkofito increases the economic value of hydropower by about 2%.

- In all cases tested, the system is able to meet the specified irrigation and environmental release requirements, in both the Acheloos and the Thessalia valleys.

The decision system can be improved and utilized in several other ways. First, additional information is needed to better represent the hydropower facilities on the Pamisos River. For example, the assumption made here is that the tailrace at Pefkofito is controlled by the Mouzaki reservoir level. Furthermore, downstream of Mouzaki there are two proposed hydropower stations, one at the exit of the Mouzaki reservoir and another at Mavromation. However, no information is available for the latter, and no attempt was made here to model it. Also, the pumping possibility at the Mouzaki hydropower station require more detailed knowledge of the downstream impoundments. Since such information is unavailable, our assumption for pump-back operations at this site is that the station is either pumping for eight hours each day or that it does not pump at all. Given this assumption, pumping operations at Mouzaki are not profitable. However, the situation may change if the facility characteristics are modeled in more detail.

The optimization process is designed to maximize the hydropower value given that it meets certain minimum release requirements for irrigation. As explained in Chapter 3, if water supply in excess of the agreed diversion amount does not generate additional benefit, the previous approach is optimal. However, if the benefit or loss functions for water excess or deficit are known, then the optimization process should be reformulated to explicitly consider the revenues/losses from irrigation.

The decision system has intentionally been developed with a flexible structure to include such modifications given additional information. This will hopefully be accomplished in the next project phase.

REFERENCES

Georgakakos, A.P., H. Yao, Y. Yu, and K.G. Noutsopoulos, "A Reservoir Control Model for the Acheloos River," Technical Report No. GIT/CEE-HYDRO-95-6, School of Civil and Environmental Engineering, Georgia Tech, Atlanta, September 1995, 124p.

Georgakakos, A.P., Yao, H., and Y. Yu, "A Control Model for Dependable Hydropower Capacity Optimization," *Water Resources Research*, 33(10), 2349-2365, 1997.

Georgakakos, A.P., H. Yao, and Y. Yu, "Control Models for Hydroelectric Energy Optimization," *Water Resources Research*, 33(10), 2367-2379, 1997.

Georgakakos, A.P., H. Yao, and Y. Yu, "A Control Model for Hydroelectric Energy Value Optimization," *ASCE J. for Wat. Res. Plan. and Mgt*, 123(1), 30-38, 1997.

APPENDIX A

RESERVOIR DATA AND CHARACTERISTIC CURVES

A.1 Elevation vs. Storage Relationships

Table A.1.1: Elevation vs. Storage Data for Mesohora

Level (m)	Area (km^2)	Storage (mcm)
640	0	0
650	0.055	0.09
660	0.24	1.56
670	0.515	5.33
680	0.925	12.53
690	1.355	23.93
700	1.873	40.07
710	2.59	62.38
720	3.22	91.43
730	3.985	127.45
740	4.751	171.13
750	5.671	223.26
760	6.738	285.28
770	7.823	358.08
780	8.983	442.11
790	10.166	537.85
800	11.57	646.53

Table A.1.2: Elevation vs. Storage Data for Sykia

Level (m)	Area (km^2)	Storage (mcm)
410	0	0
420	0.19	0.6
430	0.417	5.56
440	0.695	8.33
450	1	16.8
460	1.6	22.22
470	2.29	41.66
480	3.17	76.3
490	4.17	111.1
500	5.23	159.4
510	6.46	216.64
520	7.67	287.6
530	9.24	380.52
540	10.98	480.51
550	12.76	590.8

Table A.1.3: Elevation vs. Storage Data for Kremasta

Level (m)	Area (km^2)	Storage (mcm)
227	40	999
233	45	1420
240	50	1750
250	58	2300
255	61	2600
260	65	2900
265	68	3300

270	71	3650
275	74	4000
282	79	4500

Table A.1.4: Elevation vs. Storage Data for Kastraki

Level (m)	Area (km^2)	Storage (mcm)
142	23.3	750
142.5	23.5	755
143	23.8	765
143.2	23.9	770
143.5	24.1	775
144	24.2	785
144.2	24.4	800

Table A.1.5: Elevation vs. Storage Data for Stratos

Level (m)	Area (km^2)	Storage (mcm)
64	6.11	43.16
66	6.63	55.79
68	7.05	64.21
70	7.58	84.21

Table A.1.6: Elevation vs. Storage Data for Pyli

Level (m)	Area (km^2)	Storage (mcm)
264	0	0
280	0.11	0.64
300	0.78	9.54
320	1.66	33.94
340	2.82	78.74
360	3.4	140.94

Table A.1.7: Elevation vs. Storage Data for Mouzaki

Level (m)	Area (km^2)	Storage (mcm)
205	0	0
220	0.51	2.55
240	2.01	26.08
260	3.76	82.81
280	5.38	173.68
300	7.54	302.21
320	9.58	472.94
340	11.89	687.21
360	14.43	949.94

A.2 Power Functions

Table A.2.1: Power function for Mesohora

Power (MW)	Discharge (m^3/s)	Gross Head (m)
120	81.37	181
123	82.39	184
128	83.5	188
133	84.81	192
138	86.25	196
143	87.48	200
147	88.77	204
152	90	208
156	90	212
159	90	216
163	90	220

Table A.2.2: Power function for Sykia

Power (MW)	Discharge (m^3/s)	Gross Head (m)
95	127.23	89
101	127.23	94
107	127.23	99
114	127.23	104
120	127.23	109
126	127.23	114
132	127.23	119
137	126.26	124
138	122.16	129
138	117.82	134

138	113.86	139
138	110.24	144
138	106.90	149
138	103.78	154

Table A.2.3: Specific Generation Efficiency vs. Elevation Data for Kremasta

H (m)	227	229	233	237	241	245	249	253	261	265	271	277	283
E (m^3/kwh)	5.5	5.3	5	4.7	4.4	4.2	4	3.8	3.6	3.2	3	2.8	2.6

Table A.2.4: Specific Generation Efficiency vs. Elevation Data for Kastraki

H (meters)	142	142.5	143	143.5	144	144.5	145.0
E (cubic m^3/kwh)	5.95	5.87	5.78	5.71	5.62	5.56	5.48

Table A.2.5: Specific Generation Efficiency vs. Elevation Data for Stratos

H (m)	67	67.5	68	68.5	69
E (m^3/kwh)	11.7	11.54	11.39	11.24	11.10

Table A.2.6: Power function for Mouzaki

Generation			Pumping		
Power (MW)	Discharge (m^3/s)	Gross Head (m)	Power (MW)	Discharge (m^3/s)	Gross Head (m)
170	236.12	94	313	273.52	94
184	238.70	98	314	266.87	98
195	241.04	102	314	260.19	102
207	243.58	106	314	253.50	106
219	245.61	110	314	246.78	110
231	247.74	114	313	240.03	114
243	249.93	118	313	233.27	118
253	251.37	122	312	226.48	122

265	254.27	126	312	219.66	126
276	256.20	130	311	212.82	130
286	258.12	134	309	205.96	134

Table A.2.7: Power function for Pefkofito

Generation			Pumping		
Power (MW)	Discharge (m^3/s)	Gross Head (m)	Power (MW)	Discharge (m^3/s)	Gross Head (m)
151	104.72	195	195	86.97	195
158	105.80	200	194	84.61	200
171	107.85	210	190	79.84	210
183	109.70	220	185	75.03	220
196	111.37	230	180	70.16	230
208	112.80	240	297	105.68	240
221	114.00	250	295	101.95	250
232	114.00	260	292	98.16	260
244	114.00	270	289	94.18	270
255	114.00	280	284	90.10	280
266	114.00	290	279	85.88	290
277	114.00	300	273	81.55	300